

**DOCTORAL THESIS**

An Investigation of  
Noncovalently Bound  
Supramolecular Systems  
through Case Studies of  
Oxacalixarenes and  
Iodo-triazoles

Anna Cowart

TALLINN UNIVERSITY OF TECHNOLOGY  
DOCTORAL THESIS  
18/2021

**An Investigation of Noncovalently Bound  
Supramolecular Systems through Case  
Studies of Oxacalixarenes and  
Iodo-triazoles**

ANNA COWART



TALLINN UNIVERSITY OF TECHNOLOGY

School of Science

Department of Chemistry and Biotechnology

This dissertation was accepted for the defence of the degree 26/02/2021

**Supervisor:**

Dr. Jasper Adamson  
National Institute of Chemical Physics and Biophysics  
Tallinn, Estonia

**Co-supervisor:**

Prof. Riina Aav  
School of Science  
Tallinn University of Technology  
Tallinn, Estonia

**Opponents:**

Prof. Edvinas Orentas  
Department of Organic Chemistry  
Vilnius University  
Vilnius, Lithuania

Dr. Erki Enkvist  
Institute of Chemistry  
Faculty of Science and Technology  
Tartu University  
Tartu, Estonia

**Defence of the thesis:** 09/04/2021, Tallinn

**Declaration:**

Hereby I declare that this doctoral thesis, my original investigation and achievement, submitted for the doctoral degree at Tallinn University of Technology has not been submitted for doctoral or equivalent academic degree.

Anna Cowart

-----  
signature



European Union  
European Regional  
Development Fund



Investing  
in your future

Copyright: Anna Cowart, 2021

ISSN 2598-6989 (publication)

ISBN 978-9949-83-679-6 (publication)

ISSN 2598-6901 (PDF)

ISBN 978-9949-83-680-2 (PDF)

Printed by Koopia Niini & Rauam

TALLINNA TEHNIKAÜLIKOOL  
DOKTORITÖÖ  
18/2021

**Mittekovalentsete sidemete abil  
moodustunud supramolekulaarsete  
süsteemide uurimine oksakaliksareenide ja  
jodotriasoolide näitel**

ANNA COWART





# Contents

List of publications .....	7
Introduction .....	8
Abbreviations .....	9
1 Literature overview .....	10
1.1 Supramolecular binding event .....	10
1.2 Non-covalent interactions of calixarenes .....	11
1.2.1 Hydrogen bonding .....	11
1.2.2 Halogen bonding .....	12
1.2.3 Van der Waals forces .....	13
1.2.4 Aromatic interactions .....	14
1.2.5 Hydrophobic effect .....	15
1.3 Supramolecular hosts and receptors .....	15
1.3.1 Cucurbiturils .....	16
1.3.2 Cyclodextrins .....	17
1.3.3 Crown ethers .....	17
1.3.4 Calixarenes .....	17
1.3.5 Heteracalixaromatics .....	18
1.3.6 Oxacalixarenes .....	20
1.3.7 Conformations of oxacalix[ <i>n</i> ]arenes .....	21
1.3.8 Molecular recognition of oxacalix[4]arenes .....	23
1.4 Methods for determining the strength of noncovalent interactions .....	25
1.4.1 Complexation equilibria .....	25
1.4.2 NMR method .....	26
1.4.3 Chemical exchange .....	26
1.4.4 NMR and molecular recognition .....	26
1.4.5 Mass spectrometry and electrospray ionization .....	27
1.4.6 Ion-mobility mass-spectrometry .....	27
2 Motivation and aims for work .....	29
3 Results and discussion .....	30
3.1 Unsubstituted oxacalix[ <i>n</i> ]arenes (Publication I) .....	30
3.1.1 Introduction to the synthesis of oxacalix[ <i>n</i> ]arenes .....	30
3.1.2 Synthesis of unsubstituted oxacalix[ <i>n</i> ]arenes ( <i>n</i> = 4, 8) .....	32
3.1.3 Crystal structures of unsubstituted oxacalix[ <i>n</i> ]arenes ( <i>n</i> = 4, 8) .....	35
3.1.4 Complexation properties of unsubstituted oxacalix[4]arene .....	36
3.2 Oxacalix[4]arene carboxylic acid (Publication II) .....	38
3.2.1 Synthesis and structure of oxacalix[4]arene carboxylic acid .....	38
3.2.2 Complexation properties of oxacalix[4]arene carboxylate .....	41
3.2.3 Complexation properties of oxacalix[4]arene carboxylic acid in gas phase (ongoing investigation) .....	42
3.3 Halogen bonding systems in solution (Publication III) .....	47
3.3.1 Introduction to halogen bonding in solution .....	47
3.3.2 Triazole-based XB donors .....	47
3.3.3 XB donor – quinuclidine interaction study by <sup>1</sup> H NMR titration .....	49
3.3.4 XB donor – acceptor enantiodiscrimination study by <sup>1</sup> H NMR titration .....	49
4 Conclusions .....	51

5 Experimental section.....	52
5.1 Mass spectrometry .....	52
References .....	53
Acknowledgements.....	59
Abstract.....	60
Lühikokkuvõte.....	61
Appendix 1 .....	63
Appendix 2 .....	71
Appendix 3 .....	81
Author's other publications and conference presentations.....	87
Curriculum vitae.....	88
Elulookirjeldus.....	89

## List of publications

This thesis has been prepared based on the following publications by the author:

- I **Peterson, A.**; Kaabel, S.; Kahn, I.; Pehk, T.; Aav, R.; Adamson, J. Unsubstituted oxacalix[n]arenes (n=4 and 8): A conformational study in solution and solid state and interaction studies with aromatic guests. *ChemistrySelect* **2018**, *3*, 9091–9095.
- II **Peterson, A.**; Ludvig, M-L.; Martõnova, J.; Kaabel, S.; Kerner, P.; Uudsemaa, M.; Trummal, A.; Fomitšenko, M.; Pehk, T.; Aav, R.; Adamson, J. New oxacalix[4]arene carboxylate detects viologen in protic media. *Supramol. Chem.* **2019**, *32*, 313–319.
- III **Peterson, A.**; Kaasik, M.; Metsala, A.; Järving, I.; Adamson, J.; Kanger, T. Tunable chiral triazole-based halogen bond donors: assessment of donor strength in solution with nitrogen-containing acceptors. *RSC Advances*, **2019**, *9*, 11718–11721.

### AUTHOR'S CONTRIBUTION TO THESE PUBLICATIONS

- I Synthesized and characterized the compounds by solution NMR. Performed and analyzed the solution NMR experiments and helped to write the manuscript and the supporting information on these topics.
- II Carried out the synthesis. Planned and performed the <sup>1</sup>H NMR titration experiments and analyzed the data. Helped to write the manuscript and the supporting information on these topics.
- III Planned, conducted, and interpreted the <sup>1</sup>H NMR titration experiments. Helped to write the manuscript and supporting information.

## Introduction

Noncovalent interactions are the basis of supramolecular chemistry and are employed in several other fields of chemistry. Noncovalent interactions have an important role in assembling the fundamental biological structures of life and connecting building blocks of new synthetic materials. For example, in biological applications, hydrogen bonds and  $\pi$ - $\pi$  interactions stabilize the DNA double helix and 3D protein structures. In synthetic chemistry, they play a role in catalysis and in large capsular assemblies. One of the specific interactions studied in this thesis is halogen bonding, which is a type of electrostatic interaction. Similar to a hydrogen bond, a halogen bond forms between an electron donor and electron acceptor pair. Investigating noncovalent bonds helps to improve our understanding of large molecular entities consisting of two or more interacting compounds and can lead to the discovery of new functional materials, effective catalysts, and sensors.

In supramolecular chemistry, noncovalent interactions are used to form host-guest complexes or to assemble large capsules. The first step towards obtaining supramolecular entities is the design and synthesis of supramolecular host molecules. In this work, supramolecular entities were made based on hosts such as crown ethers, cyclodextrins, cucurbiturils, and calixarenes, with an emphasis on calixarene chemistry. The name 'calixarene' was proposed by David Gutsche in 1978,<sup>1</sup> based on 'chalice' in Greek. The term *arene* highlights that the compound contains aromatic rings. Dating back to the 19th century when Adolf von Baeyer synthesized the first cyclic aromatic oligomers by mixing aqueous formaldehyde with phenol at elevated temperatures, calixarenes have been a constantly growing family of aromatic host molecules that have been used in a wide range of applications, e.g., in peptide recognition,<sup>2,3</sup> gas sensing,<sup>4-6</sup> and anion extraction.<sup>7,8</sup>

A subclass of oxygen-bridged calixarenes, oxacalixarenes, has developed from the family of calixarenes. These compounds differ from the main class in their electronic and structural properties. A few examples of oxacalixarene supramolecular complexes have been published, yet much is still left to discover about the binding properties of these macrocycles, making them interesting targets for further investigation. One of the aims of this thesis was to contribute to the field of calixarene chemistry by synthesizing new oxacalixarene derivatives and determining their supramolecular properties and possible applications. For the investigation of the noncovalently binding systems of oxacalixarenes, the selection of the analytical methods, nuclear magnetic resonance and mass spectrometry, was based on the solubility and stability of the compounds and on the environment of interest for their potential applications.

In this thesis, the structural and complexation properties of unsubstituted oxacalixarenes in solid and solution phase are discussed in **publication I**. **Publication II** describes the synthesis of a new carboxyl group-containing oxacalixarene, as well as the properties of its complexation with the cationic aromatic guest, paraquat. The results and discussion section discuss the gas-phase study of carboxyl group-containing oxacalixarene complexes with various amines. Ion-mobility mass spectrometry was used to study the oxacalixarene complexes. **Publication III** investigated the halogen bond as a noncovalent interaction between pairs of donor and acceptor molecules. In all three publications, the stability of noncovalently interacting synthetic molecular systems was investigated by solution NMR titration.

The research findings related to oxacalixarenes have been presented by the author at international conferences in Estonia, Poland, France, and Canada.

## Abbreviations

BARF	tetrakis[3,5-bis(trifluoromethyl)phenyl]borate
CA	calixarene
CB	cucurbituril
CCS	collision cross section
CD	cyclodextrin
CPK	space-filling model
CuI	copper(I)iodide
DFT	density functional theory
DMSO	dimethyl sulfoxide
DOSY	diffusion ordered spectroscopy
DTIM	drift tube ion mobility
eq	equivalent
ES	electrospray
ESI	electrospray ionization
Fe(acac) <sub>3</sub>	iron(III)acetylacetonate
HB	hydrogen bond
HRMS	high resolution mass spectrometry
K <sub>a</sub>	equilibrium association constant
MALDI	matrix-assisted laser desorption/ionization
MEP	molecular electrostatic potential
MS	mass spectrometry
NMR	nuclear magnetic resonance
PF <sub>6</sub> <sup>-</sup>	hexafluorophosphate
RT	room temperature
SCXRD	single crystal X-ray diffraction
S <sub>N</sub> Ar	nucleophilic aromatic substitution
TBA	tetrabutylammonium
TIM	trapped ion mobility
TWIM	traveling wave ion mobility
UV-vis	ultraviolet-visible
vdW	van der Waals
VT	variable temperature
XB	halogen bond

# 1 Literature overview

## 1.1 Supramolecular binding event

Supramolecular chemistry is based on noncovalent interactions. Compared with covalent interactions, noncovalent interactions are weak and reversible. These types of interactions can be used in biological applications where the weak nature of chemical bonds mimics processes occurring at the cellular level. Different processes can be influenced through controlled and directed outside stimuli – such as changing the environmental polarity or the temperature or irradiating with light – to form or reverse noncovalent interactions.

The interactions described in supramolecular chemistry are either solvophobic or electrostatic. In many cases, the line between these interacting forces is not apparent. For clarity, in supramolecular chemistry, bond formation is described by the chemical functionalities of the interacting compounds. The weak interactions that are discussed in chapter 1.2 are hydrogen bonds, halogen bonds, van der Waals (vdW) interactions,  $\pi$ - $\pi$  stacking, and cation- $\pi$  interactions (Table 1). Supramolecular binding due to the hydrophobic effect is discussed. Interaction descriptions with illustrated examples from calixarene chemistry are given in chapter 1.2.

**Table 1.** The type of force and bond energies of common supramolecular interactions<sup>9</sup>

Interaction	Type of force	Energy (kJ mol <sup>-1</sup> )
hydrogen bond	electrostatic dipole-dipole	4–120
halogen bond	coulombic attraction	10–50
van der Waals	dispersion force	<5
	dipole-dipole force	
	dipole-induced dipole force	
aromatic interactions	London dispersion forces	2–80

The stability and longevity of a host-guest complex does not solely depend on the noncovalent interactions between the interacting components. The path to stable complex formation starts from the *complementarity* and *preorganization* of the host molecule.<sup>9</sup> Both of these terms were formulated in 1990 by D. J. Cram,<sup>10</sup> who is known for the first synthesis of three-dimensional host molecules – carcerands. *Complementarity* describes how the binding sites of the host molecule must be spatially accessible and structurally available for the specific interactions to take place. These structural features eliminate strains on the supramolecular system that weaken the complexation strength. Molecular *preorganization* describes the amount of conformational change the host molecule goes through to encapsulate a guest molecule.

The predecessors of the complementarity and preorganization models in supramolecular chemistry came from the field of biochemistry, where the first such model, the lock-and-key model for enzyme kinetics, was formulated by Emil Fischer in 1894.<sup>11</sup> The model suggests that the enzyme binding site is rigid, and only a structurally complementary substrate can interact with the binding pocket. Koshland<sup>12</sup> proposed that the interaction site of enzymes can change spatially according to the signal received from the potential substrate in order to accommodate a substrate that would not fit in the

initial binding site. In the development of synthetic receptors, the induced-fit model proved that complexation processes can be controlled by outside signals, making it possible to control the binding and release of guest molecules, i.e., substrates.

The complexes known as chelates are widely occurring and form from the interaction of a metal ion and an electron donor, also known as a ligand. The ligand forms coordination complexes with a single metal ion depending on the coordination number of the metal. In chelates, the number of coordinate covalent bonds that form between metal and ligand depends on the free electron pairs of the ligand. The stability of the complexes comes from the chelates structural organization into heterocyclic rings.<sup>13</sup> Although chelate complexes are stable by nature, they require an energy contribution so that the conformational changes can fit the targeted metal atoms. One of the ways to lower the energetic barrier of complexation and therefore increase the stability of complexes is to use rigid macrocyclic ligands such as cryptands<sup>14,15</sup> or crown ethers.<sup>16,17</sup>

## 1.2 Noncovalent interactions of calixarenes

### 1.2.1 Hydrogen bonding

Hydrogen bonding can be viewed as one of the most versatile and important noncovalent bonds in chemistry. These bonds form between a covalently bound hydrogen atom and an electronegative atom with a free pair of electrons.<sup>18</sup>

In calixarene chemistry, hydrogen bonds have been used for building supramolecular dimeric<sup>19</sup> and hexameric<sup>20</sup> capsules. The crystal structure of such a hexameric assembly was first published in 1997<sup>21</sup>. Notably, the self-assembly of resorcinarene hexamer was made possible through the formation of 60 hydrogen bonds. In 2011,<sup>22</sup> the modeled structure of the hexameric capsule **1<sub>6</sub>** was published; **1<sub>6</sub>** is composed of six resorcinarene **1** units and contains eight benzene molecules in the capsules' inner space (Figure 1).

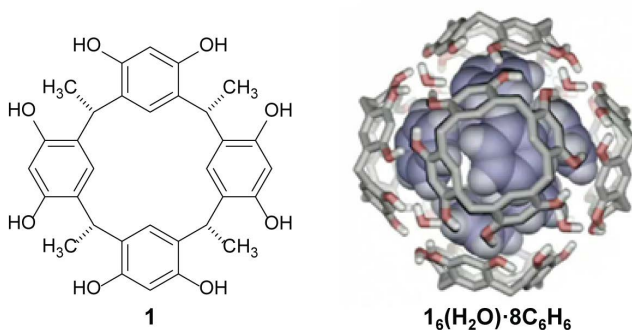


**Figure 1.** The structure of a single C-methylcalix[4]resorcinarene **1** and the supramolecular capsule **1<sub>6</sub>** assembled from six respective resorcinarenes. Fig. 1b model reprinted from Ref. [22] with permission from the Royal Society of Chemistry.

The self-assembly of calixarenes into capsules makes it possible to bind various small guest molecules in a more controlled fashion; these guests can be detained and released by changing the polarity of the environment. In the case of hexameric capsules, it has been shown that encapsulated guest molecules, such as catalysts, can have different selectivities towards reactants, directing the chemo- and regioselectivity of the reaction products.<sup>23</sup>

It has been shown that calixarenes containing carboxylic acid groups in their upper rim can self-organize into dimers in nonpolar organic solvents.<sup>24</sup> NMR measurement of this type of calix[4]arene pinched cone dimer proved that the dimer hydrogen bonds could be broken by diluting the sample or by the controlled addition of polar solvents.

### 1.2.2 Halogen bonding

Halogen bonding (XB) is the intermolecular interaction between a halogen atom with an electrophilic region (R-X) and another molecular unit with a nucleophilic region (Y). In the R-X...Y interaction (Figure 2a), the halogen atom is viewed as a halogen-bond donor and Y is the halogen-bond acceptor. R is covalently bound to the halogen atom.<sup>25,26</sup> An important detail in XB binding is the interaction angle – the XB strength increases when the angle between the acceptor and donor is close to 180°. Therefore, XB interactions can be viewed as directional.<sup>27</sup> The XB bonding strength and interaction geometry are similar to those of hydrogen bonding, with the main variance being in atom sizes; the larger atom radius of a halogen can sterically obstruct or eliminate secondary interactions.<sup>28</sup> Counterintuitive because of the strongly negative charge of halogen atoms, a halogen atom interacts with both negatively and positively charged entities due to a phenomenon called the  $\sigma$ -hole, which was first described in 1992 by Brinck.<sup>29</sup> The term  $\sigma$ -hole was brought into use in 2005 to explicitly define an XB donor's central positive electrostatic potential zone, which originates from the polarization of electronic density of the atom due to bonding.<sup>30</sup> For the formation of R-X...Y bonds, the halogen atom has to be sterically accessible, as the negative charge is located on the sides of the halogen atom, with the most positive area facing outward from the R-X bond. The stability of the halogen bond depends on various parameters, such as the direction and length of the XB bond,<sup>31</sup> and the solvent effect (which varies among neutral and charged XB donors<sup>32</sup> and counterions<sup>33</sup>).

In calixarene chemistry, this type of interaction has been found to stabilize long chains of calixarenes by being a part of a co-operative effect in the solid-state complex formation (Figure 2b).<sup>34</sup> Calixarene channels form from the interactions between ketone-calix[4]arene **2** dimer and the CH<sub>2</sub>Cl<sub>2</sub> solvent molecules. Neighboring macrocycles are stabilized by numerous hydrogen bonds and two halogen bonds.

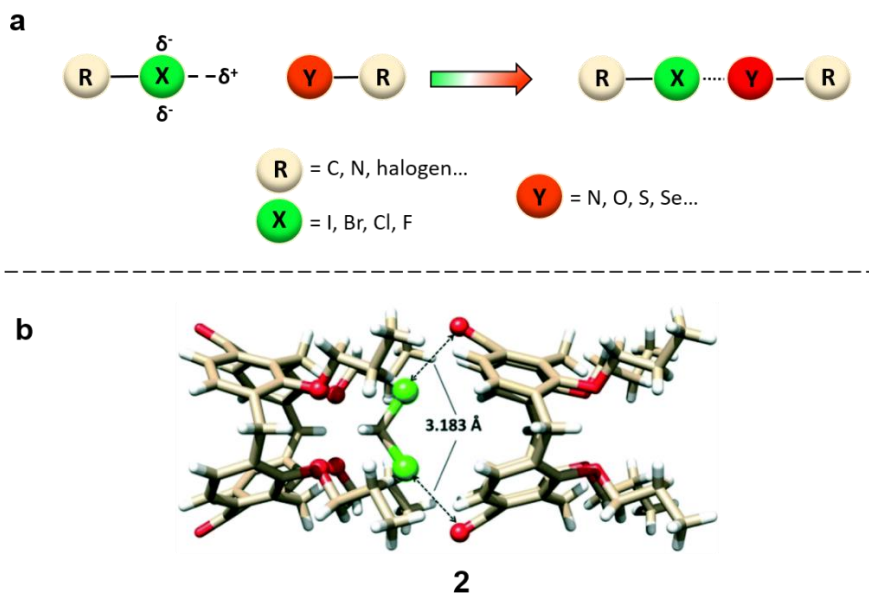


**Figure 2.** a) Schematic overview of  $R-X\cdots Y$  interaction pairs. b) Crystal structure of calixarene **2** dimer with a  $\text{CH}_2\text{Cl}_2$  molecule. Crystal structure color codes: C yellow, Cl green, O red, H white. The XB interaction is indicated by the black dotted line between  $\text{CH}_2\text{Cl}_2$  and the calixarene **2** ketone oxygen ( $\text{Cl}\cdots\text{O}$ ; distance = 3.183 Å). Fig. 2b reprinted from Ref. [34] with permission from the Royal Society of Chemistry.

### 1.2.3 Van der Waals forces

Although hydrogen and halogen bonding can be viewed as dipole–dipole interactions, they are not considered to be van der Waals (vdW) forces. VdW forces include all other dipole–dipole, induced dipole–dipole, and induced dipole–induced dipole interactions that describe intermolecular interactions between uncharged species within close spatial proximity. These forces are difficult to model compared to other noncovalent bonds. VdW forces are quite weak, but they cannot be overlooked because molecules in supramolecular systems form numerous vdW connections. The sum of these vdW connections can determine the characteristics of the system and lead to complex stability that is either higher or lower than what is theoretically predicted.<sup>13</sup> In the solution state, vdW interactions are thought to be weak. However, in systems in the gas phase or solid phase, vdW forces can be the sole contributors to host–guest system stabilization. One remarkable application of such interactions was introduced in 2002 by Atwood et al.,<sup>35</sup> where hexagonal close-packed assemblies of calixarene **3** were shown to encapsulate volatile gas molecules (methane and freon) in the solid phase (Figure 3). These calixarene-containing organic crystals captured gas molecules only through vdW interactions. The thermogravimetric analysis results proved that the complexes were surprisingly thermostable. This was one of the first examples of a thermostable supramolecular system made for gas storage.

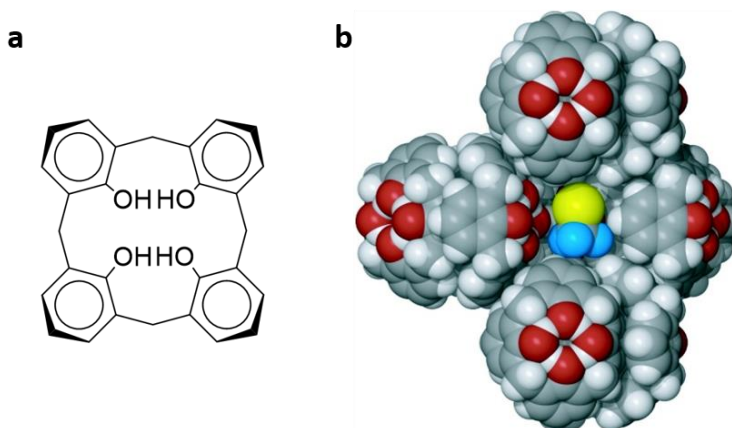


**Figure 3.** a) Structure of calix[4]arene **3** and b) space-filling model of a  $\text{CF}_3\text{Br}$  molecule captured by five units of calixarene **3** with one calixarene **3** unit left out for a clear representation of  $\text{CF}_3\text{Br}$ . Atom colors: carbon (gray), hydrogen (white), oxygen (red), fluorine (blue), and bromine (yellow). Fig. 3b reprinted from Ref. [35] with permission from AAAS.

#### 1.2.4 Aromatic interactions

The most well-known examples of aromatic interactions are  $\pi$ - $\pi$  stacking and cation- $\pi$  interactions. The  $\pi$ - $\pi$  interactions take place between two conjugated systems that can be found in four different types of geometries – parallel stacked, parallel displaced, edge-to-face, or ‘T’-shaped (Figure 4).<sup>36</sup>

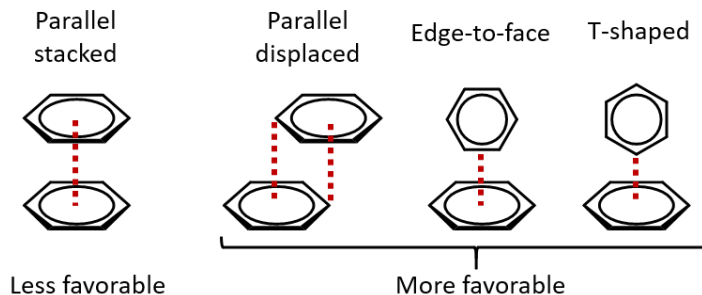


**Figure 4.** Four possible geometries of  $\pi$ - $\pi$  interactions. Adapted by permission from Springer Nature (Ref. [36]) copyright © 2017.

The rather weak, yet important, interactions in large aromatic systems are formed by repulsion and interaction of the electrostatic surfaces of arenes, which are negatively charged in the above and below planes and positively charged around the edges. The best example of a supramolecular complex that uses these interactions are buckybowls, which are polycyclic aromatic hydrocarbons that can bind fullerenes into their bowl-like cavity with  $K_a$  values reaching up to  $8.6 \times 10^3 \text{ M}^{-1}$  in toluene.<sup>37</sup>

Cation- $\pi$  interactions take place between a cation and an electron-rich  $\pi$ -system. In essence, these interactions are electrostatic because the cation interacts with the electric quadrupole of the aromatic ring. The strength of cation- $\pi$  interactions increases with the increase in electron-donating substituents. Cation- $\pi$  interactions have been utilized to encapsulate metal and organic cations by calixarenes.<sup>38</sup>

### 1.2.5 Hydrophobic effect

Although the hydrophobic effect has not been fully defined, the mode of this type of noncovalent interaction has been variously explained. One of the main theories describes how in the presence of nonpolar solutes, the water molecules are more ordered than in pure solvent, making the hydrophobic effect entropy driven.<sup>39</sup> At the same time, the decrease in entropy at the interface is common for both the water–alkane and polar aprotic solvent–alkane systems. In addition to the decreased entropy being caused by the ordered H-bonding of water, the cause for entropy decrease at the surface of the two solvent layers is the immiscibility of the solvents due to large cohesion forces between polar solvent molecules.<sup>40</sup>

It has been shown that polycationic water-soluble oxacalixarene **5** (Figure 5) can form complexes with neutral electron-rich aromatic guest molecules in water at pH 2.<sup>41</sup> Insight into the formation of the complex arose from a calculation study that showed that when water molecules were added to the interacting system, the aromatic guest was sandwiched between the two aromatic rings of oxacalixarene **5**, with -OH groups additionally interacting with solvent molecules through H-bonding. This indicated that the formation of the solvation shell was the driving force that combined nonpolar solutes. Furthermore, the same calculation for the complex *in vacuo* did not converge.

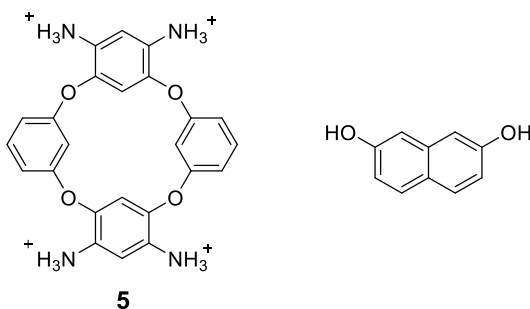


**Figure 5.** The investigated polycationic oxacalixarene **5** with the guest 2,7-dihydroxynaphthalene from Ref. [41].

## 1.3 Supramolecular hosts and receptors

The design of artificial hosts is the cornerstone of all molecular recognition studies. The examples of supramolecular hosts described in chapter 1.3 are from the classes of cucurbiturils (CB[*n*]), cyclodextrins (CD[*n*]), macrocyclic polyethers (crown ether), and calixarenes (CA[*n*]) (Figure 6). These synthetic analogs of biological receptors have received much attention, as they are synthetically accessible, easily modified, and their structures can be controlled at the molecular level. Owing to these properties, supramolecular hosts are used in drug delivery,<sup>42,43</sup> metal<sup>44</sup> and anion extraction,<sup>45</sup> sensing,<sup>46,47</sup> and molecular imaging.<sup>48,49</sup>

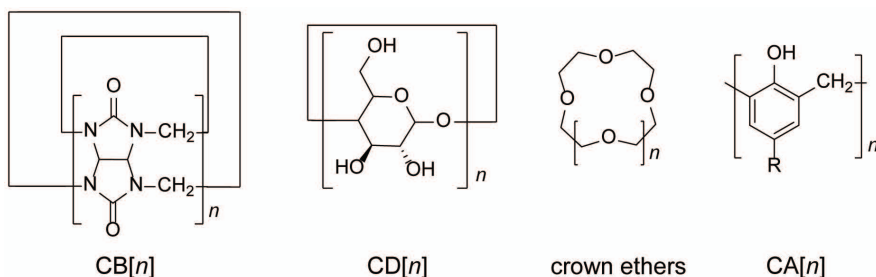


**Figure 6.** Structural representation of CB[n], CD[n], crown ether, and CA[n].

### 1.3.1 Cucurbiturils

Although the first cucurbituril was synthesized in 1905 by Behrend,<sup>50</sup> cyclic urea-based oligomers entered the supramolecular chemistry field in the 1980s and 1990s.<sup>51</sup> CB[n]s are made up of glycoluril units connected by methylene bridges. The family of cucurbiturils has grown rapidly with various CB[n] derivatives, structural homologs, and macrocycles comprised of glycoluril monomer analogs. Chiral and achiral hosts can be found in the subfamilies of cucurbiturils.<sup>52</sup> Cucurbiturils have always been compared with CDs, since the main representatives of cucurbiturils – CB[6], CB[7], and CB[8] – share similar cavity dimensions with  $\alpha$ -CD,  $\beta$ -CD, and  $\gamma$ -CD hosts. One of many comparative studies between these two host groups was conducted in 2005.<sup>53</sup> Surprisingly, CB[7] showed very high affinity towards ferrocene derivatives, forming 1:1 complexes (Figure 7) in water with association constants in the range of  $10^9$ – $10^{12}$  M<sup>-1</sup>. The  $\beta$ -CD analog complex stability was much lower,  $10^3$ – $10^4$  M<sup>-1</sup>, with hydrophobic interactions being the main interactions stabilizing the complexes in water. The stability of CB[7] complexes is connected with the partially negative charge of the macrocycles portal, which increases the affinity towards positively charged guests.

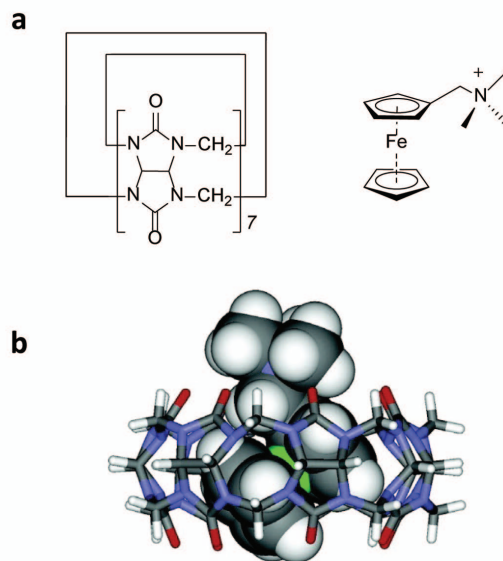


**Figure 7.** a) Structure of CB[7] and (ferrocenylmethyl)trimethylammonium. b) Crystal structure of CB[7] and (ferrocenylmethyl)trimethylammonium inclusion complex. Fig. 7b reprinted with permission from Ref. [53]. Copyright © 2005, American Chemical Society.

### 1.3.2 Cyclodextrins

CDs are cyclic oligosaccharides composed of glucopyranose units connected by  $\alpha$ -(1,4) bonds. The main representatives or “parent” CDs are six-, seven-, and eight-membered  $\alpha$ -CD,  $\beta$ -CD, and  $\gamma$ -CD, of which the most studied host is the seven-membered homolog.<sup>54</sup> These three CDs form during the enzymatic treatment of starch, and the ratio of CD formation can be controlled by employing different enzymes. Their solubility in water and lack of toxicity has led to the widespread industrial use of CDs.<sup>55</sup> For example, in the food, pharmaceuticals, and cosmetics industries, CD-containing products are applied for the stabilization, solubilization, and prolonged release of various essential compounds.<sup>56</sup>

CDs are firmly established in industrial use, but there is still much to discover about their many roles in various new functions. For example, in 2010, Stoddart et al.<sup>57</sup> showed that it is possible to prepare metal-organic frameworks (MOFs) from CDs by combining them with potassium ions. Using CDs to build MOFs has become increasingly common in recent years because CDs lack the main drawback shared by other natural compounds, that is, the inability to form highly porous frameworks due to the asymmetry of building units.<sup>58</sup>

### 1.3.3 Crown ethers

In the 1960s, Charles Pedersen studied new compounds that could form complexes with metal cations, which led to the discovery of crown ethers and their complexes with metals.<sup>16</sup> Structurally, crown ethers are made up of ethyleneoxy ( $-\text{CH}_2\text{CH}_2\text{O}-$ )<sub>n</sub> units and are described as macrocycles when the number of units is at least four (Figure 8).<sup>59</sup> The field of molecular recognition was enriched in the 1970s when three-dimensional multidentate ligands called cryptands were synthesized. In 1987, the Nobel Prize for Chemistry was collectively awarded to Lehn,<sup>60</sup> Cram,<sup>61</sup> and Pedersen<sup>62</sup> for their work on the synthesis and application of macrocyclic ligands. The crown ethers are used in complexes with metal cations as phase-catalysts; a well-known example of these catalysts is the six oxygen-containing 18-crown-6, which binds small metal ions such as potassium.<sup>63</sup>

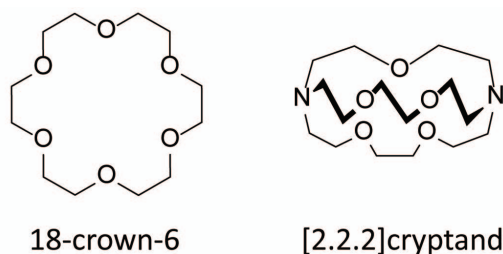


**Figure 8.** Structures of 18-crown-6 and [2.2.2]cryptand.

### 1.3.4 Calixarenes

CAs form a group of aromatic host molecules that have a long history in synthetic chemistry. The parent CA structure consists of four *p*-*tert*-butyl phenols connected by methylene bridges into a cyclic tetramer. Controlling the macrocycles' geometry can be achieved by modifying the upper rim, the lower rim, or the methylene bridge.<sup>64</sup> Macrocyces form during a base-catalyzed condensation reaction when mixing *p*-functionalized phenol and formaldehyde<sup>65</sup> and can be found in four conformations – cone, partial cone, 1,3-alternate, and 1,2-alternate (Figure 9).

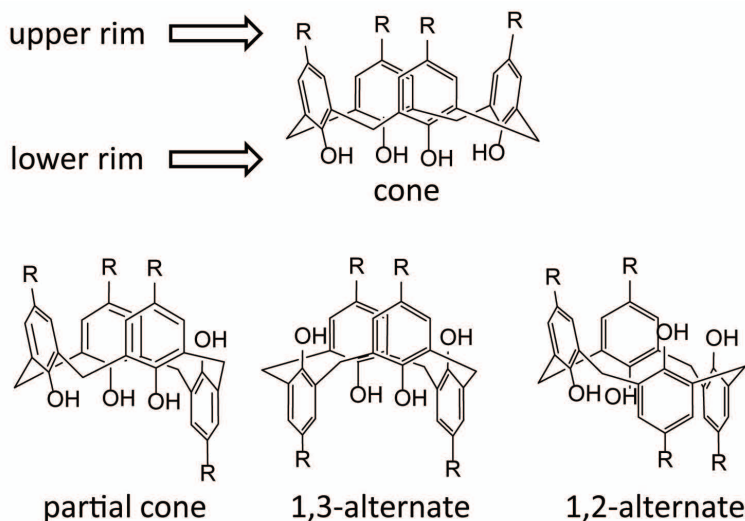


**Figure 9.** The four conformations of calix[4]arene.

The CAs main size homologs vary from 4- to 8-membered, with the 4-membered CA products being the most researched owing to their synthetic approachability. Nevertheless, large-sized CA homologs with progressively larger ring sizes have been observed as well, with the largest documented calixarene being a 90-membered calixarene.<sup>66</sup>

### 1.3.5 Heteracalixaromatics

When the aromatic units of calixarenes are connected by heteroatoms instead of by methylene bridges, the formed macrocycles are called heteracalixarenes (Figure 10).<sup>67,68</sup>

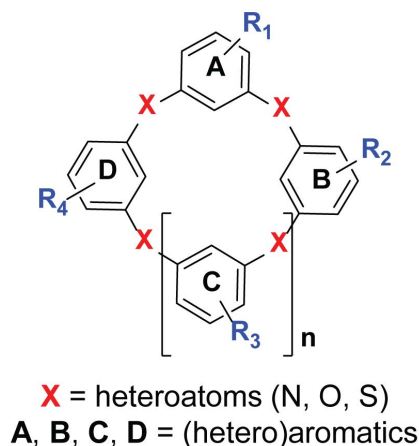


**Figure 10.** Illustrative representation of the heteracalixaromatic core with possible derivatization sites.

The type of bridging atoms can considerably change the internal diameter and the electronic and steric properties of the host molecules, making heteracalixarenes distinct from traditional calixarenes. Depending on the heteroatom used as the linkage, heteracalixarenes can be allocated into three large subclasses: aza-, thia-, and

oxacalixarenes.<sup>68</sup> In addition to N-, O-, and S-bridged macrocycles, selenium-bridged heteracalixarenes have also been synthesized.<sup>69</sup>

All the heteracalixaromatics (N, O, S) share a common geometrical shape in the solid state – either a 1,3-alternate or a twisted 1,3-alternate conformation.<sup>70</sup> 1,3-Alternate is the main conformation of aza- and oxacalix[4]arenes.<sup>68</sup> In the 1,3-alternate configuration, the macrocycle nitrogen and oxygen bridges adopt an  $sp^2$  configuration. The  $sp^2$  configuration makes the heteracalix[4]aromatics more rigid, as they are divided into two planar dimeric segments. In addition to the electronic properties, one other influence on the heteracalixarene synthetic availability and molecular recognition is the electronegativity of the bridging atoms.

Azacalixarenes have been found to specifically interact with various metals, e.g., methylazacalix[4]pyridine with  $Zn^{2+}$  ion.<sup>71</sup> The same azacalixarene derivative can recognize and bind aromatic and aliphatic diols.<sup>72</sup>

O-substituted thiacalixarene has been shown to selectively bind transition metals over  $Na^+$  and  $K^+$  ions.<sup>73</sup> A competition study performed with NMR showed that when  $Ag^+$  was added to a thiacalixarene- $Na^+$  complex, the chemical shifts of the complex changed to signals corresponding to a thiacalixarene- $Ag^+$  complex.

Water-soluble sulfonato(thia)calixarenes have been shown to bind pyridine and pyridine derivatives in both acidic and neutral conditions, with  $K_a$  values in the range of  $10^2$ – $10^3$   $M^{-1}$ .<sup>74</sup> Sulfonato(thia)calixarenes have been added to water purification resins due to their ability to form inclusion complexes with various halogenated compounds.<sup>75</sup>

Various anion-binding ureido-substituted calixarenes in 1,3-alternate conformation have been developed,<sup>76</sup> among them thiacalixarenes.<sup>77</sup> In 2016, Yamato and co-workers showed that the 1,3-alternate thiacalixarene **6** bearing urea moieties in the *p*-position of the phenyl groups can bind halogen and acetate ions and dihydrogen phosphate.<sup>78</sup> The most stable complexes were formed between thiacalixarene and  $F^-$  in chloroform–acetonitrile 10:1 mixture, where the anion was clasped between the four NH groups of thiacalixarene through hydrogen bonding. This was evidenced by  $^1H$  NMR titration data that showed the NH protons shifting downfield while the methylene protons near the NH groups were shifting slightly upfield. The proposed structure of thiacalixarene binding to a fluoride atom is depicted in Figure 11.

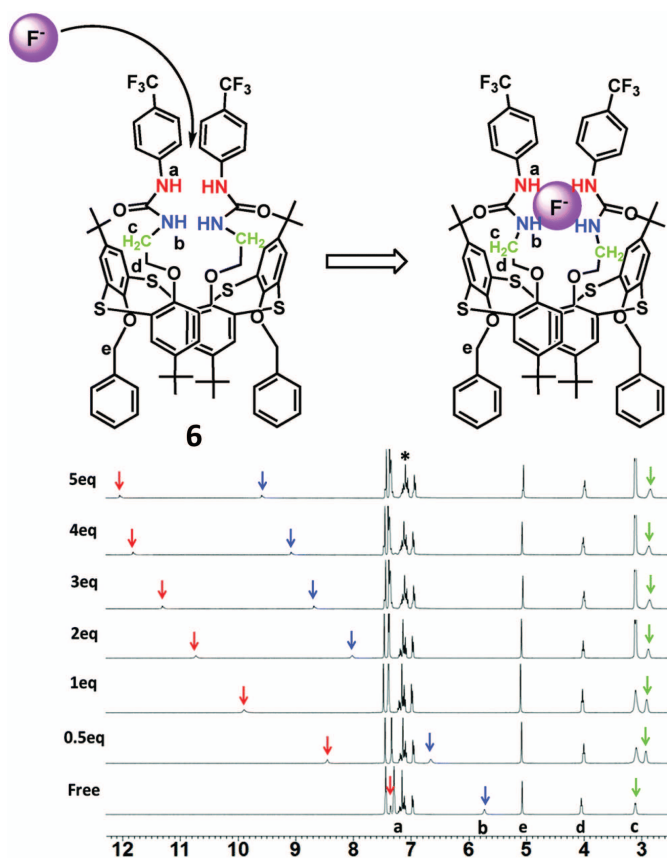


**Figure 11.** The suggested structure of thiacalixarene **6**-F<sup>-</sup> coordination complex investigated by Yamato and co-workers.<sup>78</sup> The flexibility of the side arms was proposed based on NH (marked with red and blue) and CH<sub>2</sub> (marked with green) protons. <sup>1</sup>H NMR titration data (below the structure) obtained in CDCl<sub>3</sub>-CD<sub>3</sub>CN (10:1, v/v) solution, showing the chemical shifts of thiacalixarene **6** host throughout the titration. Fig. 11 reprinted from Ref. [78] with permission from the Royal Society of Chemistry.

Various heterocalixarenes have been proposed for the design and discovery of potential drug candidates. Among them are thiacalixarene tetracarboxylic acid derivatives that can bind dopamine hydrochloride<sup>79</sup> and azacalix[2]arene[2]pyrimidines that exhibit anticancer activity.<sup>80</sup>

### 1.3.6 Oxacalixarenes

Oxacalixarenes combine the characteristic properties of calixarenes and crown ethers. Similar to crown ethers, the free electron pairs on the oxygens have been found to bind metals, as they are possible sites for electrostatic and charge-transfer interactions. The ether bonds keep the macrocycle rigid and fixed in a 1,3-alternate conformation, which leads to close packing of the macrocycles, making it possible to form dimeric compounds with a shared binding pocket. The molecular recognition of neutral aromatic compounds can be achieved through  $\pi$ - $\pi$  interactions with the oxacalixarene aromatic units (Figure 12).

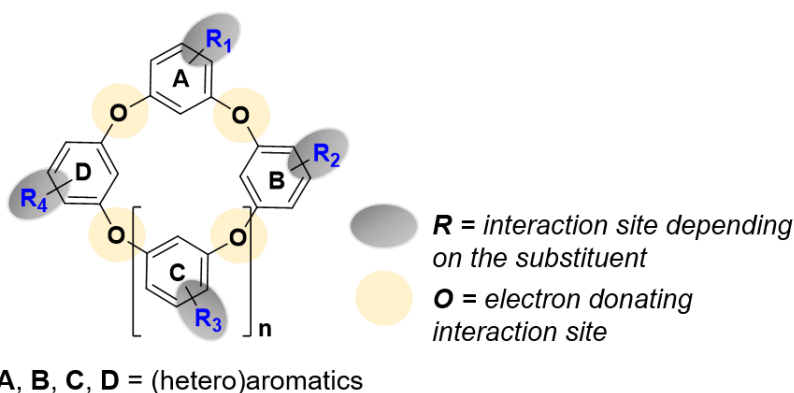


**Figure 12.** Oxacalixarene core and possible interaction sites.

### 1.3.7 Conformations of oxacalix[*n*]arenes

Various groups have shown that oxacalix[4]arenes, regardless of substitution, form a twisted 1,3-alternate conformation,<sup>81–83</sup> which means that neighboring aromatic rings are oriented in opposite directions, away from each other. The aromatic rings facing each other are located almost in parallel, which makes the macrocycles' entire cavity highly symmetrical. The size of the binding cavity is approximately 4.5 Å – too small for traditional guest encapsulation.<sup>84</sup> Nevertheless, the rigid conformation does not interfere with other host–guest binding types and can be used as a starting point for receptor design.

The small dimensions of the annulus have led to the development of larger sized isomers that vary from 5–8-membered to 10–14-membered macrocycles.<sup>82,85–89</sup> SCXRD studies of these oxacalix[*n*]arenes found a continued trend of a twisted conformation. Unfortunately, this type of twisted conformation indicates rapid conformational turnover, making these macrocycles undesirable as host compounds. The macrocycles' rapid structural changes in solution have been observed via variable temperature NMR (VT-NMR) by our group and others.<sup>81,90</sup>

To increase the size of the core and circumvent the quick structural turnover, the triptycene-<sup>91</sup> and naphthalene-derived<sup>84</sup> oxacalixarenes (Figure 13) were synthesized. Naphthalene **8**- and 1,8-naphthyridine **9**-containing oxacalixarenes could moderately bind neutral guests such as phenol, benzoic acid, and *o*-salicylic acid mainly through hydrogen bonding, as no interactions were observed with toluene.

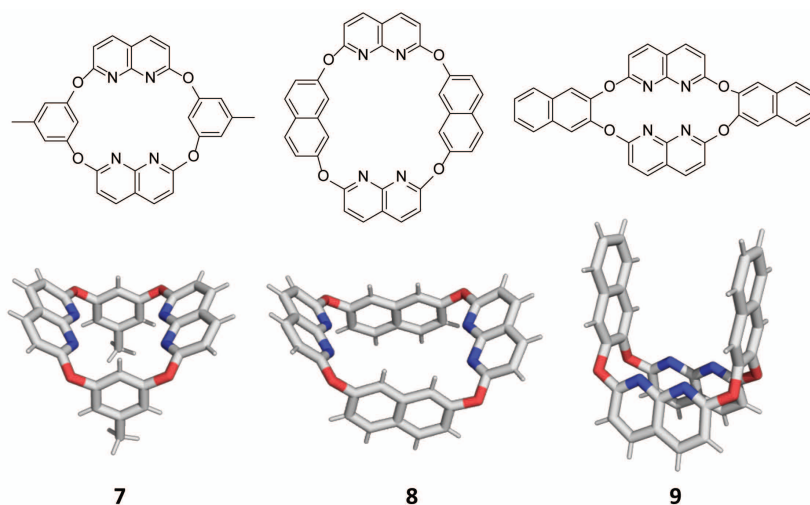


**Figure 13.** a) Planar and b) crystal structures of naphthalene–naphthyridine mixed oxacalixarenes **7**, **8**, and **9** investigated by Katz, Geller and Foster in Ref. [84].

Both the host naphthalene and the guest aromatic showed an upfield shift in their NMR spectra (Figure 14), indicating anisotropic shielding of the aromatic rings and suggesting the occurrence of  $\pi$ – $\pi$  interactions between the two components. In addition to the upfield shifts, the 1,8-naphthyridine part showed a downfield shift that was intrinsic to hydrogen bonding. In comparison, the benzene-containing oxacalixarene **7** did not form any host–guest complexes with the neutral guests.

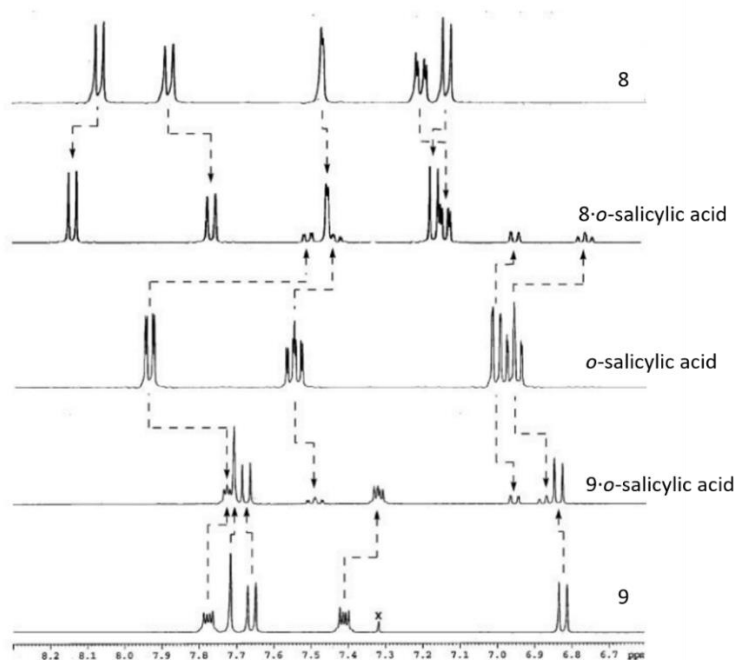


**Figure 14.**  $^1\text{H}$  NMR of the aromatic region (8.3–6.6 ppm). Fig. 15 reprinted from Ref. [84] with permission from the Royal Society of Chemistry.

### 1.3.8 Molecular recognition of oxalix[4]arenes

As noted in previous examples, oxalixarenes can bind neutral guests in protic<sup>41</sup> and aprotic<sup>84</sup> solvents, but those preliminary studies are only examples of several investigations that have explored the development of real-life applications.

One of the first studies published focusing on the oxalixarene complexation properties investigated different nitro-substituted oxalixarenes that were shown to interact with electrochemically active ferrocene/ferrocenium<sup>+</sup> **11** and cobaltocene/cobaltocenium<sup>+</sup> redox couples.<sup>92</sup> These interactions were confirmed using cyclic voltametric experiments that were measured for calixarene **10** and **11/11**<sup>+</sup> pairs in dichloromethane (Figure 15). The  $K_a$  value obtained for the calixarene **10** redox pair in the case of charged compound **11**<sup>+</sup> was  $K_{ox} = 7400 \text{ M}^{-1}$  and that of the neutral compound **11** was  $K_{red} = 87 \text{ M}^{-1}$ . These results suggested that the two orders of magnitude difference in binding resulted from the cation- $\pi$  interactions between the **11**<sup>+</sup> and hydroxyl-substituted aromatic units.

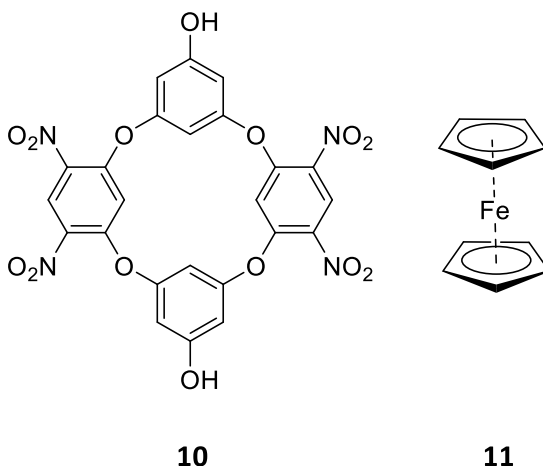


**Figure 15.** Nitro-substituted calixarene **10** and ferrocene **11** investigated in Ref. [92].

One possible field of application for oxalixarenes is in chemosensing. Examples of molecular tweezers used for chemosensing are the tetraoxalix[2]arene[2]triazine derivatives that form consistently stable complexes specifically with  $\text{Cu}^{2+}$  ions through the chelation effect, regardless of the structural differences and bulkiness of the side "arms".<sup>93</sup> The UV-vis and fluorescence studies of diquinolated oxalixarene **12** (Figure 16a) titrated with various metals showed that oxalixarene **12** selectively binds  $\text{Cu}^{2+}$  in acetonitrile.<sup>94</sup> The binding event was confirmed with UV-vis via the observed redshift of the host when the copper ions were added. Furthermore, the complex formation quenched the host's fluorescence signal, demonstrating that oxalixarene **12** is a sensitive  $\text{Cu}^{2+}$  sensor. The same research group found that dinaphthoylated oxalixarene **13** (Figure 16b) selectively binds  $\text{Ce}^{3+}$  ions in acetonitrile at a 1:1 stoichiometry.<sup>95</sup> Unlike other rare earth cations, the specific binding was only found for the oxalixarene **13**· $\text{Ce}^{3+}$  complex.

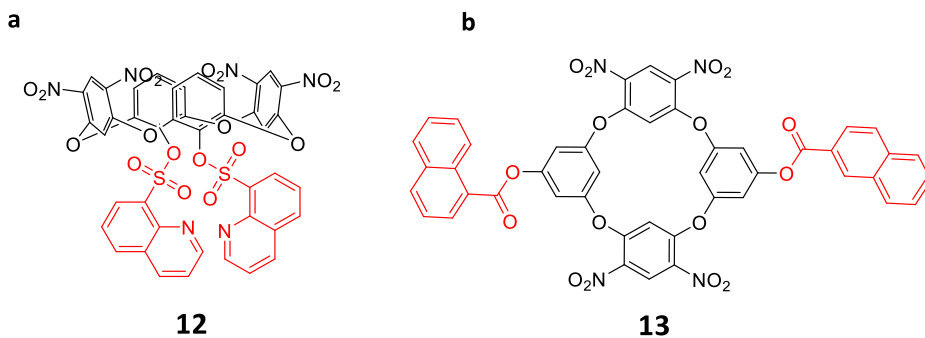


**Figure 16.** Structures of fluorescent oxacalixarene **12** and **13** hosts. Interaction sites of fluorescent units are marked with red. Oxacalixarene **12** was investigated in Ref. [94] and oxacalixarene **13** in Ref. [95].

The use of crown ethers in drug design has made oxacalixarenes desirable candidates for this application. One of the first studies of oxacalixarenes as drug candidates was conducted in 2019 by the group of Xiaoxing Yin,<sup>96</sup> who carried out the first pharmacological study of the novel oxacalix[2]arene[2]pyrimidine derivatives as an anticancer treatment. Fifteen derivatives were tested in cell inhibition and cell apoptosis assays and were compared against the anticancer drug fluorouracil **14** as the positive control. From the library of oxacalix[2]arene[2]pyrimidine derivatives, compound **15a**, bearing two 2-aminoethanol linkers, had equivalent anticancer activity as **14** (Figure 17). It was hypothesized that the tumor cells were inhibited with a higher efficacy due to the suitable hydrophilic–lipophilic balance of compound **15a**. Originally, the most hydrophilic oxacalixarene derivative, compound **15b**, was expected to be the best drug candidate, yet it exhibited low inhibitory activity. Based on these results, it was suggested that cell apoptosis was induced through the -NH groups of the macrocycle.

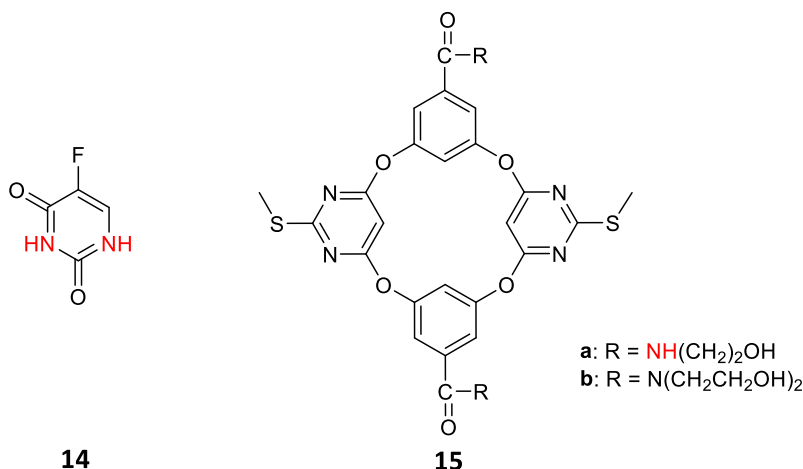


**Figure 17.** Structures of reference compound **14** and examples of oxacalixarene drug candidates **15a** and **15b** examined in Ref. [96]. The predicted interaction sites are marked with red.

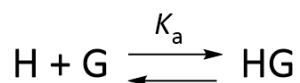
These results are encouraging for the use of oxacalixarenes in real-life applications. Only recently have oxacalixarene molecular recognition studies received more attention, and these hosts have much potential in the field of supramolecular chemistry.

## 1.4 Methods for determining the strength of noncovalent interactions

In supramolecular chemistry, the quantitative methods used for studying the strength of noncovalent interactions all feature the same principle – tying the concentration of the complex to the monitored physical change of a spectroscopic or calorimetric feature. That change can be either the chemical shift of one of the components in NMR, shifted absorption band wavelengths, UV signal quenching, or a change of temperature in isothermal titration calorimetry. The qualitative and structural data of the binding site interactions in solution can be obtained with 1D and 2D NMR. Studying supramolecular complexes in the gas phase has been made possible by the development of soft ionization techniques – electrospray ionization (ESI), developed in 1983,<sup>97</sup> and matrix-assisted laser desorption ionization (MALDI), first mentioned in 1985 by Hillenkamp and colleagues,<sup>98</sup> with the diversity of the method further demonstrated by Tanaka in 1988.<sup>99</sup> In the solid state, the most informative method is SCXRD, which works well for the structural determination of synthetic hosts and receptors and for strongly binding host–guest complexes. The bottleneck in the analysis of such complexes is the single crystal formation and the crystallization forces that influence the complex geometry.

### 1.4.1 Complexation equilibria

Formation of the host–guest complex can be described by a pseudo first-order reaction equation (Equation 1), where H is the host, G is the guest and HG is the complex.<sup>100</sup>



**Equation 1.** *Supramolecular equilibrium in the case of simple 1:1 binding.*

The equilibrium of this reaction can be assessed with a binding constant, also referred to as the association constant –  $K_a$ , which indicates the amount of free host and guest in comparison with the amount of the complex (Equation 2). [H], [G], and [HG] are the molar concentrations of the interacting components.

$$K_a = \frac{[\text{HG}]}{[\text{H}][\text{G}]}$$

**Equation 2.** *The supramolecular equilibrium constant.*

To calculate the  $K_a$  value, [H], [G], and [HG] at different stages of the experiment need to be determined. Traditionally, the “host” describes the macrocycle or the largest and most intricate component in the supramolecular system. During the titration experiment, the host is viewed as the component whose concentration is kept constant throughout the experiment, and the “guest” is the component whose concentration is changed gradually. To create the titration curve (also known as the binding isotherm), the added guest concentration is plotted on the x-axis, and the observed shift in spectroscopic property is plotted on the y-axis. An example of a 1:1 <sup>1</sup>H NMR titration binding isotherm

is shown in Figure 18,<sup>101</sup> where a *p*-carboxylatocalix[4]arene **16** is titrated with paraquat, and the protons of the alkyl chain (Figure 18a) and aryl rings (Figure 18b) are monitored.

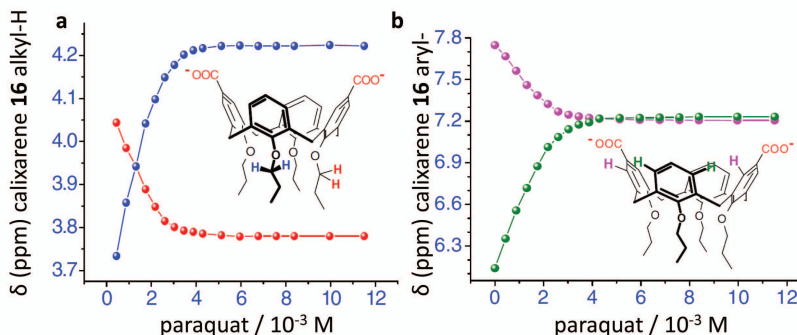


**Figure 18.** <sup>1</sup>H NMR titration of the binding isotherms of a 1:1 host–guest complex between calixarene **16** and paraquat. The chemical shifts of the host protons a) alkyl-H (marked with blue and red) and b) aryl-H (marked with green and pink) are plotted on the y-axis. The paraquat concentration is plotted on the x-axis. Titration graphs are reprinted from Ref. [101], with permission from Elsevier. Copyright © 2008

#### 1.4.2 NMR method

Structural and dynamic information of reversible and ever-changing supramolecular systems can be extracted from a single <sup>1</sup>H NMR titration experiment. The chemical shift resonance ( $\delta$ ) is different for the individual H and G compounds. This is in contrast to the noncovalently bound HG complex in which H and G interact with each other. Therefore, influencing the chemical environment of the atoms in the strong magnetic field translates to the change in the resonance ( $\Delta\delta$ ) of an isolated component.

#### 1.4.3 Chemical exchange

For mixtures of various molecular species that interact with one another, slow, intermediate, and fast exchange of the new formed entity can be differentiated at the NMR timescale. Two methods can be applied to determine the  $K_a$  value depending on the exchange rate.<sup>63</sup> In the case of fast exchange, where the  $\delta$  of free host and the  $\delta$  of the host in complex cannot be differentiated because  $\Delta\delta$  is the weighted average of the two,  $K_a$  can be calculated from the chemical shift data obtained from the NMR titration experiment. By knowing the chemical shifts of free host and guest, it is possible to monitor the host–guest complexation resonance  $\delta_{HG}$  and link it back to the relative molar concentrations of free and bound host. In the case of slow exchange, the peaks of free and bound host are not averaged and can be observed separately, making the calculation of  $K_a$  possible based on the peak area integration that is directly related to the mass balance (Equation 2). The results from this method are harder to interpret because the slow exchange covers a timeframe that is typically a mixture of slow and intermediate exchange; this complicates the integration of peak areas and data analysis.

#### 1.4.4 NMR and molecular recognition

The  $K_a$  value is not the only information gathered from an NMR titration experiment. Structural information of the host–guest complex can be analyzed as well by observing the host and guest signals throughout the experiment. In the NMR spectrum, the atoms in the interaction site experience the largest  $\Delta\delta$  changes. Depending on the manner of the upfield or downfield shifts, it is possible to distinguish whether the guest is

encapsulated by the host (*endo* complexation) or is coordinated outside of the host's macrocyclic cavity (*exo* complexation). For example, the *endo* complexes between various trisulfonated calixarenes and trimethyllysine were proven based on  $^1\text{H}$  NMR titration data.<sup>102</sup>

Another NMR method for determining the  $K_a$  value of supramolecular complexes is diffusion ordered spectroscopy (DOSY). This method is used to analyze mixtures (e.g., host and guest samples), where components differ in size and shape and therefore have separate diffusion coefficients. DOSY has been used to analyze supramolecular capsules, more specifically, capsules that are assembled through hydrogen bonding.<sup>103</sup> This method has advantages over traditional chemical shift-based NMR titration, as it can prevent errors such as misinterpretation of data due to self-aggregation, proton transfer, or acid–base equilibrium. The disadvantages of the method lie in the prerequisites of the supramolecular system; the system needs to undergo fast exchange, and the molecular weights of the interacting components must differ by approximately tenfold.<sup>104</sup>

#### 1.4.5 Mass spectrometry and electrospray ionization

The main principle in supramolecular gas phase analysis is to successfully generate a charged ion of the noncovalently preassembled complex without fragmenting it during ionization. Additionally, when fragmentation occurs, it is important to differentiate fragmentation units arising from covalent and noncovalent interactions. The ESI method is slightly favored over other soft ionization techniques when considering the main prerequisites for the supramolecular MS analysis.

ESI-MS can be used to study host–guest complexes and self-associated macrocyclic capsules, and it can confirm the presence of complexes in complicated mixtures.<sup>105</sup> It must be emphasized that the stability of a supramolecular complex differs depending on whether it is in the solution or gas phase. Hydrogen bonded complexes are more stable in the gas phase, as there is no competition between the interacting components and the solvent. However, the lack of solvent can be a drawback if the hydrophobic effect is the main interaction keeping the complex together in solution.<sup>106</sup>

#### 1.4.6 Ion-mobility mass-spectrometry

Ion-mobility mass-spectrometry (IM-MS) adds another element to the standard MS analysis by providing accurate data for the ion dimension.<sup>107</sup> The time it takes for the ion to pass through a carrier gas in the mass analyzer can indicate the ion size. This means that the method is quite sensitive, as it is possible to differentiate between structural isomers with the same mass-to-charge ( $m/z$ ) ratio. The traditional mass analyzer can be coupled with one of the three ion mobility spectrometers: drift tube IM (DTIM), traveling wave IM (TWIM), or trapped IM (TIM). A further explanation of the instrumental setup is based on DTIM, as it was the mass spectrometer used in the current work.

In DTIM, the sample moves through a gas-filled tube that is exposed to a homogeneous electric field (Figure 19). The separation of analytes is based on the collisions with carrier gas molecules. For example, spherical ions move through the drift tube at higher velocity, whereas their nonspherical counterparts with identical  $m/z$  values migrate slower because there are more collisions with the gas molecules.

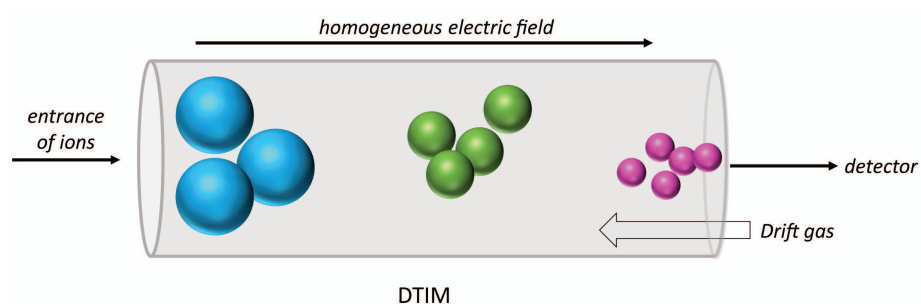


**Figure 19.** Scheme of drift tube ion mobility unit. Ions are separated according to their dimension. Ions with the smallest dimension (pink) elute first.

The final registered parameter of the experiment is the drift time ( $t_d$ ), which is one of the necessary base parameters in calculating the collision cross-section (CCS).<sup>108</sup> An initial assessment of the complex geometry can be made based on the drift time, as was shown by Nau and colleagues with different CB-azoalkane *endo* complexes, where the drift times of the free CB host and CB complex were identical.<sup>109</sup> The ions' structural information can be resolved by comparing the CCS values of the IM-MS experiment to the CCS values calculated based on the structural data of a previously optimized geometry.<sup>110</sup>

The IM-MS method has mainly been employed in the analysis of biomolecules, but it is becoming more common for analyzing synthetic receptors.<sup>107</sup> Regarding host–guest chemistry, there have only been a few examples that have used this technique for supramolecular host and complex structure elucidation. These examples include the structure analysis of chiral hemicucurbituril,<sup>111</sup> cucurbituril,<sup>112</sup> and cyclodextrin<sup>113</sup> inclusion complexes. In calixarene chemistry, no oxacalixarene complexes have been investigated so far, although there is one example from calixarene chemistry with pyridine[4]arenes,<sup>114</sup> which indicates a promising outlook for the versatility of using the IM-MS technique to study oxacalixarene host–guest chemistry. When analyzing the complex, the method was sensitive enough to confirm a multicomponent ternary complex between pyridine[4]arene,  $\text{PF}_6^-$  anion, and  $\text{CHCl}_3$  in the gas phase.<sup>114</sup> The CCS value measured for the pyridine[4]arene dimer· $2\text{PF}_6^-$ (exo)· $\text{CHCl}_3$ (endo) complex (2.2 nm) aligned with the CCS values calculated by SCXRD (1.9 nm) and DOSY-NMR (2.0 nm).

## 2 Motivation and aims of this work

In supramolecular chemistry, calixarenes have been described as host compounds with “(almost) unlimited possibilities”<sup>115</sup>. Calixarenes are known to arrange spatially into conformations that favor guest encapsulation. The structure and multiple guest-binding sites have led to the extensive synthesis and design of calixarene derivatives, as the structural variability can be easily accessed synthetically.

This PhD thesis aimed to develop new oxygen-bridged calixarenes with new host–guest binding properties. The main role of the calixarene cavity has been similar to a template, acting to pre-organize substituents, while the attached sidechains have been used as the main interaction site. As yet, molecular recognition studies of oxacalixarenes have focused on oxacalixarenes comprising aromatic groups bearing substituents. However, in this work, one focus was on the unsubstituted macrocycles and the binding abilities of the oxacalixarene core. To investigate the possibilities of unsubstituted oxacalixarene, electron-rich unsubstituted oxacalixarenes were analyzed with various electron-deficient guests in nonpolar solvents. The limited solubility of unsubstituted oxacalixarenes ( $n = 4, 8$ ) in protic solvents provided the incentive to modify the parent structure (e.g., with carboxyl groups), thereby expanding the guest library. Next, host–guest studies with oxacalixarene containing a carboxylate group were undertaken. Finally, the structural features that govern halogen bonding strength in solution were investigated; this information could potentially be utilized in oxacalixarene chemistry. The complexation experiments conducted in this work have great value because little is known about oxacalixarene host–guest properties. A better understanding of oxacalixarene structural behavior in different media can lead to new potential applications of these hosts in drug delivery or as chemical sensors for recognizing toxic compounds.

### The specific aims of this study were:

- To synthesize unsubstituted homologs of oxacalix[ $n$ ]arenes ( $n = 4, 8$ );
- To synthesize the water-soluble derivative of oxacalixarene – monocarboxylic oxacalix[4]arene;
- To investigate the properties of the obtained oxacalixarenes as supramolecular hosts; and
- To determine the structural characteristics that govern the formation of highly directional interactions in halogen bonds.

### 3 Results and discussion

Chapter 3 presents the results of three publications. The focus of chapter 3.1 is on the synthesis and host–guest complexation studies of oxacalixarene macrocycles. In **Publication I**, the synthesis and structural analysis from the solid- and solution-phase studies of the unsubstituted 4- and 8-membered oxacalixarenes is discussed. The topic of oxacalixarenes continues in chapter 3.2 with the synthesis and structural studies of the new monocarboxylic oxacalix[4]arene and an exploration of the binding properties of the host in solution, applying NMR, and in the gas phase, applying IM-MS (**Publication II** and the results from ongoing investigation).

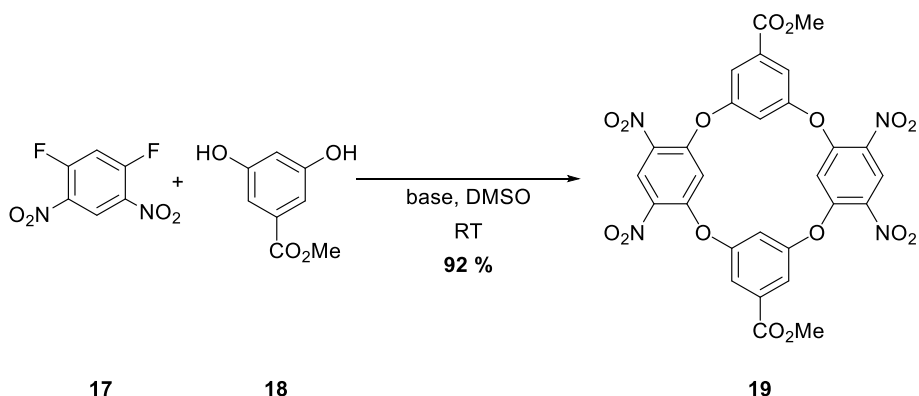
In chapter 3.3, the NMR titration study of the binding of iodo-triazole based XB donors to selected XB acceptors is presented. Based on these results, the outlook of applying solution NMR titration as a preliminary screening tool for investigating various XB donor–acceptor pairs is examined (**Publication III**).

#### 3.1 Unsubstituted oxacalix[*n*]arenes (Publication I)

##### 3.1.1 Introduction to oxacalix[*n*]arene synthesis

The synthesis of oxacalixarenes has been approached using two main synthetic pathways – the metal catalyst-mediated fragment coupling methods, such as Ullmann coupling,<sup>86</sup> and one-pot nucleophilic aromatic substitution reactions.<sup>116</sup> New oxacalixarenes can be formed through post-macrocyclization modifications, e.g., functional group modifications<sup>117</sup> or re-macrocyclization reactions.<sup>118</sup>

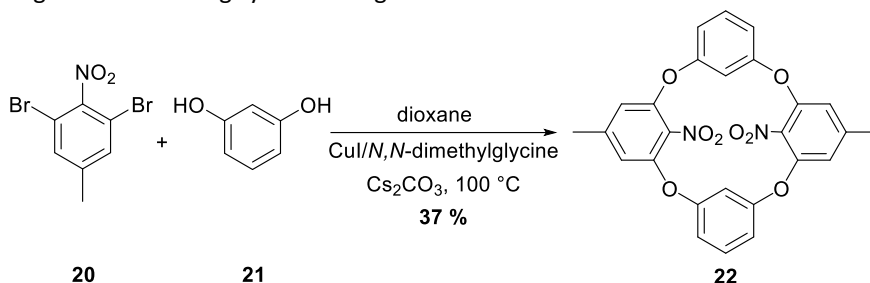
The first cyclic aryl ethers, which can now be identified as oxacalixarenes, were synthesized in 1966 by Sommer and Staab, but the low yields and low solubility of the products hindered the purification and full characterization of these compounds.<sup>119</sup> Therefore, these cyclic aryl ether compounds did not spark curiosity in the scientific community. It was not until 2005, when Katz and co-workers synthesized nitro-substituted oxacalixarenes (such as compound **19**) with a one-pot reaction at very high yields, that interest returned to this overlooked potential subclass of calixarenes.<sup>90</sup> The cyclization reaction between compound **17** and compound **18** yielded 92 % oxacalixarene **19** (Scheme 1).



**Scheme 1.** One-pot  $S_NAr$  preparation of oxacalixarene **19**.

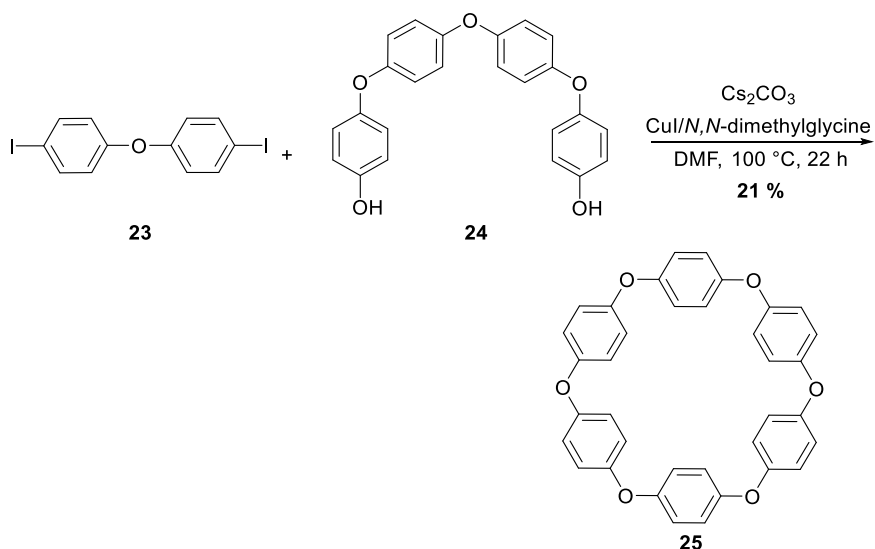
$S_NAr$  reactions were used by the Wang group to synthesize parent oxa- and azacalixarenes.<sup>70</sup> Notably,  $S_NAr$  reactions were used first to assemble macrocycles from heteroaromatic rings such as pyridines and pyrazines.<sup>120</sup> Later, the  $S_NAr$  reactions were successfully deployed to synthesize symmetric oxacalixarene macrocycles from asymmetric starting compounds.<sup>121</sup>

An alternative way to synthesize unfunctionalized oxacalixarenes is Ullmann coupling, which is a well-known reaction used for creating aryl ether bonds.<sup>122</sup> In 2006, the synthesis of functionalized oxacalixarenes and their differently sized homologs via Ullmann coupling was reported.<sup>123</sup> The substrates for the model reaction (Scheme 2) were compound **20** and compound **21**, yielding oxacalix[4]arene **22**. The reaction scope showed the importance of the *N,N*-dimethylglycine ligand as a part of the copper catalytic system for the synthesis of oxacalixarene **22**. However, in the case of larger-sized isomers, the presence of the dimethylglycine ligand in the formation of macrocycles was found to be unnecessary. In that study, it was emphasized that “large fully aromatic crown ethers are rare”<sup>123</sup>, where all oxygens are linked by aromatic groups, making them interesting synthetic targets.



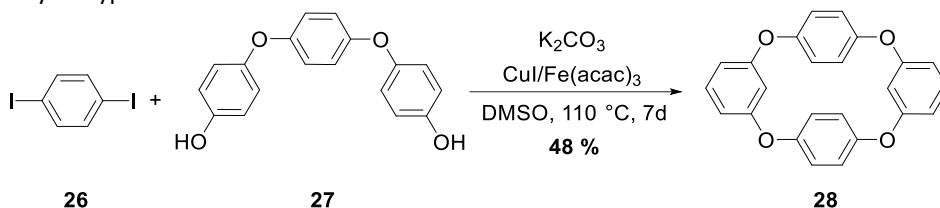
**Scheme 2.** Ullmann coupling reaction conditions that resulted in a 37 % yield of oxacalixarene **22**.

In the same year, Osakada et al. showed that with similar CuI/*N,N*-dimethylglycine reaction conditions it was possible to synthesize 6- to 10-membered unsubstituted cyclophanes from linear oligo(*p*-phenylene oxide)s with modest yields.<sup>89</sup> The 6-membered cyclophane **25** was constructed from linear compound **23** and compound **24** (Scheme 3). The crystal structures revealed nearly planar structures of the macrocycles, with large inner diameters ranging from 1.0–1.5 nm. Nevertheless, each benzene ring was tilted from the plain of the neighboring ring, indicating the absence of conjugation between monoaromatic rings.



**Scheme 3.** Ullmann coupling reaction yielding 21 % cyclophane **25**.

In 2014, Zhou et al. presented a library of unsubstituted aryl ether macrocycles, that could be easily accessed with a Cu(I)/iron(III) catalytic system.<sup>86</sup> The macrocyclization reaction was screened using compound **26** and compound **27** as starting substrates (Scheme 4). To find the best reaction conditions, the model reaction was screened over the temperature range of 100–140 °C, and the effect of the solvent on the yield was compared between 1,4-dioxane, DMSO, and DMF. Various copper sources, bases, and the presence or absence of ligands and iron catalysts were analyzed. The highest yield of oxcalixarene **28** was with the 10 mol% CuI/Fe(acac)<sub>3</sub> catalytic system, using K<sub>2</sub>CO<sub>3</sub> as the base in DMSO at 110 °C under an inert atmosphere. Using the same reaction conditions, a library of oxcalixarenes was compiled by involving numerous diiodoarenes and dihydroxyphenols.

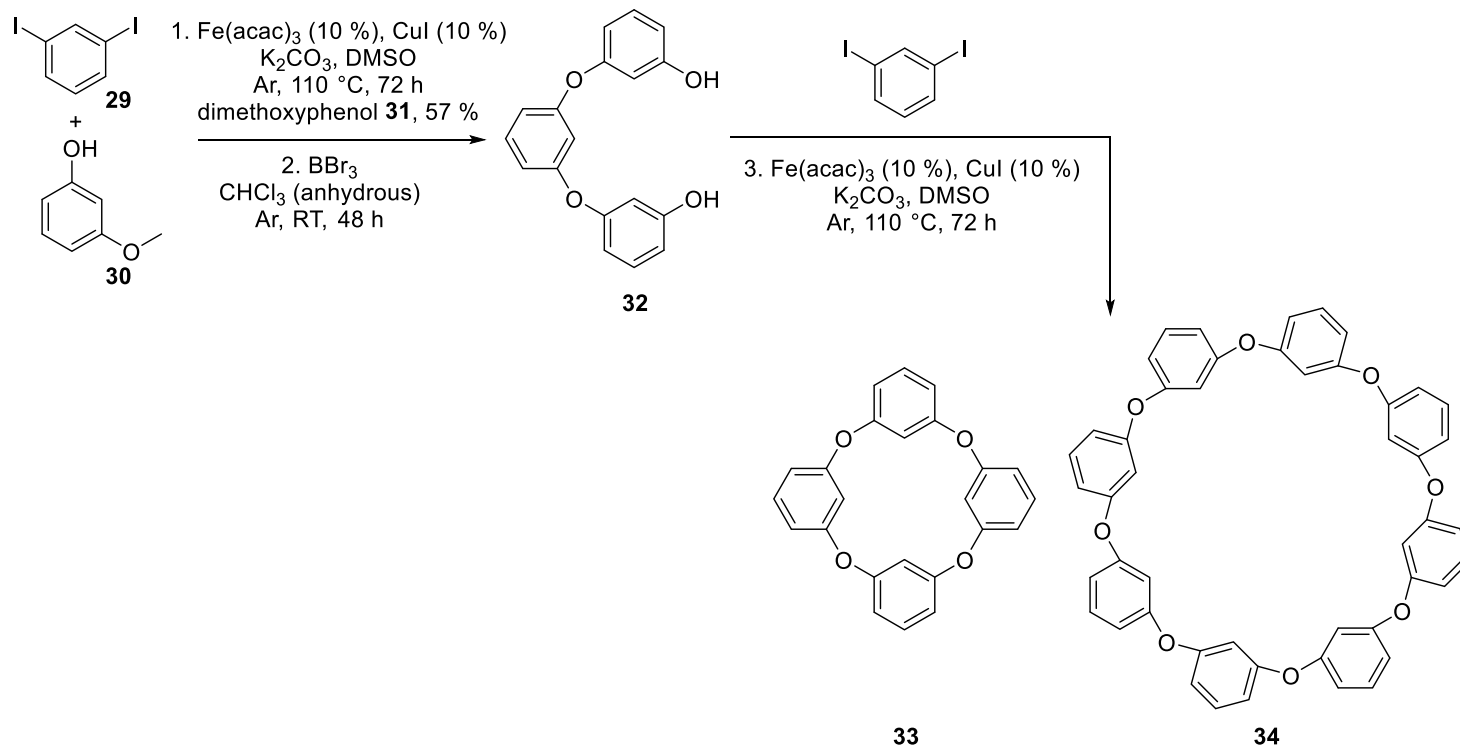


**Scheme 4.** Model reaction of unsubstituted oxcalixarene **28**.

### 3.1.2 Synthesis of unsubstituted oxcalix[*n*]arenes (*n* = 4, 8)

The three-step copper-catalyzed synthesis procedure described in section 3.1.1<sup>86</sup> was utilized in my thesis work to synthesize unsubstituted oxcalixarene **33** and **34** (Scheme 5). In the first step, equimolar amounts of compound **29** and compound **30** were coupled in the presence of a copper/iron catalytic system and K<sub>2</sub>CO<sub>3</sub>. The coupling reaction was relatively slow and yielded 57 % of compound **31** in 72 h at 110 °C in DMSO. In the second step, compound **31** was demethylated by BBr<sub>3</sub>, with a high yield (97 %) of compound **32**. In the final step, Ullmann coupling of compound **32** and compound **29** yielded 40 % oxcalix[4]arene **33** and 2 % oxcalix[8]arene **34** after careful

chromatographic separation. The main by-products of the reaction were linear oligomers. The  $^1\text{H}$  NMR spectra of the reaction mixture evidenced the formation of linear oligomers as broad peaks appearing in the range of 6–7 ppm. The obtained oxacalixarenes were, however, of very high purity, and this allowed us to concentrate on evaluating the properties of these macrocycles.



**Scheme 5.** 3-Step fragment coupling synthesis procedure of oxacalixarene **33** and **34**.

### 3.1.3 Crystal structures of unsubstituted oxcalix[*n*]arenes (*n*= 4, 8)

The oxcalix[4]arene **33** crystal structure showed the macrocycle in a 1,3-alternate conformation, which is intrinsic to 4-membered oxcalixarenes.<sup>81–83,116</sup> Intriguingly, the oxcalix[4]arene **33** was found packed in two crystal polymorphs (Figure 20a).

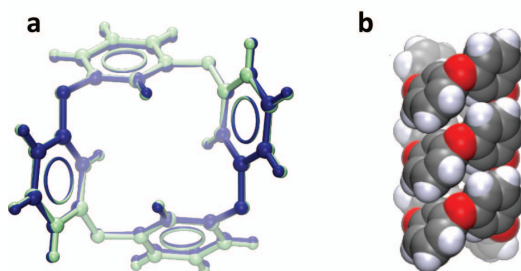


**Figure 20.** a) Overlay of the two oxcalix[4]arene **33** crystal structures. Polymorph I is marked with green and polymorph II with blue. b) CPK visualization of the oxcalix[4]arene **33**. Fig. 20a and 20b were adapted with permission from **Publication I**.

It was presumed that the polymorphism did not occur due to conformational changes but because of the influence of crystal packing, as conformations were the same in both polymorphs. It was deduced that only one conformation exists in the solid state, with small structural differences between the two polymorphs.

Similar columnar packing and stabilizing interactions were seen for the 8-membered oxcalix[8]arene **34** (Figure 21b), which was found in one twisted conformation intrinsic to larger sized heteracalixarene isomers (Figure 21a).

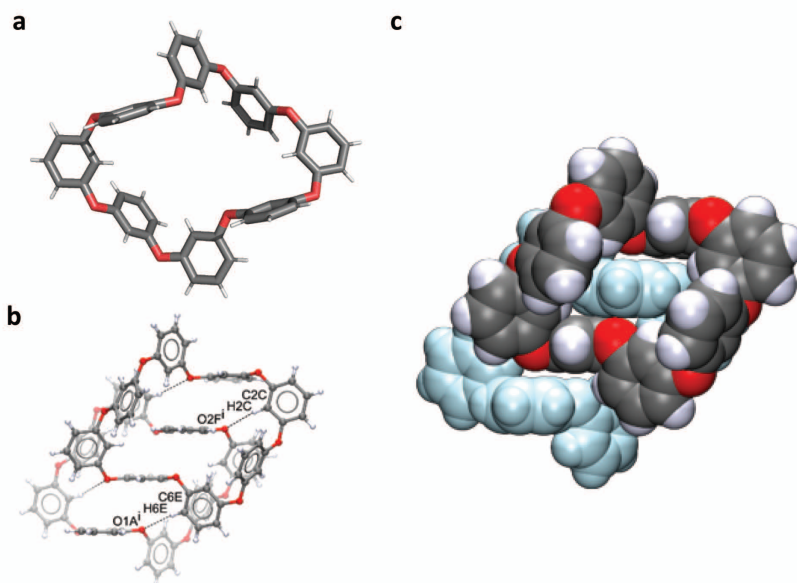


**Figure 21.** 8-Membered oxcalixarene **34** a) isolated crystal structure; b) dimeric unit representation of the crystal structure where macrocycles are connected through four C–H...O hydrogen bonds (marked with dotted lines) and off-center  $\pi$ – $\pi$  stacking; c) CPK visualization of dimeric units. Fig. 21b and 21c were adapted with permission from **Publication I**.

Building large calixarenes has been the focus of several previous studies.<sup>82,88,124,125</sup> The development of larger macrocycles has been hindered by the occurrence of rapid conformational changes that interfere with directed complexation. In this work, the crystal structures of the 8-membered oxacalixarene **34** showed tight packing (Figure 21b, c) of macrocycles through off-center  $\pi$ - $\pi$  interactions and multiple HBs; therefore, binding guests through similar interactions was thought promising. The selectivity of the core of the electron-rich 8-membered oxacalixarene **34** was investigated with fullerene C<sub>60</sub> **39** and the electrochemically active compound ferrocene **11**. Compound **39**, with its electron-deficient double bonds, appeared to be a good guest for validating both the  $\pi$ - $\pi$  interactions and the size compatibility of the interaction pair. Compound **11** was selected because it has been shown to form complexes with oxacalixarenes in previous studies.<sup>92</sup> Preliminary complexation studies with <sup>1</sup>H NMR in chloroform and toluene showed that the binding event was energetically unfavored. The plausible reason for the lack of affinity could have been in the flexibility of the host or the lack of size compatibility between the host and the guests. The complexation studies were continued with the more abundant tetrameric product.

### 3.1.4 Complexation properties of unsubstituted oxacalix[4]arene

The molecular electrostatic potential (MEP) image was obtained for the oxacalix[4]arene **33** macrocycle (Figure 22). The MEP image revealed that the outward edges of the aromatic ring were electron-deficient, with the electron density gradually increasing towards the cavity and near the oxygen bridge. The selection of guest molecules to investigate the binding of oxacalix[4]arene **33** was based on two possible interactions with the macrocycle:

- 1) hydrogen bonding between the guest hydrogen and the macrocycle oxygen bridge;
- 2)  $\pi$ - $\pi$  interactions between the host's electron-rich  $\pi$ -system and the  $\pi$ -system of the neutral guests.

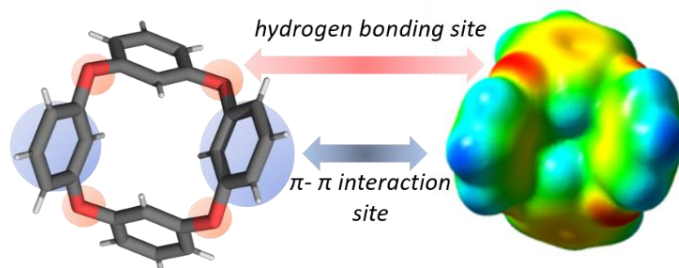


**Figure 22.** Crystal structure of oxacalix[4]arene **33** (left) and MEP image (right) visualized with GaussView 5.0.8. High electron density is marked with red and low electron density is marked with blue. MEP image adapted with permission from **Publication I**.

The six guest molecules investigated in this work were benzoic acid **35**, ferrocene **11**, 1,5-dimethylnaphthalene **36**, neocuproine **37**, 3-methylcatechol **38**, and fullerene **39** (Figure 23). Benzoic acid **35** and 3-methylcatechol **38** were chosen to analyze the formation of the complex through hydrogen bonding. Aromatic acid and alcohol were chosen to analyze the possibility of further complex stabilization arising from the  $\pi$ - $\pi$  interactions. The planar electron-deficient nitrogen-containing heterocycle neocuproine **37** was selected to assess the possibility of face-to-face stacking of the adversarial aromatic components. 1,5-Dimethylnaphthalene **36** was used to compare the complexation differences between the naphthalene and heterocyclic aromatics.

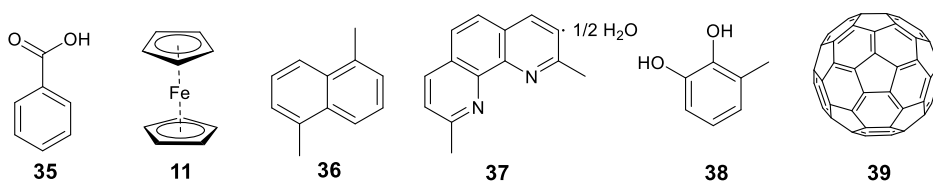


**Figure 23.** Guest molecules for the preliminary screening with oxacalix[4]arene **33**.

The preliminary NMR study of the oxacalix[4]arene **33** complexes with compounds **36**, **37**, and **38** in a 1:2 host–guest ratio were obtained from measurements in  $\text{CDCl}_3$  or toluene- $d_8$ . In the case of compound **39**, a solution containing oxacalix[4]arene **33** and **39** in a 5:1 ratio was measured in  $\text{CDCl}_3$ , targeting the possible formation of the 2:1 oxacalix[4]arene **33**·**39** complex. The NMR analysis showed weak complexation between oxacalix[4]arene **33** and compounds **36** and **37** in chloroform and **38** in toluene, and no interactions were observed with compound **39**.

After the preliminary NMR results, the next aim was to measure the association constants of the complexes with guests **36**, **37**, and **38** using the NMR titration method. However, due to the low solubility of the guests, the  $K_a$  values could not be determined. Yet, the NMR titration experiments could be performed for the **33**·**35** (Figure 24a) and **33**·**11** complexes. In the case of the benzoic acid **35** complex, experiments were conducted in two concentration ranges of oxacalix[4]arene **33**. At 4.5 and 45 mM, similar weak interactions were observed between host–guest pairs, and no reliable association constant could be determined. No reliable association constant could be determined for the **33**·**11** host–guest complex either. These results clarified that derivatization of oxacalixarenes is important for molecular recognition, as the bare oxacalixarene core lacked directed binding. To our knowledge, the unsubstituted oxacalixarene complexation study with aromatic guest molecules was the first interaction study using unsubstituted oxacalixarenes.

Additionally, NMR was used to investigate how the oxacalix[4]arene **33** proton shifts are influenced by environmental acidity. The non-aromatic acid TFA was used in this study to help clarify whether the changes observed with compound **35** were indeed induced by  $\pi$ – $\pi$  interactions. The TFA titration results showed no noticeable shifts of  $\text{H}_4$  or  $\text{H}_5$ , but  $\text{H}_2$  shifted upfield when adding up to 100 eq of TFA to a solution of oxacalix[4]arene **33** (Figure 24b). This proves that the downfield shifts detected with compound **35** were connected with the **33**·**35** host–guest interactions and were not the result of changes in the environment. In addition, it was hypothesized that the oxacalix[4]arene **33** 1,3-alternate conformation was the probable structure inhabited by the host in solution. This was based on the inward-facing  $\text{H}_2$  protons' noticeable upfield shifts, which could be explained by the cone shielding anisotropy created by the neighboring benzene rings.

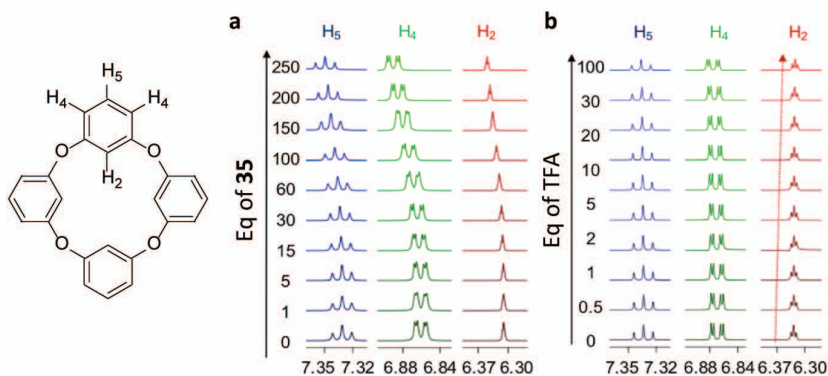
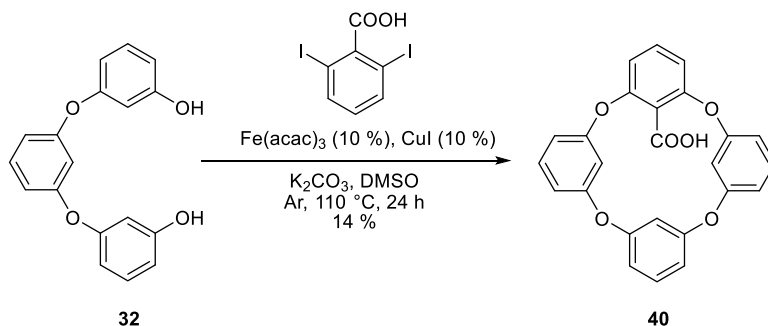


**Figure 24.**  $^1\text{H}$  NMR (800 MHz,  $\text{CDCl}_3$ ) titration results of oxcalix[4]arene **33** and a) compound **35**; b) TFA. Titration data adapted with permission from **Publication I**.

## 3.2 Oxcalix[4]arene carboxylic acid (Publication II)

### 3.2.1 Synthesis and structure of oxcalix[4]arene carboxylic acid

After analyzing the binding properties of the oxcalix[4]arene core, it was evident that oxcalix[4]arene **33** required functionalization to enhance its solubility in protic solvents. It was hypothesized that enhancing the solubility in protic solvents would change the host–guest binding modes, thereby influencing the selectivity of the host towards biologically interesting guests. To achieving this, a functionalized aryl group was added to the oxcalix[4]arene **33** structure by changing compound **29** in the third fragment-coupling step to 2,6-diiodobenzoic acid (Scheme 6). The reaction product was oxcalix[4]arene carboxylic acid **40** in 14 % yield. The low reaction yield was explained by the tendency of the product to decarboxylate during the product isolation.



**Scheme 6.** Synthesis of oxcalix[4]arene carboxylic acid **40** from precursor.

In the crystal structure (Figure 25b), the crystal packing was mainly stabilized by HBs between the carboxylic acid groups and the opposing unsubstituted oxcalixarenes, where macrocycles were packed together via aromatic–aromatic dispersive forces. Single crystals of oxcalix[4]arene **40** were found in 1,3-alternate conformation. The hydrogen bonding in the crystal structures showed potential for the binding of guest molecules between the aromatic units. In solution, the upfield proton resonance position of proton  $\text{H}_6$  in comparison (Figure 25c) with the  $\text{H}_9$  proton signal indicated a static 1,3-alternate saddle-like conformation. Lehmann proposed<sup>126</sup> that the noticeable upfield shift of aryl ether inward-facing aromatic protons might be the result of aromatic cone shielding anisotropy.

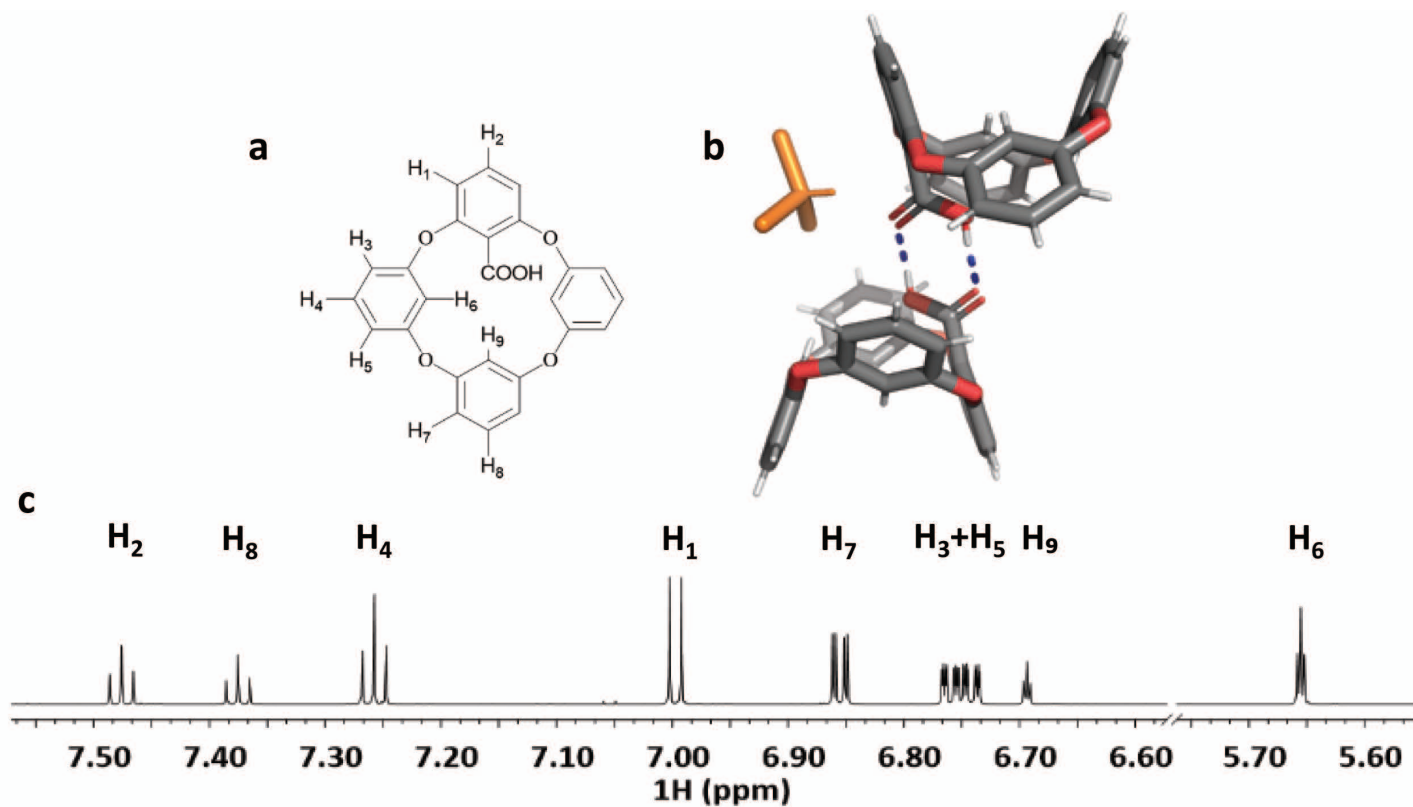


**Figure 25.** Oxacalix[4]arene **40** a) chemical structure with marked protons; b) hydrogen-bonded dimer (HB marked with blue dotted lines) with co-crystallized CHCl<sub>3</sub> solvent molecule (marked with orange) in the background; c) <sup>1</sup>H NMR (CD<sub>3</sub>OD, 800 MHz) spectrum with marked proton signals.

Depending on the solvent, carboxylic acid can be influenced by either dissociation or dimerization effects, and it is important to understand the mechanisms before planning the complexation experiment. The presence of HB bonds between the carboxylic acid groups of oxacalix[4]arene **40** in the crystal structure was a promising characteristic for building a dimeric capsule that would form a larger binding pocket. Whether or not the dimeric capsule was present in chloroform was investigated. For this, an NMR dilution study was performed in which the macrocycle was measured in the concentration range of 0.04–1.00 mM (Figure 26).

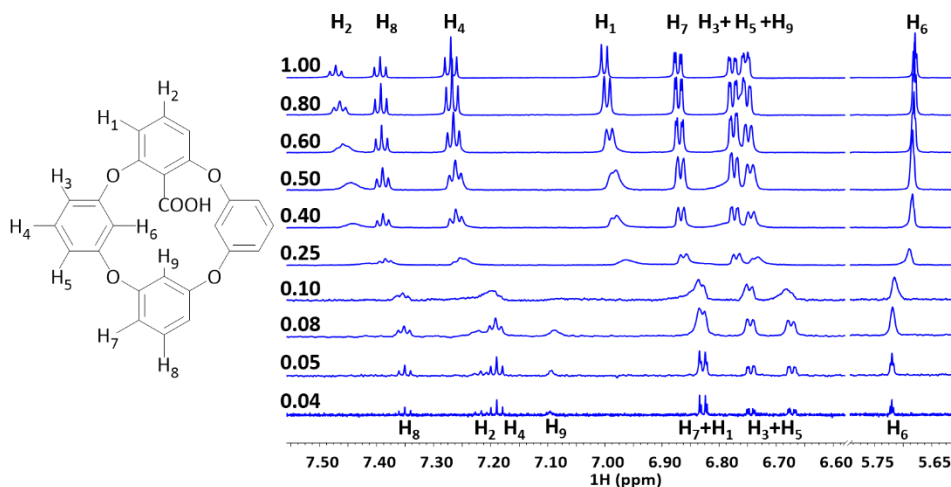


**Figure 26.**  $^1\text{H}$  NMR ( $\text{CDCl}_3$ , 800 MHz) dilution study of oxacalix[4]arene **40**.

When the concentration was increased, the downfield shifts of the macrocycles outward-facing protons and upfield shifts of protons  $\text{H}_6$  and  $\text{H}_9$  indicated that dimer formation did not take place in chloroform. In the case of dimerization, opposite shifts of the peaks should have been observed. This was seen in previously reported data of similar carboxylic acid macrocycles;<sup>24,127</sup> for example, in the case of dimer formation, opposite chemical shifts were visible in the NMR spectra. Another hint came from the BindFit dimer aggregation model that could not fit the data points.

The structure of oxacalix[4]arene **40** was also studied in methanol. The possibility of acid dissociation was investigated by measuring oxacalixarene in  $\text{CD}_3\text{OD}$  in acidic and basic environments (Figure 27). TFA was added to a dilute 0.08 mM sample of oxacalix[4]arene **40**. The observed shifts corresponded to the shifts seen with the 1.00 mM oxacalix[4]arene **40** sample. When TEA was added to the 1.00 mM oxacalix[4]arene **40** sample, the resulting spectra coincided with that of the 0.04 mM oxacalix[4]arene **40** sample. This was in good agreement with an increased dissociation fraction of a weak acid upon dilution.

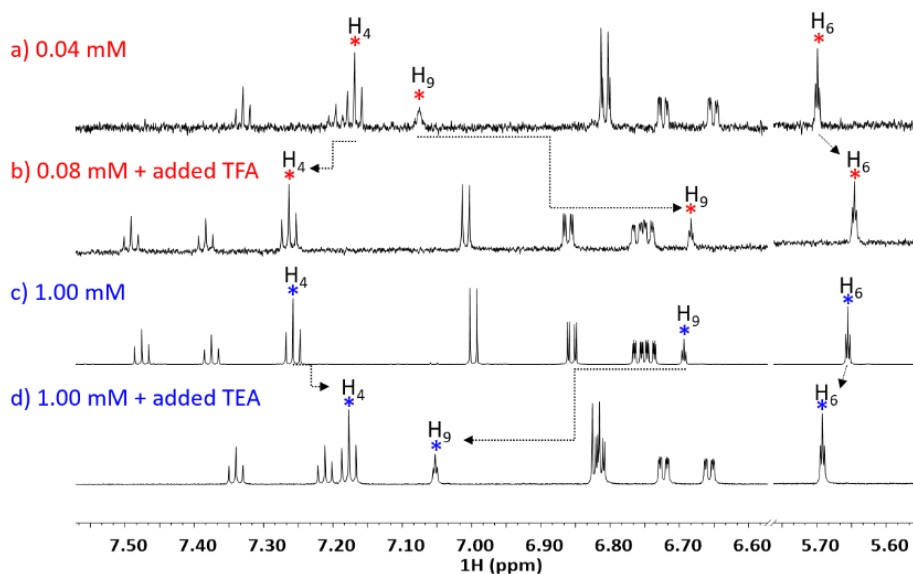


**Figure 27.**  $^1\text{H}$  NMR ( $\text{CD}_3\text{OD}$ , 800 MHz) spectra of oxacalix[4]arene **40** a) 0.04 mM sample; b) 0.08 mM dilute sample + TFA (20 eq); c) 1.00 mM sample; d) 1.00 mM sample + TEA (20 eq). NMR spectra adapted with permission from **Publication II**.

These experimental data clearly indicated that analyzing the complexation of this macrocycle by NMR would be complicated owing to the additional acid–base equilibrium, as the macrocycle chemical shifts were very sensitive to environmental pH changes. To circumvent the potential issues of inexplicable data from host–guest complexes in solution, the macrocycles' carboxylate form was used in the subsequent experiments.

### 3.2.2 Complexation properties of oxacalix[4]arene carboxylate

The carboxylic acid substitution can easily be modified into a carboxylate salt, which enhances the solubility of the aromatic macrocycle in protic solvents. Solubility in water is important when using the macrocycle host–guest interaction properties in biological applications<sup>128,129</sup> or as synthetic scavengers.<sup>130</sup> The affinity towards neutral guests in water has been demonstrated with various calixarene-like macrocycles, but there is only one example of a water-soluble polycationic oxacalixarene, **5**,<sup>41,131</sup> that can bind neutral and, surprisingly, cationic aromatic guests when in a suitable protonation state.

Inspired by the design of water-soluble oxacalixarenes, the targeted binding of nitrogen-containing biologically relevant guests was investigated. For this, oxacalix[4]arene **40** was treated with TBAOH, forming the TBA-salt oxacalix[4]arene derivative **41**. The bulky TBA counterion was chosen because it is too large to interfere with the macrocycle's binding pocket, fully isolating the carboxylate ion binding site. The bipyridinium compound paraquat was selected for the guest template, as it is a popular target compound for toxic guest molecule neutralization by host–guest encapsulation processes. It was predicted that the complex would assemble through the formation of a salt bridge, that is, through electrostatic interactions between the negatively charged carboxylate oxygen and the paraquat nitrogen, or through additional  $\pi$ – $\pi$  interactions.

An  $^1\text{H}$  NMR titration study was performed in methanol (Figure 28), and the data were fitted using the BindFit<sup>100,132</sup> online analysis tool. The oxacalixarene **41**-paraquat complex showed a  $K_a$  value in methanol of  $2020 \pm 70 \text{ M}^{-1}$ , corresponding to 1:1 binding

stoichiometry. Notably, this is the highest binding affinity reported for any oxcalixarene with an organic cation.

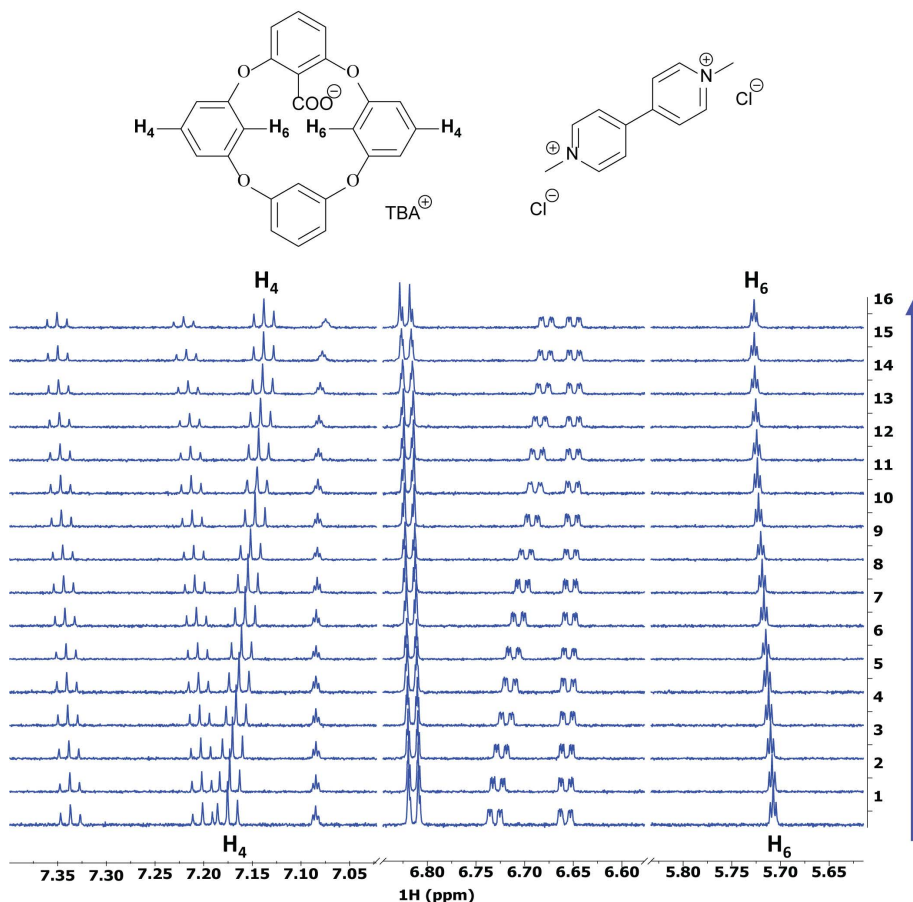


**Figure 28.**  $^1\text{H}$  NMR ( $\text{CD}_3\text{OD}$ , 800 MHz) titration data of **41** (0.2 mM) and paraquat with 0.1, 0.4, 0.8, 1.1, 1.5, 2.2, 3.0, 3.9, 6.0, 7.6, 8.4, 10.9, 14.0, 17.0 and 20.2 eq added guest. The  $\text{H}_4$  and  $\text{H}_6$  proton shifts were used for  $K_a$  calculation. NMR titration spectra adapted with permission from **Publication II**.

The inward-facing  $\text{H}_6$  protons' downfield shift and the outward-facing  $\text{H}_4$  protons' upfield shift indicated that the oxcalix[4]arene slightly changed conformation to fit the guest compound. Unfortunately, no single crystals of this complex were obtained.

### 3.2.3 Complexation properties of oxcalix[4]arene carboxylic acid in the gas phase (ongoing investigation)

A gas-phase study of oxcalixarenes was conducted under the supervision of Dr. Elina Kalenius at the Department of Chemistry, University of Jyväskylä, Finland.

The previous results of the oxcalix[4]arene **41**·paraquat complex showed promise that oxcalix[4]arene **40** can be used as a host for amines. The method of choice for the initial complex screening was ESI-MS. ESI-MS is an excellent method for analyzing supramolecular complexes. Because electrospray is not a destructive ionization method,

it is possible to ionize structures held together by weak noncovalent interactions without causing fragmentation.<sup>105</sup> From the mass spectrum, it is possible to observe the potential structure of the complex and the interaction stoichiometry. It was anticipated that the affinity of oxalix[4]arene **40** towards ammonium cations would be driven by salt bridges forming between carboxylates and ammonium. This type of ion pair formation in the gas phase is known in the field of resorcinarene chemistry,<sup>133–135</sup> yet in oxalixarene chemistry, this was described for the first time here. The formation of a salt bridge is influenced by electrostatic interactions and hydrogen bonding.<sup>136</sup> This led to establishing the use of ammonium cations **42–48** (Figure 29), which could be measured under the same ionization conditions. These compounds were further characterized by drift tube ion mobility mass spectrometry (DTIM-MS).

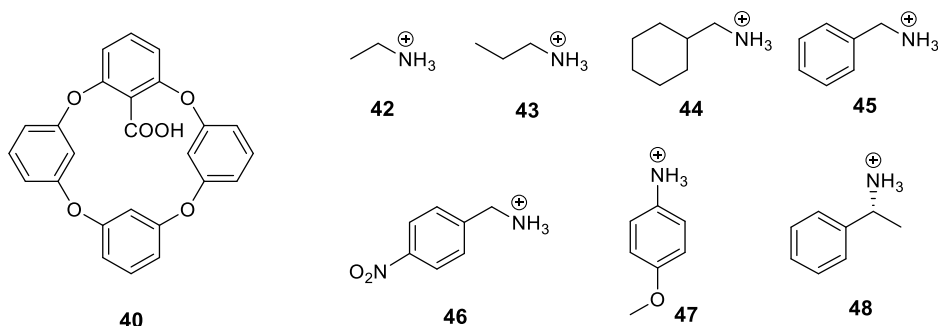


**Figure 29.** Oxalixarene **40** host and the list of ammonium cations.

There were two categories of guest molecules. In the first category, the ethylammonium **42**, propylammonium **43**, and cyclohexanemethylammonium **44** cations were selected to assess differences in complexation between a bulky cycloalkane group and an alkyl chain. In the second category, various benzylammoniums were analyzed to evaluate whether the complex was further stabilized by aromatic interactions and how much the distance between the ammonium cation and the aromatic ring (**45**, **47**, **48**), and between the aromatic rings' electron-withdrawing **46** and -donating **47** substituents, influenced the interaction strength. The guest (**42–48**) screening was analyzed using acetonitrile with ESI-MS in positive mode (Figure 30). Oxalix[4]arene **40** was also analyzed in negative ESI mode, yet the only product ion found was decarboxylated compound [**40** – COOH]<sup>+</sup>, even after thorough tuning of the ionization conditions. Therefore, further analysis was not carried out in the negative mode due to fragmentation of the macrocycle.

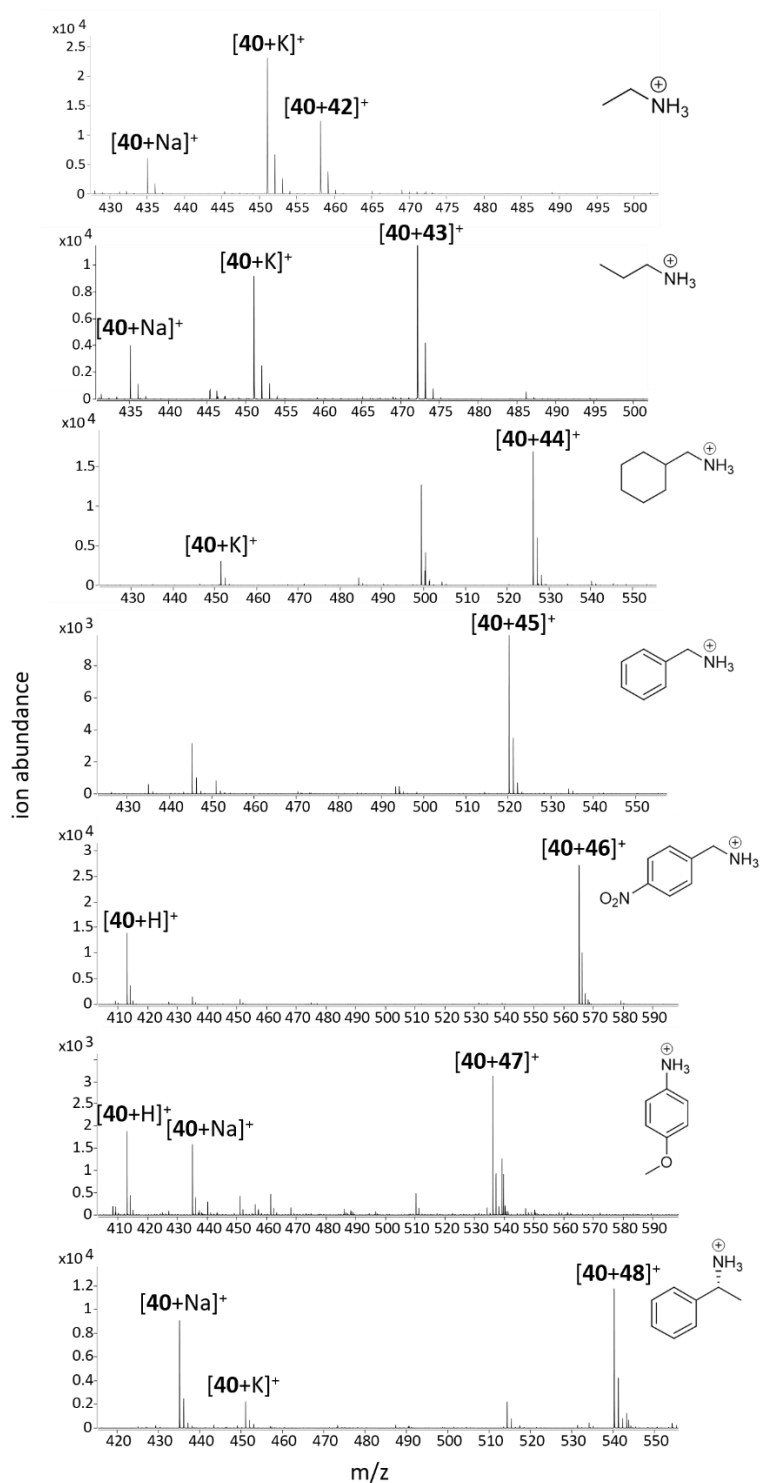


**Figure 30.** (+)ESI-MS spectra of oxacalixarene **40** plus an equimolar amount of guests **42** – **48**.

Based on the (+)ESI-MS spectra, it was assumed that the aromatic guests **42** – **48** had similar interaction profiles. The complexed ions in all host–guest pairs showed a 1:1 stoichiometry, and no ions with a double-charge or ions revealing other cooperative binding modes were detected. Dimer  $[40_2+Na]^+$  was present in all the spectra in low abundance, but no peaks corresponding to **40**<sub>2</sub> dimer encapsulating the amine guest were found.

Additional structural information of the oxacalix[4]arene **40** gas-phase complexes was obtained by IM-MS. Measuring drift times of the complexes and comparing them to  $Na^+$  adduct of oxacalix[4]arene **40**, as the “free host” ion drift time, increased our understanding of the binding geometry of the complex. As mentioned in the literature overview, in the case of *endo* binding, the drift times are expected to be roughly equivalent, as the ion drift times are mainly dependent on the dimensions of the ion. Ion mobilograms are depicted in Figure 31.

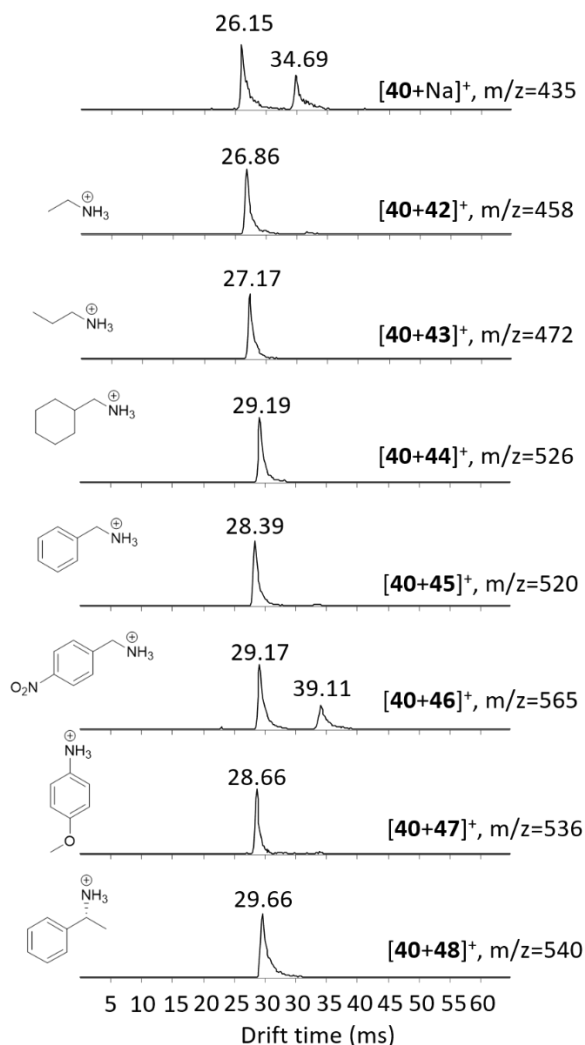


**Figure 31.** Results of IM-MS analysis. The ion mobility times of  $[40+Na]^+$  and the complexes are depicted.

The results depicted in Figure 31 show varying complex ion drift times compared to the initial  $[40+Na]^+$  drift time (26.15 ms). This variation indicates that the ammonium cations are located outside the macrocycle cavity, as all of the complex drift times were longer than the “free host” ion drift time. Additional evidence for this is that the ion drift times increased as the guest molecule size increased, indicating that the guests were similar to each other in their complex formation and were located at the macrocycle portal. Additionally, in the case of the  $[40+46]^+$  complex ion, two peaks under the same ion signal can clearly be distinguished, which usually indicates that there are two different complex geometries present or dimer fragmentation has occurred in the drift tube. When analyzing the  $[40+Na]^+$  ion, two peaks were present with similar peak separation times of  $\sim 10$  ms, proving that dimer fragmentation was more likely.

The CCS values were calculated based on the measured ion mobility drift times and are comparable because the experiments were conducted under tuned and equilibrated drift gas pressure and temperature conditions. The CCS theoretical values were based on structural information (Figure 32) gathered from DFT calculations\*. The CCS theoretical and experimental values were in good agreement (see Table 2), evidencing the similarity between the gas-phase complexes and the predicted structures. From the structures, it can be seen that the guest molecules interact with the host via hydrogen bond and C–H... $\pi$  interactions. No further complex stabilization occurred through  $\pi$ – $\pi$  interactions for **40·45** or **40·46**.

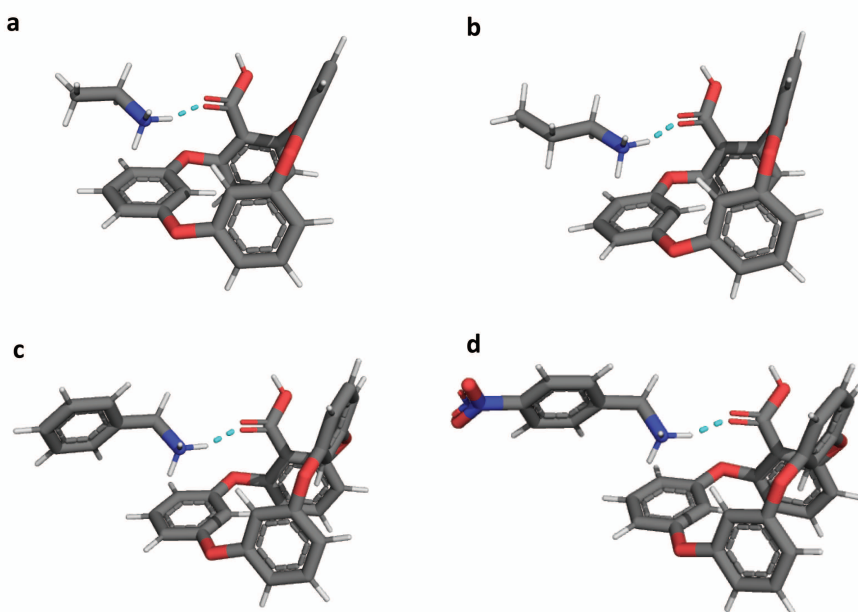


**Figure 32.** Structures of oxacalix[4]arene **40** complexes a) **40·42**; b) **40·43**; c) **40·45**; d) **40·46**. Hydrogen bonds are marked in cyan. Calculated at the B97D/6-311+G(2d,p) level of theory.

\*Geometry optimization conducted by Dr. Aleksander Trummal and Dr. Merle Uudsemaa at NICPB.

**Table 2.** Oxocalix[4]arene **40** complex ion drift times and CCS values.

Guest	m/z	DT (mS)	CCS <sub>exp</sub> (Å)	CCS <sub>theor</sub> (Å)
			N <sub>2</sub>	N <sub>2</sub>
<b>42</b>	458	26.86	202.1	192.1
<b>43</b>	472	27.17	205.0	199.4
<b>44</b>	526	29.19	218.1	-
<b>45</b>	520	28.39	211.8	216.2
<b>46</b>	565	29.17	216.9	231.0
<b>47</b>	536	28.66	212.7	-
<b>48</b>	540	29.66	221.5	-

### 3.3 Halogen bonding systems in solution (Publication III)

#### 3.3.1 Introduction to halogen bonding in solution

Compared to hydrogen bonding, the investigation of halogen bonds (XBs) in solution is a newer field of study. It has led to applications in host-guest chemistry<sup>137–140</sup> and has shown promise for building larger supramolecular structures through self-assembly.<sup>141–143</sup>

Calixarenes capable of forming XBs can be prepared by direct derivatization, as demonstrated by Lhotak et al. in 2014.<sup>144</sup> In that work, that the regioselectivity of the halogen to the thiacalixarene core was influenced by the starting conformation of the unsubstituted thiacalixarene. Depending on whether the macrocycle was in the cone or in the 1,3-alternate conformation, the halogenation took place in either the *meta* and *para* positions, or only in the *meta* position, respectively. The authors suggested that the halogenated thiacalixarenes could be used as synthetic intermediates.

In addition to using halogenated intermediates in organic synthesis, various organic halogen bond donors have become promising targets as a new group of catalysts. These catalysts can carry out anion-recognition type reaction activation or they can be used as analogs for hydrogen bond-activated reactions. The idea that halogen bonding could be a successful and versatile way to accelerate reactions comes from the well-known catalyst I<sub>2</sub>, which has been used for the initiation and acceleration of different types of organic reactions.<sup>145,146</sup> The organic halogen-donating catalysts in noncovalent organocatalysis have been investigated since the first work of Bolm et al. in 2008.<sup>147</sup> Since then, there have been several examples of XB interactions being used in organic synthesis and organocatalysis.<sup>148</sup>

#### 3.3.2 Triazole-based XB donors

In XB chemistry, anion recognition by halogen donors has been studied more than the recognition and activation of neutral halogen acceptors. Activating neutral compounds is more challenging, as the formed XBs are weaker. Thus, for the XB interactions to take place, stronger XB donors are needed.<sup>28,149</sup> In catalysis, the structural effects and compatibility of the catalyst–substrate binding site is of great importance. Screening for optimal catalyst candidates has revealed the advantage of halotriazoles, which is their structural approachability – halotriazoles can be constructed from azides (including chiral azides) and alkynes by applying classic Cu-catalyzed click reactions.

Halo-triazolium salts have shown high association constants when binding anions; this shows the promise of halo-triazolium XB donors being a good option for binding neutral acceptors. In this work, the suitability of these donors to interact with neutral acceptors was investigated with a selection of monodentate XB donors (Figure 33). For the neutral

acceptor, the strong Lewis base, quinuclidine **56**, was chosen as the reference compound. The triazolium salt structures were modified by phenyl, perfluorophenyl, and *p*-nitrophenyl substituents, changing the counterions (triflate (OTf), tetrafluoroborate (BF<sub>4</sub>), and tetrakis[3,5-bis(trifluoromethyl)phenyl]borate (BARF)) and the halogen (-I and -Br). As control compounds, a neutral XB donor **55** and the nonhalogenated donor **54** were added to the selection.

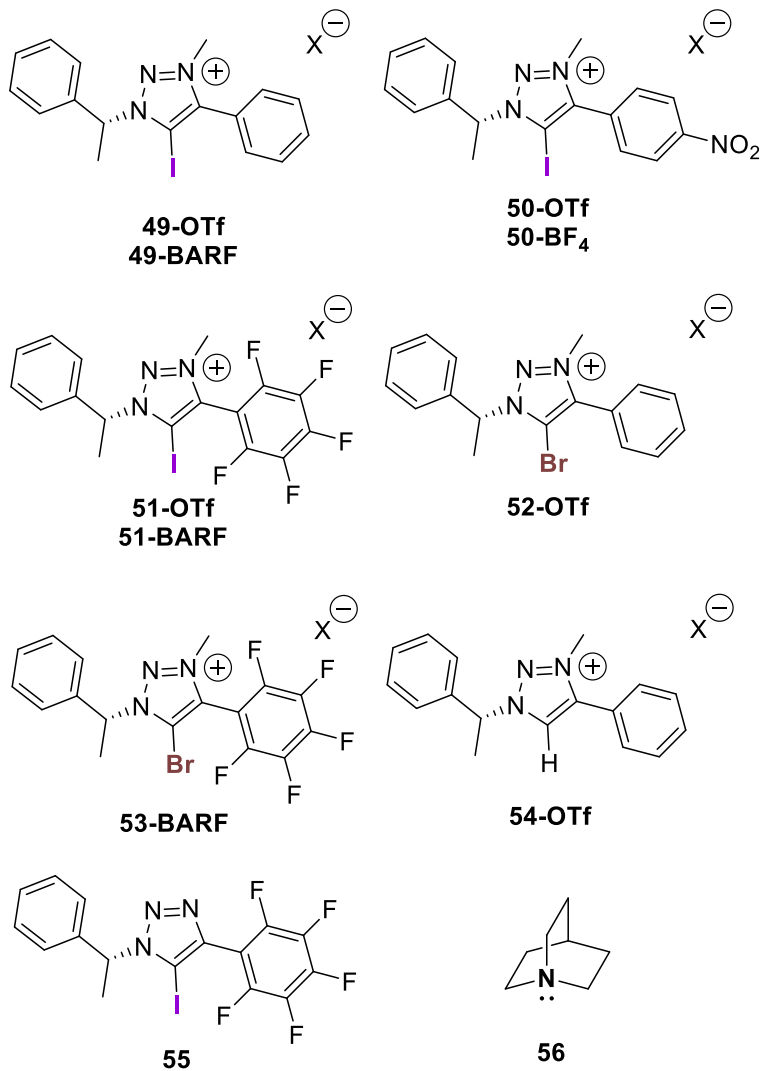


**Figure 33.** XB donors and reference acceptor **56**. List of compounds adapted with permission from *Publication III*.

### 3.3.3 XB donor – quinuclidine interaction study by <sup>1</sup>H NMR titration

The XB strengths were assessed by <sup>1</sup>H NMR titration in CDCl<sub>3</sub> at RT. The NMR titrations were carried out for every XB donor–acceptor pair in two independent experiments. The results of the NMR titration experiments are presented in Table 3.

**Table 3.** *K<sub>a</sub>* values<sup>a</sup> of XB donor–acceptor pairs.

Entry	XB donor	<i>K<sub>a</sub></i> , M <sup>-1</sup>
1	<b>49-OTf</b>	57 ± 5
2	<b>49-BARF</b>	(1.23 ± 0.01) × 10 <sup>3</sup>
3	<b>50-OTf</b>	257 ± 12
4	<b>50-BF<sub>4</sub></b>	284 ± 12
5	<b>51-OTf</b>	703 ± 6
6	<b>51-BARF</b>	(1.1 ± 0.3) × 10 <sup>4</sup>
7	<b>52-OTf</b>	< 1
8	<b>53-BARF</b>	n.d <sup>b</sup>
9	<b>54-OTf</b>	< 1
10	<b>55</b>	2.0 ± 0.3

<sup>a</sup>The titration data were fitted with the 1:1 binding isotherm of BindFit ([www.supramolecular.org](http://www.supramolecular.org)). The given association constant is the mean value of two independent experiments. <sup>b</sup>*K<sub>a</sub>* not determined due to XB donor dehalogenation during the experiment.

Substituents in the aromatic ring that are directly connected to the triazole unit can have a significant effect on the XB interactions.<sup>32</sup> The *K<sub>a</sub>* values (Table 3, entries 1, 3, 5) showed the binding strengths to decrease in the order of **49-OTf** > **50-OTf** > **51-OTf**. The XB donor with a perfluoro-substituted aromatic ring had the strongest interaction with the acceptor due to a previously recorded effect<sup>150</sup> in which the electron-deficient aryl substituents (–C<sub>6</sub>F<sub>5</sub>) influence the C-X carbon by increasing the carbon's positive area of σ-hole. The NMR titration was performed with **54-OTf** (the nonhalogenated analog of **49-OTf**) to confirm whether the observed interactions were indeed caused by halogen bonding (Table 3, entry 9). The result, *K<sub>a</sub>* < 1, verified that the previous interactions were due to halogen bonding.

Changing the counterion (OTf, BARF, or BF<sub>4</sub>) showed that the XB interaction strength was substantially affected by the counterion coordination ability. The affinities towards quinuclidine were quite similar for **50-BF<sub>4</sub>** and **50-OTf**, with the least coordinating tetrafluoroborate having slightly higher affinity towards quinuclidine than the triflate salt (Table 3, entries 3 and 4). However, considerable changes in the interaction strengths were induced with the BARF counterion (Table 3, entries 2 and 6). The *K<sub>a</sub>* value of **51-BARF** and quinuclidine (1.1 ± 0.3) × 10<sup>4</sup> M<sup>-1</sup> is one of the highest reported so far.

When the halogen atom was changed from -I to -Br, the decrease in the interaction strength corresponded to the increase in electronegativity. The bromine analog **52-OTf** showed little to no affinity towards the acceptor, in contrast to the high affinity of iodo-triazolium **49-OTf** (Table 3).

### 3.3.4 XB donor – acceptor enantiodiscrimination study by <sup>1</sup>H NMR titration

The enantiodiscrimination ability of halotriazoles was assessed with <sup>1</sup>H NMR titration in solution. For the experiment, **51-BARF** was chosen as the best XB donor candidate based on a previous study. The two chiral XB acceptors, imine **57** and amine **58**, are shown in Figure 34, and the association constant values for the XB pairs are shown in Table 4.

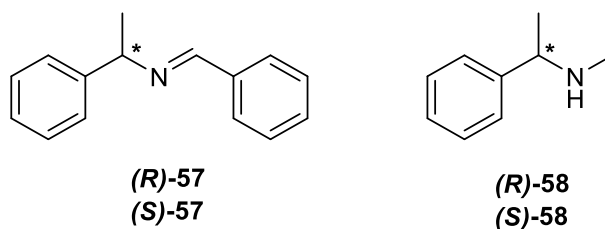


**Figure 34.** Structures of chiral imine and amine XB acceptors.

**Table 4.**  $K_a$  values<sup>a</sup> of **51-BARF** donor and chiral acceptor XB pairs.

Entry	XB acceptor	$K_a$ , M <sup>-1</sup>
1	<b>(R)-57</b>	6.1 ± 0.7
2	<b>(S)-57</b>	6.0 ± 0.8
3	<b>(R)-58</b>	94 ± 7
4	<b>(S)-58</b>	91 ± 5

<sup>a</sup>The <sup>1</sup>H NMR titration data were fitted using the software described under Table 3.

From the results in Table 4, it can be concluded that no preferential binding of enantiomers was achieved with **51-BARF**, as there were no remarkable changes in the association constant values between enantiomers. One of the possible reasons for the lack of directed affinity towards one enantiomer could have been the structure of the donors' triazole core, where bulkier substituents should be used to induce enantioselective complex formation.

## 4 Conclusions

To develop new supramolecular assemblies, it is necessary to investigate the binding specificities of new hosts. In this thesis, various oxacalixarene hosts were studied, and an additional investigation of iodo-triazole based halogen bond donor ability was undertaken.

The unsubstituted oxacalix[*n*]arenes (*n*= 4 and 8) were prepared through a 3-step fragment coupling pathway and isolated with 40 % and 2 % yield in high purity. A solid state crystallographic study revealed that oxacalix[4]arene **33** was in a 1,3-alternate conformation and oxacalix[8]arene **34** was in a twisted conformation. The solution study also revealed the presence of the 1,3-alternate conformation. The host–guest interactions of oxacalix[4]arene **33** were evidenced by <sup>1</sup>H NMR in chloroform and toluene. A selection of guests that could form complexes through  $\pi$ – $\pi$  interactions and hydrogen bonding (benzoic acid, ferrocene, 1,5-dimethylnaphthalene, neocuproine, 3-methylcatechol, and fullerene) were screened. Oxacalix[4]arene **33** showed weak affinity towards all the guests except fullerene. However, the preliminary solution NMR studies showed no affinity of large oxacalix[8]arene **34** towards the guests due to the rapid conformational change of the host.

Functionalized oxacalix[4]arene carboxylic acid was synthesized with the analogous fragment coupling method. In the solid state, the macrocycle was found to form hydrogen-bonded carboxylic acid dimers. By contrast, studies in chloroform showed no dimer formation in solution. In the carboxylate form, the solubility of the macrocycle was enhanced in protic solvents. The oxacalix[4]arene carboxylate tetrabutylammonium salt formed a complex with paraquat in methanol, with  $K_a = 2020 \pm 70 \text{ M}^{-1}$ . To our knowledge, this value is the highest published  $K_a$  value for an oxacalix[4]arene macrocycle derivative and an organic cation. These findings indicate that the newly synthesized oxacalix[4]arene **40** has promising features that could lead to its application in toxic compound detection and encapsulation.

In the gas phase, oxacalix[4]arene **40** complexes with different ammonium cations were observed. The ESI-MS study of seven amine guests showed the formation of single-charged host–guest complexes with 1:1 stoichiometry. CCS values were obtained from IM-MS experiments for the seven complexes, and four of the structures were confirmed by quantum chemical calculations. The  $\text{CCS}_{\text{theor}}$  and  $\text{CCS}_{\text{exp}}$  values were in good agreement, evidencing that it is possible to gain insight into small calixarene complex gas-phase structures by using a combination of IM-MS and DFT calculations.

The results of the triazole-based XB donor characterization in solution demonstrate the importance of the counterion's effect on XB donor ability. The binding of neutral XB acceptor was more influenced by the counterion effect than by the donor's electron-deficient phenyl substituents. The  $K_a$  values of triazole-based donors and a neutral acceptor varied from  $10^1$  to  $10^4 \text{ M}^{-1}$ . The triazole-based XB donor did not differentiate between the chiral XB acceptors, i.e., imine and amine enantiomers.

The findings of this thesis contribute to the understanding of oxacalixarene synthesis and binding properties and, similarly, to XB systems. This information is important for designing structures with the capacity for molecular recognition that employ oxacalixarene structures or make use of XB motifs.

## 5 Experimental section

### 5.1 Mass spectrometry

All the gas-phase studies were performed on an Agilent 6560 Ion Mobility Quadrupole Time-of-Flight (IM-QTOF) spectrometer (Agilent Technologies, Santa Clara, CA), equipped with micro-ESI source. All the measurements were conducted in positive mode. The stock solutions of oxalix[4]arene **40** and amines were prepared in methanol. For the MS analysis, a 5  $\mu$ M oxalix[4]arene **40** sample was prepared in MeCN and added to an equimolar amount of amine. The sample flow rate was set to 2  $\mu$ L/min in the IM-MS experiments.

The mass range for the ESI-MS and IM-MS experiments was set to 300–1000 m/z. All gas-phase measurements were operated in the extended dynamic range mode with a 3200 m/z range. The source conditions for the IM-MS experiments were kept consistent throughout the screening of amines, with the following parameters: capillary voltage 4.5 kV, source gas temperature 225 °C, drying gas 7 L/min, nebulizer 4 psi, fragmentor 400 V, and Oct 1 RF Vpp 750 V. The IM-MS spectra were measured with N<sub>2</sub> as the drift gas. According to the N<sub>2</sub> drift gas settings, the stepped field IM-MS spectra were gathered by varying the drift tube entrance voltages from 1074 to 1674 V in 100 V steps. The drift tube and trap funnel pressures were tuned before each IM-MS experiment. The readiness and reproducibility of the spectrometer was checked using the ES tuning mix standard solution (Agilent Technologies).<sup>150</sup>

The ESI-MS and ion-mobility spectra were analyzed with Agilent Masshunter software. Theoretical CCS values were calculated with the ion mobility calculator IMoS Suite version 1.06.<sup>151</sup> The calculation was based on recorded experimental parameters that include gas, temperature and pressure. The trajectory method with Lennard-Jones parameters was used and showed good agreement between predicted and measured CCS values. The coordinates of the complexes for CCS<sub>theor</sub> calculation were obtained from DFT calculations (B97D/6-311+G(2d,p)).

## References

- 1 C. D. Gutsche and R. Muthukrishnan, *J. Org. Chem.*, 1978, **43**, 4905–4906.
- 2 Z. Xu, S. Jia, W. Wang, Z. Yuan, B. J. Ravoo and D.-S. Guo, *Nat. Chem.*, 2019, **11**, 86–93.
- 3 Y. Hamuro, M. C. Calama, H. S. Park and A. D. Hamilton, *Angew. Chemie Int. Ed. English*, 1997, **36**, 2680–2683.
- 4 G. V Zyryanov, Y. Kang and D. M. Rudkevich, *J. Am. Chem. Soc.*, 2003, **125**, 2997–3007.
- 5 G. V Zyryanov and D. M. Rudkevich, *J. Am. Chem. Soc.*, 2004, **126**, 4264–4270.
- 6 B. B. Ahuja and A. Vigalok, *Angew. Chemie Int. Ed.*, 2019, **58**, 2774–2778.
- 7 J. Scheerder, J. F. J. Engbersen, A. Casnati, R. Ungaro and D. N. Reinhoudt, *J. Org. Chem.*, 1995, **60**, 6448–6454.
- 8 X. Ji, X. Chi, M. Ahmed, L. Long and J. L. Sessler, *Acc. Chem. Res.*, 2019, **52**, 1915–1927.
- 9 J. W. Steed and P. A. Gale, *Supramolecular chemistry: from molecules to nanomaterials*, John Wiley & Sons New York, 2012.
- 10 D. J. Cram, *From Design to Discover*, Amer Chemical Society, 1990, vol. 1.
- 11 E. Fischer, *Berichte der Dtsch. Chem. Gesellschaft*, 1894, **27**, 2985–2993.
- 12 D. E. Koshland Jr, *Proc. Natl. Acad. Sci. U. S. A.*, 1958, **44**, 98.
- 13 B. Wang and E. V Anslyn, *Chemosensors: principles, strategies, and applications*, John Wiley & Sons, 2011, vol. 15.
- 14 E. Graf and J. Lehn, *Chem. Informationsd.*, 1981, **12**, 1040–1057.
- 15 J. M. Lehn and J. P. Sauvage, *J. Am. Chem. Soc.*, 1975, **97**, 6700–6707.
- 16 C. J. Pedersen, *J. Am. Chem. Soc.*, 1967, **89**, 7017–7036.
- 17 H. K. Frensdorff, *J. Am. Chem. Soc.*, 1971, **93**, 600–606.
- 18 E. Arunan, G. R. Desiraju, R. A. Klein, J. Sadlej, S. Scheiner, I. Alkorta, D. C. Clary, R. H. Crabtree, J. J. Dannenberg and P. Hobza, *Pure Appl. Chem.*, 2011, **83**, 1619–1636.
- 19 Z. Xiao, W. Yang, F. Yan, L. Ji, W. Li and W. Wang, *CrystEngComm*, 2019, **21**, 439–448.
- 20 Q. Zhang, L. Catti and K. Tiefenbacher, *Acc. Chem. Res.*, 2018, **51**, 2107–2114.
- 21 L. R. MacGillivray and J. L. Atwood, *Nature*, 1997, **389**, 469–472.
- 22 L. Avram, Y. Cohen and J. Rebek Jr, *Chem. Commun.*, 2011, **47**, 5368–5375.
- 23 A. Cavarzan, A. Scarso, P. Sgarbossa, G. Strukul and J. N. H. Reek, *J. Am. Chem. Soc.*, 2011, **133**, 2848–2851.
- 24 H. Miyaji, M. Dudic, J. H. R. Tucker, I. Prokes, M. E. Light, T. Gelbrich, M. B. Hursthouse, I. Stibor, P. Lhoták and L. Brammer, *Supramol. Chem.*, 2003, **15**, 385–390.
- 25 G. R. Desiraju, P. S. Ho, L. Kloo, A. C. Legon, R. Marquardt, P. Metrangolo, P. Politzer, G. Resnati and K. Rissanen, *Pure Appl. Chem*, 2013, **85**, 1711–1713.
- 26 G. Cavallo, P. Metrangolo, R. Milani, T. Pilati, A. Priimagi, G. Resnati and G. Terraneo, *Chem. Rev.*, 2016, **116**, 2478–2601.
- 27 K. Rissanen, *CrystEngComm*, 2008, **10**, 1107–1113.
- 28 L. C. Gilday, S. W. Robinson, T. A. Barendt, M. J. Langton, B. R. Mullaney and P. D. Beer, *Chem. Rev.*, 2015, **115**, 7118–7195.
- 29 T. Brinck, J. S. Murray and P. Politzer, *Int. J. Quantum Chem.*, 1992, **44**, 57–64.

- 30 P. Politzer, J. S. Murray, T. Clark and G. Resnati, *Phys. Chem. Chem. Phys.*, 2017, **19**, 32166–32178.
- 31 P. Metrangolo, H. Neukirch, T. Pilati and G. Resnati, *Acc. Chem. Res.*, 2005, **38**, 386–395.
- 32 M. G. Sarwar, B. Dragisic, L. J. Salsberg, C. Gouliaras and M. S. Taylor, *J. Am. Chem. Soc.*, 2010, **132**, 1646–1653.
- 33 S. M. Walter, F. Kniep, L. Rout, F. P. Schmidtchen, E. Herdtweck and S. M. Huber, *J. Am. Chem. Soc.*, 2012, **134**, 8507–8512.
- 34 P. Slavík, V. Eigner and P. Lhoták, *CrystEngComm*, 2016, **18**, 4964–4970.
- 35 J. L. Atwood, L. J. Barbour and A. Jerga, *Science*, 2002, **296**, 2367–2369.
- 36 A. J. Neel, M. J. Hilton, M. S. Sigman and F. D. Toste, *Nature*, 2017, **543**, 637–646.
- 37 A. Sygula, F. R. Fronczek, R. Sygula, P. W. Rabideau and M. M. Olmstead, *J. Am. Chem. Soc.*, 2007, **129**, 3842–3843.
- 38 P. Lhoták and S. Shinkai, *J. Phys. Org. Chem.*, 1997, **10**, 273–285.
- 39 D. Chandler, *Nature*, 2005, **437**, 640–647.
- 40 F. A. Greco, *J. Phys. Chem.*, 1984, **88**, 3132–3133.
- 41 N. Manganaro, G. Lando, I. Pisagatti, A. Notti, S. Pappalardo, M. F. Parisi and G. Gattuso, *Supramol. Chem.*, 2016, **28**, 493–498.
- 42 M. E. Davis and M. E. Brewster, *Nat. Rev. Drug Discov.*, 2004, **3**, 1023–1035.
- 43 M. J. Webber and R. Langer, *Chem. Soc. Rev.*, 2017, **46**, 6600–6620.
- 44 B. O. Okesola and D. K. Smith, *Chem. Soc. Rev.*, 2016, **45**, 4226–4251.
- 45 N. Busschaert, C. Caltagirone, W. Van Rossom and P. A. Gale, *Chem. Rev.*, 2015, **115**, 8038–8155.
- 46 I. V. Kolesnichenko and E. V. Anslyn, *Chem. Soc. Rev.*, 2017, **46**, 2385–2390.
- 47 R. Kumar, A. Sharma, H. Singh, P. Suating, H. S. Kim, K. Sunwoo, I. Shim, B. C. Gibb and J. S. Kim, *Chem. Rev.*, 2019, **119**, 9657–9721.
- 48 X. Ma and Y. Zhao, *Chem. Rev.*, 2015, **115**, 7794–7839.
- 49 W.-F. Lai, A. L. Rogach and W.-T. Wong, *Chem. Soc. Rev.*, 2017, **46**, 6379–6419.
- 50 R. Behrend, E. Meyer and F. Rusche, *Justus Liebigs Ann. Chem.*, 1905, **339**, 1–37.
- 51 J. Lagona, P. Mukhopadhyay, S. Chakrabarti and L. Isaacs, *Angew. Chemie Int. Ed.*, 2005, **44**, 4844–4870.
- 52 R. Aav, S. Kaabel and M. Fomitšenko, *Comprehensive Supramolecular Chemistry II*, Elsevier, 2017.
- 53 W. S. Jeon, K. Moon, S. H. Park, H. Chun, Y. H. Ko, J. Y. Lee, E. S. Lee, S. Samal, N. Selvapalam and M. V. Rekharsky, *J. Am. Chem. Soc.*, 2005, **127**, 12984–12989.
- 54 E. M. M. Del Valle, *Process Biochem.*, 2004, **39**, 1033–1046.
- 55 J. Szejtli, *Chem. Rev.*, 1998, **98**, 1743–1754.
- 56 A. R. Hedges, *Chem. Rev.*, 1998, **98**, 2035–2044.
- 57 R. A. Smaldone, R. S. Forgan, H. Furukawa, J. J. Gassensmith, A. M. Z. Slawin, O. M. Yaghi and J. F. Stoddart, *Angew. Chemie Int. Ed.*, 2010, **49**, 8630–8634.
- 58 T. Rajkumar, D. Kukkar, K.-H. Kim, J. R. Sohn and A. Deep, *J. Ind. Eng. Chem.*, 2019, **72**, 50–66.
- 59 G. W. Gokel, W. M. Leevy and M. E. Weber, *Chem. Rev.*, 2004, **104**, 2723–2750.
- 60 J. Lehn, *Angew. Chemie Int. Ed. English*, 1988, **27**, 89–112.
- 61 D. J. Cram, *Angew. Chemie Int. Ed. English*, 1988, **27**, 1009–1020.
- 62 C. J. Pedersen, *Angew. Chemie Int. Ed. English*, 1988, **27**, 1021–1027.

- 63 B. Wang and E. V. Anslyn, *Chemosensors: principles, strategies, and applications*, John Wiley & Sons, 2011.
- 64 P. Neri, J. L. Sessler and M.-X. Wang, *Calixarenes and beyond*, Springer, 2016.
- 65 C. D. Gutsche, B. Dhawan, K. H. No and R. Muthukrishnan, *J. Am. Chem. Soc.*, 1981, **103**, 3782–3792.
- 66 V. Guérineau, M. Rollet, S. Viel, B. Lepoittevin, L. Costa, P. Saint-Aguet, R. Laurent, P. Roger, D. Gimes and C. Martini, *Nat. Commun.*, 2019, **10**, 1–14.
- 67 B. König and M. H. Fonseca, *Eur. J. Inorg. Chem.*, 2000, **2000**, 2303–2310.
- 68 M.-X. Wang, *Chem. Commun.*, 2008, 4541–4551.
- 69 J. Thomas, W. Van Rossom, K. Van Hecke, L. Van Meervelt, M. Smet, W. Maes and W. Dehaen, *Chem. Commun.*, 2012, **48**, 43–45.
- 70 M.-X. Wang, *Acc. Chem. Res.*, 2012, **45**, 182–195.
- 71 H.-Y. Gong, Q.-Y. Zheng, X.-H. Zhang, D.-X. Wang and M.-X. Wang, *Org. Lett.*, 2006, **8**, 4895–4898.
- 72 H. Gong, D. Wang, J. Xiang, Q. Zheng and M. Wang, *Chem. Eur. J.*, 2007, **13**, 7791–7802.
- 73 C. P. Casas and T. Yamato, *J. Incl. Phenom. Macrocycl. Chem.*, 2005, **53**, 1–8.
- 74 Y. Liu, Y.-H. Ma, Y. Chen, D.-S. Guo and Q. Li, *J. Org. Chem.*, 2006, **71**, 6468–6473.
- 75 N. Iki, T. Fujimoto, T. Shindo, K. Koyama and S. Miyano, *Chem. Lett.*, 1999, **28**, 777–778.
- 76 J. N. Babu, V. Bhalla, M. Kumar, R. K. Mahajan and R. K. Puri, *Tetrahedron Lett.*, 2008, **49**, 2772–2775.
- 77 J. Kroupa, I. Stibor, M. Pojarova, M. Tkadlecova and P. Lhotak, *Tetrahedron*, 2008, **64**, 10075–10079.
- 78 S. Rahman, H. Tomiyasu, H. Kawazoe, J.-L. Zhao, H. Cong, X.-L. Ni, X. Zeng, M. R. J. Elsegood, T. G. Warwick, S. J. Teat, C. Redshaw, P. E. Georghiou and T. Yamato, *New J. Chem.*, 2016, **40**, 9245–9251.
- 79 O. A. Mostovaya, P. L. Padnya, A. A. Vavilova, D. N. Shurpik, B. I. Khairutdinov, T. A. Mukhametzyanov, A. A. Khannanov, M. P. Kuttyreva and I. I. Stoikov, *New J. Chem.*, 2018, **42**, 177–183.
- 80 Y. Addepalli, X. Yang, M. Zhou, D. P. Reddy, S.-L. Zhang, Z. Wang and Y. He, *Eur. J. Med. Chem.*, 2018, **151**, 214–225.
- 81 R. D. Chambers, P. R. Hoskin, A. R. Kenwright, A. Khalil, P. Richmond, G. Sandford, D. S. Yufit and J. A. K. Howard, *Org. Biomol. Chem.*, 2003, **1**, 2137–2147.
- 82 H. Konishi, K. Tanaka, Y. Teshima, T. Mita, O. Morikawa and K. Kobayashi, *Tetrahedron Lett.*, 2006, **47**, 4041–4044.
- 83 W. Maes, W. Van Rossom, K. Van Hecke, L. Van Meervelt and W. Dehaen, *Org. Lett.*, 2006, **8**, 4161–4164.
- 84 J. L. Katz, B. J. Geller and P. D. Foster, *Chem. Commun.*, 2007, 1026–1028.
- 85 W. Van Rossom, K. Robeyns, M. Ovaere, L. Van Meervelt, W. Dehaen and W. Maes, *Org. Lett.*, 2011, **13**, 126–129.
- 86 Q. Zhou, L. Su, T. Jiang, B. Zhang, R. Chen, H. Jiang, Y. Ye, M. Zhu, D. Han, J. Shen, G. Dai and Z. Li, *Tetrahedron*, 2014, **70**, 1125–1132.
- 87 L. Wu, L. Jiao, Q. Lu, E. Hao and Y. Zhou, *Spectrochim. Acta Part A Mol. Biomol. Spectrosc.*, 2009, **73**, 353–357.

- 88 W. Van Rossom, M. Ovaere, L. Van Meervelt, W. Dehaen and W. Maes, *Org. Lett.*, 2009, **11**, 1681–1684.
- 89 D. Takeuchi, I. Asano and K. Osakada, *J. Org. Chem.*, 2006, **71**, 8614–8617.
- 90 J. L. Katz, M. B. Feldman and R. R. Conry, *Org. Lett.*, 2005, **7**, 91–94.
- 91 S.-Z. Hu and C.-F. Chen, *Chem. Commun.*, 2010, **46**, 4199–4201.
- 92 D. Sobransingh, M. B. Dewal, J. Hiller, M. D. Smith and L. S. Shimizu, *New J. Chem.*, 2008, **32**, 24–27.
- 93 H.-B. Yang, D.-X. Wang, Q.-Q. Wang and M.-X. Wang, *J. Org. Chem.*, 2007, **72**, 3757–3763.
- 94 M. Panchal, M. Athar, P. C. Jha, A. Kongor, V. Mehta and V. Jain, *J. Lumin.*, 2017, **192**, 256–262.
- 95 M. Panchal, A. Kongor, M. Athar, V. Mehta, P. C. Jha and V. K. Jain, *New J. Chem.*, 2018, **42**, 311–317.
- 96 T. Huang, X. Wu, T. Liu, L. An and X. Yin, *Med. Chem. Res.*, 2019, **28**, 580–590.
- 97 M. Yamashita and J. B. Fenn, *J. Phys. Chem.*, 1984, **88**, 4451–4459.
- 98 M. Karas, D. Bachmann and F. Hillenkamp, *Anal. Chem.*, 1985, **57**, 2935–2939.
- 99 K. Tanaka, H. Waki, Y. Ido, S. Akita, Y. Yoshida, T. Yoshida and T. Matsuo, *Rapid Commun. mass Spectrom.*, 1988, **2**, 151–153.
- 100 P. Thordarson, *Chem. Soc. Rev.*, 2011, **40**, 1305–1323.
- 101 T. Pierro, C. Gaeta, F. Troisi and P. Neri, *Tetrahedron Lett.*, 2009, **50**, 350–353.
- 102 K. D. Daze, M. C. F. Ma, F. Pineux and F. Hof, *Org. Lett.*, 2012, **14**, 1512–1515.
- 103 L. Avram and Y. Cohen, *Chem. Soc. Rev.*, 2015, **44**, 586–602.
- 104 K. S. Cameron and L. Fielding, *J. Org. Chem.*, 2001, **66**, 6891–6895.
- 105 M. Przybylski and M. O. Glocker, *Angew. Chemie Int. Ed. English*, 1996, **35**, 806–826.
- 106 B. Baytekin, H. T. Baytekin and C. A. Schalley, *Org. Biomol. Chem.*, 2006, **4**, 2825–2841.
- 107 E. Kalenius, M. Groessl and K. Rissanen, *Nat. Rev. Chem.*, 2019, **3**, 4–14.
- 108 J. C. May, C. B. Morris and J. A. McLean, *Anal. Chem.*, 2017, **89**, 1032–1044.
- 109 T.-C. Lee, E. Kalenius, A. I. Lazar, K. I. Assaf, N. Kuhnert, C. H. Grün, J. Jänis, O. A. Scherman and W. M. Nau, *Nat. Chem.*, 2013, **5**, 376–382.
- 110 J. Boschmans, S. Jacobs, J. P. Williams, M. Palmer, K. Richardson, K. Giles, C. Laphorn, W. A. Herrebout, F. Lemièrre and F. Sobott, *Analyst*, 2016, **141**, 4044–4054.
- 111 M. Öeren, E. Shmatova, T. Tamm and R. Aav, *Phys. Chem. Chem. Phys.*, 2014, **16**, 19198–19205.
- 112 D. V Dearden, T. A. Ferrell, M. C. Asplund, L. W. Zilch, R. R. Julian and M. F. Jarrold, *J. Phys. Chem. A*, 2009, **113**, 989–997.
- 113 H. Zhang, M. Grabenauer, M. T. Bowers and D. V Dearden, *J. Phys. Chem. A*, 2009, **113**, 1508–1517.
- 114 A. Kiesilä, L. Kivijärvi, N. K. Beyeh, J. O. Moilanen, M. Groessl, T. Rothe, S. Götz, F. Topić, K. Rissanen and A. Lützen, *Angew. Chemie Int. Ed.*, 2017, **56**, 10942–10946.
- 115 V. Böhmer, *Angew. Chemie Int. Ed. English*, 1995, **34**, 713–745.
- 116 W. Maes and W. Dehaen, *Chem. Soc. Rev.*, 2008, **37**, 2393–2402.
- 117 W.-S. Ren, L. Zhao and M.-X. Wang, *Org. Lett.*, 2016, **18**, 3126–3129.
- 118 M. H. Patel and P. S. Shrivastav, *Chem. Commun.*, 2009, 586–588.

- 119 N. Sommer and H. A. Staab, *Tetrahedron Lett.*, 1966, **7**, 2837–2841.
- 120 J. W. Wackerly, J. M. Meyer, W. C. Crannell, S. B. King and J. L. Katz, *Macromolecules*, 2009, **42**, 8181–8186.
- 121 J.-X. Ma, X. Fang, M. Xue and Y. Yang, *Org. Biomol. Chem.*, 2019, **17**, 5075–5085.
- 122 S. V Ley and A. W. Thomas, *Angew. Chemie Int. Ed.*, 2003, **42**, 5400–5449.
- 123 F. Yang, L. Yan, K. Ma, L. Yang, J. Li, L. Chen and J. You, *European J. Org. Chem.*, 2006, **2006**, 1109–1112.
- 124 E. Hao, F. R. Fronczek and M. G. H. Vicente, *J. Org. Chem.*, 2006, **71**, 1233–1236.
- 125 X. Li, T. G. Upton, C. L. D. Gibb and B. C. Gibb, *J. Am. Chem. Soc.*, 2003, **125**, 650–651.
- 126 P. A. Lehmann F, *Tetrahedron*, 1974, **30**, 727–733.
- 127 A. Arduini, M. Fabbi, M. Mantovani, L. Mirone, A. Pochini, A. Secchi and R. Ungaro, *J. Org. Chem.*, 1995, **60**, 1454–1457.
- 128 M. I. N. Xue, Y. Yang, X. Chi, Z. Zhang and F. Huang, *Acc. Chem. Res.*, 2012, **45**, 1294–1308.
- 129 J. Ma, Q. Meng, X. Hu, B. Li, S. Ma, B. Hu, J. Li, X. Jia and C. Li, *Org. Lett.*, 2016, **18**, 5740–5743.
- 130 A. Fernando, T. L. Mako, A. M. Levenson, P. T. Cesana, A. M. Mendieta, J. M. Racicot, B. DeBoef and M. Levine, *Supramol. Chem.*, 2019, 1–13.
- 131 N. Manganaro, G. Lando, C. Gargiulli, I. Pisagatti, A. Notti, S. Pappalardo, M. F. Parisi and G. Gattuso, *Chem. Commun.*, 2015, **51**, 12657–12660.
- 132 D. Brynn Hibbert and P. Thordarson, *Chem. Commun.*, 2016, **52**, 12792–12805.
- 133 M. Cametti, M. Nissinen, A. Dalla Cort, L. Mandolini and K. Rissanen, *J. Am. Chem. Soc.*, 2007, **129**, 3641–3648.
- 134 N. K. Beyeh, D. P. Weimann, L. Kaufmann, C. A. Schalley and K. Rissanen, *Chem. Eur. J.*, 2012, **18**, 5552–5557.
- 135 N. Kodiah Beyeh, M. Göth, L. Kaufmann, C. A. Schalley and K. Rissanen, *European J. Org. Chem.*, 2014, **2014**, 80–85.
- 136 S. K. Seth, A. Bauzá and A. Frontera, *New J. Chem.*, 2018, **42**, 12134–12142.
- 137 A. Caballero, N. G. White and P. D. Beer, *Angew. Chemie Int. Ed.*, 2011, **50**, 1845–1848.
- 138 A. Vargas Jentsch, D. Emery, J. Mareda, P. Metrangolo, G. Resnati and S. Matile, *Angew. Chemie*, 2011, **123**, 11879–11882.
- 139 D. Mungalpara, S. Stegmüller and S. Kubik, *Chem. Commun.*, 2017, **53**, 5095–5098.
- 140 C. Gropp, B. L. Quigley and F. Diederich, *J. Am. Chem. Soc.*, 2018, **140**, 2705–2717.
- 141 X. C. Yan, P. Schyman and W. L. Jorgensen, *J. Phys. Chem. A*, 2014, **118**, 2820–2826.
- 142 C. Han, D. Zhao and S. Dong, *Chem. Commun.*, 2018, **54**, 13099–13102.
- 143 S. R. Kennedy, M. U. Main, C. R. Pulham, I. Ling and S. J. Dalgarno, *CrystEngComm*, 2019, **21**, 786–790.
- 144 J. Lukášek, S. Böhm, H. Dvořáková, V. Eigner and P. Lhoták, *Org. Lett.*, 2014, **16**, 5100–5103.
- 145 H. Togo and S. Iida, *Synlett*, 2006, **2006**, 2159–2175.
- 146 M. Breugst and D. von der Heiden, *Chem. Eur. J.*, 2018, **24**, 9187–9199.
- 147 A. Bruckmann, M. A. Pena and C. Bolm, *Synlett*, 2008, **2008**, 900–902.

- 148 R. L. Sutar and S. M. Huber, *ACS Catal.*, 2019, **9**, 9622–9639.
- 149 O. Dumele, D. Wu, N. Trapp, N. Goroff and F. Diederich, *Org. Lett.*, 2014, **16**, 4722–4725.
- 150 V. Gabelica, A. A. Shvartsburg, C. Afonso, P. Barran, J. L. P. Benesch, C. Bleiholder, M. T. Bowers, A. Bilbao, M. F. Bush and J. L. Campbell, *Mass Spectrom. Rev.*, 2019, **38**, 291–320.
- 151 C. Larriba and C. J. Hogan Jr, *J. Phys. Chem. A*, 2013, **117**, 3887–3901.

## Acknowledgments

The research work presented in this thesis was conducted in the Laboratory of Chemical Physics, National Institute of Chemical Physics and Biophysics (Estonia); in the Department of Chemistry and Biotechnology, Tallinn University of Technology (Estonia); and in the Department of Chemistry, University of Jyväskylä (Finland). This work was supported by the Estonian Research Council (PRG399, PSG400, PUT692, and MOBJD39), the European Regional Development Fund Project CoE TK134, CoE No. 2014-2020.4.01.15-0013, and partially by the Graduate School of Functional Materials and Technologies (2014-2020.4.01.16-0032).

I would like to thank my supervisors Dr. Jasper Adamson and Prof. Riina Aav for providing me with the opportunity to conduct research in the diverse and challenging field of supramolecular chemistry. I am forever grateful for all the years of support and encouragement they provided. I would also like to acknowledge the National Institute of Chemical Physics and Biophysics for its support during my PhD studies. I want to thank Prof. Tõnis Kanger for the opportunity to do research on the topic of halogen bonding and Dr. Elina Kalenius for her supervision of my research work at University of Jyväskylä. I value dearly all the knowledge gained at the mass spectrometry laboratory in Jyväskylä.

I am very grateful to all the co-authors from Laboratory of Chemical Physics at NICPB, and Department of Chemistry and Biotechnology at TalTech for their work and inspiring discussions. I want to thank Dr. Aleksander Trummal and Dr. Merle Uudsemaa for providing computational data of the gas-phase complex studies and Dr. Mikk Kaasik for all his help in halogen bond topic. I want to thank the Lab 429 members who I have had the pleasure to work with throughout the years and members of TalTech Supramolecular group with whom I have been working with on one topic or another over the years and who have helped me with my work by giving me feedback and sharing their professional knowledge.

I am forever grateful to my family and closest friends for their unconditional support. Estelle, thank you for all the amazing university memories. Finally, to my husband, thank you for always being by my side, you are my best friend.

## Abstract

### An investigation of noncovalently bound supramolecular systems through case studies of oxacalixarenes and iodo-triazoles

The importance of noncovalent bonding on its own has been an area of interest in catalysis; for example, halogen bond (XB)-forming catalysts have been utilized. Another important aspect of noncovalent binding is in the design of supermolecules, e.g., macrocycles and their self-assemblies. The success of calixarene macrocycles lies in their synthetic approachability, which has led to the development of macrocycles that are used in many applications. In the literature overview of this thesis, the various noncovalent bonds and their formation properties are discussed, with examples drawn from calixarene supramolecular assemblies and host–guest complexes. The concept of supramolecular hosts is explained, with a brief overview of cyclodextrins, crown ethers, and cucurbiturils; further insight is given regarding calixarenes and its heteracalixaromatic subclass. The last chapter of the literature overview provides a brief introduction to select solution and gas-phase methods that are used to measure binding constants of noncovalently interacting systems.

The results are divided into three chapters. The first chapter includes an introduction to oxacalixarene synthesis methods, with an emphasis on the fragment coupling pathways used in this work to synthesize macrocycles, and the results of the solid-state structure analysis of unsubstituted oxacalix[*n*]arenes (*n* = 4, 8) are given. The host–guest properties were evaluated by solution NMR, with various neutral aromatic guests. Unsubstituted oxacalix[4]arene exhibited weak interactions with aromatic guests (benzoic acid, ferrocene, 1,5-dimethylnaphthalene, neocuproine, 3-methylcatechol), while no complex formation was detected for oxacalix[8]arene. In the second chapter of the oxacalixarene studies, the oxacalixarene solubility was expanded to protic solvents, thereby making it possible to study binding in a new media. The carboxyl-substituted oxacalix[4]arene was synthesized, and its structure was characterized in the solid state and in solution by employing SCXRD and NMR. The macrocycle was found in its dimeric form only in the solid state. In its anionic form, the oxacalixarene carboxylate formed a complex with the herbicide paraquat in methanol, with an association constant of  $K_a = 2020 \pm 70 \text{ M}^{-1}$ , which is one of the highest  $K_a$  values published for an organic cation–oxacalixarene complex. The chapter concludes with a gas-phase study of the carboxyl-substituted macrocycle and various amine complexes. Seven host–guest complexes were detected by ESI-MS; for four of them, gas-phase host–guest structures were confirmed by IM-MS. Gas-phase structures of the complexes were further confirmed with a combination of IM-MS and computational chemistry methods. This study showed that reliable structure elucidation of oxacalixarene complexes can be achieved with these methods. In the third chapter, a selection of triazole-salts was analyzed to understand the structural effects of the XB donor on XB formation in solution. The results revealed that the counterions had the highest effect on neutral XB acceptor binding. The best XB donor candidate found in the study did not display any enantiodiscrimination towards amine and imine enantiomers.

Overall, the findings of this work demonstrate the importance of understanding the structural effects of oxacalixarenes and iodo-triazole XB donors and contribute to our knowledge of their noncovalently formed assemblies. This work will aid in the future development and design of oxacalixarenes and XB donors with increased binding efficiency.

## Lühikokkuvõte

### Mittekovalentsete sidemete abil moodustunud supramolekulaarsete süsteemide uurimine oksakaliksareenide ja jodotriasoolide näitel

Mittekovalentsed interaktsioonid on tuntud organokatalüüsis, kus nii vesinik- kui ka halogeensidemeid on kasutatud erinevate substraatide aktiveerimiseks. Mittekovalentsete sidemete moodustumine on samuti keskne idee supramolekulaarses keemias tuntud makrotsükli iseorganiseerumise uurimises ja “võõrustaja-külaline” kompleksühendite tekkes. Üks enim uuritud makrotsükli klasse on kaliksareenid, kuhu kuuluvad makrotsükliidid sünteesiti esmakordselt juba 19. sajandil, kuid mille “võõrustaja-külaline” interaktsioonide abil moodustuvaid molekulideüleseid materjale uuritakse senimaani. Kaliksareenid on kergesti derivatiseeritavad ning sõltuvalt asendajatest jagatakse alamliikideks. Üheks alamliigiks loetakse oksakaliksareene, mida iseloomustab hapnikusildade olemasolu metüleensildade asemel. Doktoritöö kirjanduse osas antakse lühike ülevaade mittekovalentsete interaktsioonide tüüpidest, mis on illustreeritud näidetega kaliksareenide keemiast. Sellele järgnevas kirjanduse osas iseloomustatakse lähemalt supramolekulaarsete “võõrustaja” ühendite klasse nagu tsükloodekstriinid, krooneetrid ja kukurbituriinid ning selgitatakse nende makrotsükliidide struktuuride põhjal kompleksühendite moodustumisvõimaluste erinevusi heterakaliksareenidest ning nende perspektiive erinevates rakendustes. Kirjanduse ülevaate viimases osas kirjeldatakse erinevaid lahuse ja gaasifaasi meetodeid, mida selles töös kasutati iseorganiseerunud kompleksühendite sidumiskonstantide määramiseks.

Doktoritöö tulemused ja arutelu on jagatud kolmeks peatükiks. Esimeses peatükis tutvustatakse erinevaid sünteesiteid oksakaliksareenide moodustamiseks ning makrotsükliidide monokristall-röntgendifraktsioon analüüsi ja TMR spektroskoopia tulemusi tahkes faasis ja lahuses. Oksakaliks[4]areeni komplekseerumisomadusi hinnati kuue külalismolekuliga ning interaktsioone bensoehappe ja ferrotseeniga analüüsiti kloroformis  $^1\text{H}$  TMR tiitrimismeetodiga. Teostatud analüüside tulemused näitasid oksakaliks[4]areeni madalat afiinsust aromaatsete ühendite suhtes. Edasine eesmärk oli parandada oksakaliksareenide lahustuvust protoonsetes lahustites, et hinnata makrotsükli vee lahustuvate toksiliste külalismolekulide sidumise võimet. Teises peatükis kirjeldataksegi uue karboksüülasedatud oksakaliks[4]areeni sünteesi ning makrotsükliidide struktuuranalüüsi. Karboksüülasedatud oksakaliks[4]areeni kristallstruktuur näitas, et makrotsükkel on dimeeri kujul. Dimeerse kapsli olemasolu kontrolliti ka lahuses, kus vastavat struktuuri ei leitud. Sidumiskonstantide määramiseks analüüsiti karboksüülasedatud oksakaliks[4]areeni tetrabutüülammooniumi soola kujul. Makrotsükliidide komplekseerumisvõimet parakvaadiga, inimesele mürgise herbitsiidiga, hinnati metanoolis ja vees. Metanoolis mõõdeti kompleksi  $K_a$  väärtuseks  $2020 \pm 70 \text{ M}^{-1}$ , mis on seni üks kõrgemaid sidumiskonstante, mis on avaldatud oksakaliksareeni ja orgaanilise katiooni kompleksile. Oksakaliksareenide teema viimases osas uuriti karboksüülasedatud oksakaliks[4]areeni komplekseerumisomadusi amiinidega. Komplekse uuriti ESI-MS ja IM-MS meetoditega. Isoleeritud kompleksi ioonidele mõõdeti ioonmobiilsusajad, mis vastasid kompleksite suurustele. Nelja kompleksi kvantkeemiliste meetodite abil optimeeritud geomeetriad langesid hästi kokku mõõdetud parameetritega (CCS), mis tõestas teoreetiliste struktuuride samasust gaasifaasis mõõdetud kompleksühenditega. Töö kolmandas peatükis analüüsiti halogeensidemete

doonorite sidumiskonstante neutraalse halogeensideme aktseptoriga. Triasooli-põhiste doonorite struktuuride erisuse mõju käituda halogeensideme doonorina, analüüsiti kloroformis  $^1\text{H}$  TMR tiitrimismeetodiga. Leiti, et halogeensideme doonori vastasioonidel oli kõige suurem mõju halogeensideme moodustumisele. TMR tiitrimiskatsed kiraalsete halogeensidemete aktseptoritega näitasid, et triasooli-põhised doonorid ei erista enantiomeere.

Antud doktoritöö tulemused aitavad hinnata oksakaliksareenide ja halogeensidemete doonorite kompleksühendite moodustumist. Saadud tulemustel põhinedes saab tulevikus sünteesida uusi ja efektiivsemate sidumisomadustega oksakaliksareene ja halogeensidemete doonoreid.

## Appendix 1

### Publication I

Peterson, A.; Kaabel, S.; Kahn, I., Pehk, T.; Aav, R., Adamson, J. Unsubstituted Oxacalix[*n*]arenes (*n*=4 and 8): A Conformational Study in Solution and Solid State and Interaction Studies with Aromatic Guests. *ChemistrySelect* **2018**, 3, 9091-9095.

Reprinted with permission. Copyright © 2018, Wiley-VCH Verlag GmbH & Co. KGaA, Weinheim.



## Organic &amp; Supramolecular Chemistry

Unsubstituted Oxacalix[*n*]arenes (*n* = 4 and 8): A Conformational Study in Solution and Solid State and Interaction Studies with Aromatic GuestsAnna Peterson,<sup>[a, b]</sup> Sandra Kaabel,<sup>[b]</sup> Iiris Kahn,<sup>[b]</sup> Tõnis Pehk,<sup>[a]</sup> Riina Aav,<sup>\*[b]</sup> and Jasper Adamson<sup>\*[a]</sup>

We present single crystal structures of unsubstituted oxacalix[4]arene and oxacalix[8]arene macrocycles and investigate the weak supramolecular interactions that govern their packing in the solid state. We further show that the unsubstituted oxacalix[4]arene shows weak complexation with two aromatic guest species, benzoic acid and ferrocene, in CDCl<sub>3</sub>, whereas the oxacalix[8]arene host does not complex with these guest

molecules. We also present NMR titration experiments with non-aromatic acids and DFT calculations that signify the importance of  $\pi$ - $\pi$  interactions for complexation with benzoic acid. Weak complexation is also observed between electron-rich aromatic guest molecules and the unsubstituted oxacalix[4]arene host.

## Introduction

Macrocycles are cyclic oligomers that are widely investigated in modern supramolecular science due to their broad capacity for molecular recognition. A number of families of macrocycles, e.g., crown ethers,<sup>[1,2]</sup> cyclodextrins,<sup>[3]</sup> cucurbiturils,<sup>[4,5]</sup> and calix[*n*]arenes<sup>[6,7]</sup> are well-established and their host-guest complexation properties well-investigated.

Although oxacalix[*n*]arenes or oxa[1*n*]metacyclophanes are formally related to the third generation of synthetic receptors or calix[*n*]arenes, these potential host compounds are comparatively much less investigated.<sup>[8]</sup> In the structures of oxacalix[*n*]arenes, oxygen-bridges replace the methylene linkages between aromatic linkers that results in macrocycles combining the key features of crown ethers and calix[*n*]arenes. Therefore, oxacalix[*n*]arenes have unique cavity sizes and shapes as well as capability for both hydrogen-bonding and  $\pi$ - $\pi$  interactions.

In fact, the first of these compounds was discovered in 1966, however, isolation of pure substances was challenged by poor synthetic yields and solubility of the products.<sup>[9]</sup> Interest in oxacalix[*n*]arenes was revived in 2005 when Katz and coworkers realized the great potential of nucleophilic aromatic substitution (S<sub>N</sub>Ar) protocols for the synthesis of a number of nitro-substituted oxacalix[4]arenes in high yields.<sup>[10]</sup> Since then, other research groups have complemented the library of oxacalix[*n*]arenes by utilizing various aromatic linkers,<sup>[11,12]</sup> substituents

(e.g., aliphatic,<sup>[13]</sup> amine,<sup>[14]</sup> halide<sup>[15]</sup> groups) and introducing larger odd- and even-numbered oxacalix[*n*]arenes (*n* = 5–8).<sup>[16,17]</sup> The emerging subclass of oxacalix[*n*]arenes that incorporates heterocyclic aromatic linkers is known as oxacalix[*n*]hetarenes.<sup>[8]</sup>

Despite the synthetic endeavors in the field, host-guest recognition properties of oxacalix[*n*]arenes remain poorly understood and have a primary focus on substituted oxacalix[4]arenes or oxacalix[4]hetarenes. Specific examples include the work by Katz and coworkers who studied *o*-salicylic acid complexation with oxacalix[4]naphthalene[2]naphthyridine<sup>[11]</sup> and by Shimizu et al. who showed ferrocene and its oxidized form ferrocenium to complex with nitro-substituted oxacalix[4]arenes.<sup>[18]</sup> In 2015, the group of Gattuso showed polycationic oxacalix[4]arenes to complex with paraquat and neutral aromatic guests in aqueous media.<sup>[19,20]</sup>

Another class of macrocycles that are comparable with oxacalix[4]arenes are unsubstituted or dehydroxylated calix[4]arenes that have capacity for  $\pi$ - $\pi$  interactions alone.<sup>[21]</sup> Investigation of such macrocycles started with the work of Biali and coworkers,<sup>[22]</sup> however, to the best of our knowledge, their host-guest complexation studies are also relatively scarce.<sup>[23]</sup>

In this work, we prepared oxacalix[4]arene (**1a**) and oxacalix[8]arene (**1b**) (Figure 1) hosts based on the fragment-coupling synthesis procedure, published originally by Zhou et al.,<sup>[24]</sup> to explore their conformation in solution and solid state and to determine their complexation properties in comparison to other oxacalix[*n*]arenes and oxacalix[*n*]hetarenes. Herein, we present, for the first time, the crystal structures of **1a** and **1b**, together with a study of the weak supramolecular forces directing the aggregation of these molecules in the solid state. Furthermore, we describe the complexation properties of **1a** and **1b** with aromatic guest molecules, which indicates the strength of complexation of the “naked” oxacalix[*n*]arene scaffold.

[a] A. Peterson, Prof. T. Pehk, Dr. J. Adamson  
Chemical Physics Laboratory, National Institute of Chemical Physics and Biophysics, Akadeemia tee 23, 12618, Tallinn, Estonia  
E-mail: jasper.adamson@kbfi.ee

[b] A. Peterson, S. Kaabel, Dr. I. Kahn, Prof. R. Aav  
Department of Chemistry and Biotechnology, Tallinn University of Technology, Akadeemia tee 15, 12618 Tallinn, Estonia  
E-mail: riina.aav@ttu.ee

Supporting information for this article is available on the WWW under <https://doi.org/10.1002/slct.201801590>

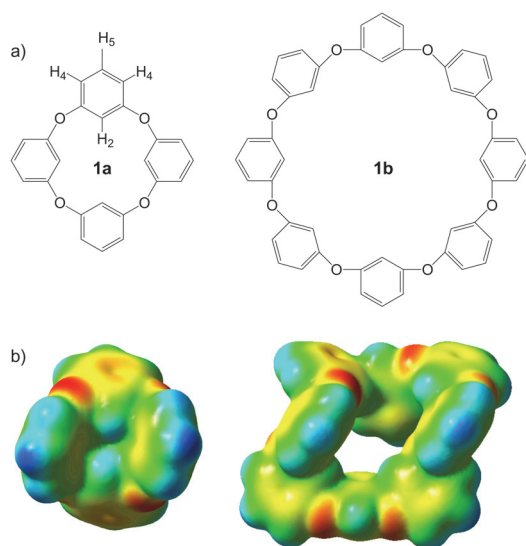


**Figure 1.** a) Structure of oxacalix[4]arene (**1a**) with indication of proton numbers and oxacalix[8]arene (**1b**) investigated in this work. b) molecular electrostatic potential images for **1a** and for **1b** as visualized by GaussView 5.0.8.

## Results and Discussion

### Crystal structures of **1a** and **1b**

Two polymorphs of the compound **1a** were obtained, one in a centrosymmetric space group  $C2/c$ , with half of the macrocycle in the asymmetric unit and second in a polar non-centrosymmetric space group  $P-42_1c$  with one quarter of **1a** in the asymmetric unit; see Supporting information (SI) for crystallographic details. Overlay of the oxacalix[4]arene molecules in polymorphs I and II shows that the conformation of **1a** changes very little between the two crystal structures (Fig-

ure S1), indicating that the polymorphism of these structures does not root from conformational differences, but is rather the result of differences in crystal packing.

Dominant intermolecular interactions within the crystal structures of the two polymorphs of **1a** were explored by the whole-molecule approach of energy framework analysis<sup>[25,26]</sup> using the *CrystalExplorer*<sup>[27]</sup> software (See SI for details), together with a more detailed look on specific intermolecular contacts. Packing of the macrocycles is mainly directed by off-center aromatic-aromatic interactions, known for electron-rich aromatic systems,<sup>[28]</sup> and multiple weak C–H...O hydrogen bonds. Oxacalix[4]arene adopts a 1,3-alternate saddle-shaped conformation in the crystal structures, which leads to a columnar stacking of **1a** in both of the polymorphs (Figure 2c). Based on the calculated energy frameworks the stacking forces are the dominant intermolecular interactions in both polymorphs (Figure 2a, b). Interaction energies between nearest neighboring molecules in the two polymorphic structures are included in the Supporting Information (Table S1 and S2)

Discrepancies in the packing of the two polymorphs I and II becomes evident when comparing the hydrogen bonding motifs in the respective crystal structures. In polymorph I, four outgoing hydrogen bonds, C6–H6...O1<sup>i</sup> ( $d(\text{H}\cdots\text{O})=2.573 \text{ \AA}$ ), and its symmetry equivalents, connect **1a** into wavy ribbons along the crystallographic  $c$  axis (Figure 2c), which are further interconnected through a ladder arrangement of four outgoing hydrogen bonds: C9–H9...O2<sup>ii</sup> ( $d(\text{H}\cdots\text{O})=2.690 \text{ \AA}$ ) and its symmetry equivalents (Figure 2d). In the oriented non-centrosymmetric crystal structure of polymorph II, eight outgoing hydrogen bonds, C4–H4...O1<sup>i</sup> ( $d(\text{H}\cdots\text{O})=2.646 \text{ \AA}$ ) and its symmetry equivalents, connect the columnar stacks of **1a** in helical motifs along the crystallographic axis  $c$  (Figure 2e).

The compound **1b** crystallized in space group  $P2_1/c$ , with the whole molecule of **1b** in the asymmetric unit. Weak C–H...O hydrogen bonds and  $\pi$ - $\pi$  stacking appear to direct the supramolecular aggregation of this crystal structure. Two molecules of **1b**, connected through four hydrogen bonds  $C2C\cdots H2C\cdots O1^i$  ( $d(\text{H}\cdots\text{O})=2.677 \text{ \AA}$ ),  $C6E\cdots H6E\cdots O1A^i$  ( $d(\text{H}\cdots\text{O})=2.414 \text{ \AA}$ ) and their symmetry equivalents, form a dimer, in

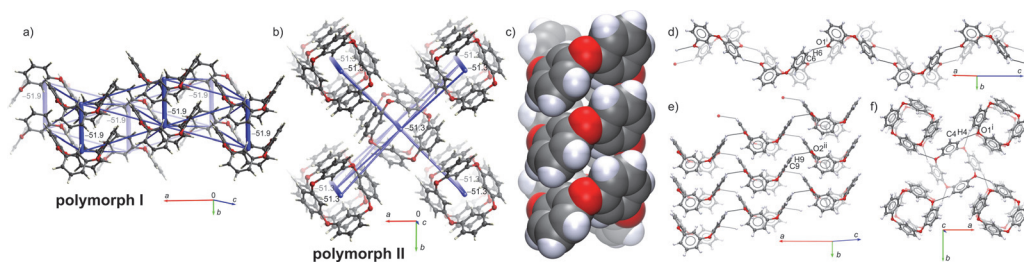


**Figure 2.** Energy-framework diagrams for the polymorphs I a) and II b) of **1a** (CCDC 1836367 and 1836368 respectively), showing the total energy  $E_{\text{tot}}$  in blue cylinders, whose thickness represents the relative strength of molecular packing in different directions within the crystal structure. Both diagrams use a scale factor of 50 and a threshold of  $5 \text{ kJ mol}^{-1}$ . The  $E_{\text{tot}}$  contribution from the stacking interaction is indicated on the figures.<sup>[27]</sup> c) The CPK visualisation of the columnar stacking of **1a**. Ribbon d) and ladder e) hydrogen bonding motifs in polymorph I of **1a**. Symmetry codes: i)  $1-x, -y, 1-z$ ; ii)  $1/2-x, -1/2+y, 1.5-z$ . f) Helical arrangement of the eight outgoing hydrogen bonds in the polymorph II. Symmetry code: i)  $1/2+x, 1/2-y, 1/2-z$ . Colour codes: C grey, O red and H white. The C–H...O hydrogen bonds  $d(\text{C}\cdots\text{H}\cdots\text{O}) \leq \sum(r(\text{vdW})[\text{H}, \text{O}])$  are drawn in black stippled lines.

which four aromatic rings are arranged parallel, indicative of off-center  $\pi$ - $\pi$  interactions (Figure 3c, d). These dimers are

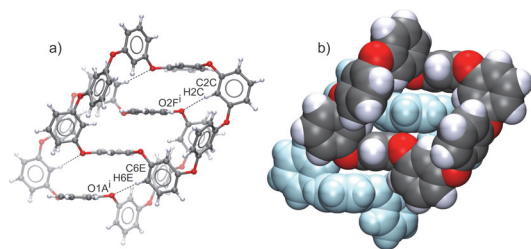


**Figure 3.** a) Dimeric units in the crystal structure of **1b**, interconnected through four C-H...O hydrogen bonds and off-center aromatic-aromatic stacking. b) CPK visualization of the tight packing of the **1b** molecules in the dimer. Symmetry code: 1-x, 1-y, 1-z. The C-H...O hydrogen bonds ( $C-H\cdots O \leq \Sigma r(vdW)[H, O]$ ) are drawn in black stippled lines.

further packed tightly side-by-side, so that the resulting crystal structure contains no voids (determined using probe radius 1 Å).

### Conformations of **1a** and **1b** in solution

For an investigation of the conformations of **1a** and **1b** in solution, we performed variable temperature solution  $^1\text{H}$ NMR and  $^{13}\text{C}$ NMR experiments on **1a** and **1b** in  $\text{CDCl}_3$ . No line broadening was seen in the temperature region 230–288 K (Figure S11), evidencing that either the structures are in a static conformation in solution or alternatively the rate of exchange between different conformations is so fast on the NMR time scale that no significant line broadening is seen at these temperatures for either macrocycle. Such observations have been made by other researchers for previous studies of substituted oxalix[4]arenes and oxalix[4]hetarenes.<sup>[10,29,30]</sup>

Moreover, we observe an upfield shift for the  $\text{H}_2$  and  $\text{C}_2$  proton and carbon resonances upon cooling. These proton and carbon atoms point towards the inner cavity of **1a** and **1b**, and this result is in agreement with previous studies that suggest that these upfield shifts could originate from some degree of reorientation of the atoms in the anisotropic shielding cone of adjacent aromatic groups and indicate that similarly to other oxalix[4]arenes and oxalix[4]hetarenes, conformations of **1a** and **1b** in solution might resemble their static conformations in the solid state.<sup>[8]</sup>

### Complexation in solution (NMR titrations)

Our following pursuit was to investigate complexation properties of **1a** and **1b** with a set of aromatic guest molecules in solution state (Figure 4). All the selected guest species have potential to form  $\pi$ - $\pi$  interactions with **1a** and **1b**, which could be complemented by hydrogen-bonding in the case of benzoic acid (**2**) and 3-methyl-catechol (**6**).

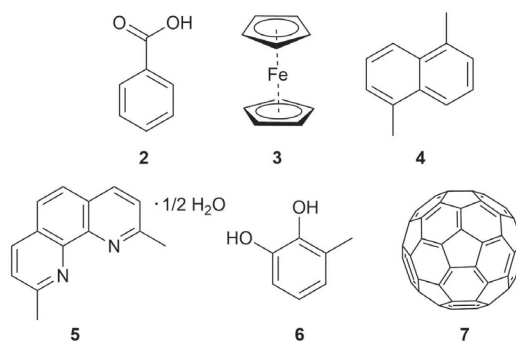


**Figure 4.** Guest molecules studied for complexation in this investigation.

It is noteworthy that **1a** and **1b** are aromatic molecules, where benzene linkers are connected by oxygen-bridges. The oxygen atoms in the linkages bear free electron pairs that can be conjugated with the aromatic moieties in the macrocycle, making the aromatic groups electron-rich. The calculated molecular electrostatic potential (MEP) images for **1a** and **1b** show that the edges of the aromatic linkers are electron-rich and the center of the aromatic linkers is electron-deficient (Figure 1b). Systems of this kind could form off-center or T-shaped  $\pi$ - $\pi$  interactions with other aromatic species<sup>[31]</sup> as well as serve as hydrogen-bond acceptors through the oxygen-linkages.

The first complexation experiments in this work were performed between **1a** and the electron-deficient guest molecule **2**, which carries functional groups that allow for hydrogen-bonding and  $\pi$ - $\pi$  interactions. Two sets of NMR titration experiments were carried out in this work, at 4.5 mM and 45 mM concentrations of **1a** in  $\text{CDCl}_3$ , which both indicated weak binding with the guest species (Figure 5a), however, the binding was not sufficiently strong to reach the data points with the binding probability between 0.2 and 0.8,<sup>[32,33]</sup> and therefore the association constant values reported in the SI are meant to serve as estimations.

We next undertook an NMR titration experiment with trifluoroacetic acid (TFA) to probe NMR shift changes of **1a** by the change of the acidity of the media. TFA is a stronger acid ( $\text{p}K_a = 0.23$ )<sup>[34]</sup> than **2** ( $\text{p}K_a = 4.20$ ).<sup>[35]</sup> Therefore, if NMR shift changes would be induced by the acidity of the media, one would expect pronounced changes in **1a** signals. Contrary to that, a negligible change in the shifts of  $\text{H}_2$  and  $\text{H}_4$  and an upfield shift of  $\text{H}_2$  in **1a** upon addition of TFA was observed (Figure 5b). Downfield shifts of all host hydrogens upon binding of **2** (Figure 5a) show that interaction with benzoic acid has different character compared to acidic non-aromatic guest molecules. Since TFA is a non-aromatic acid,  $\pi$ - $\pi$  interactions for complexation are excluded for both these molecules, which allows us to conclude that  $\pi$ - $\pi$  interactions have a key contribution to binding between **1a** and **2** and that the

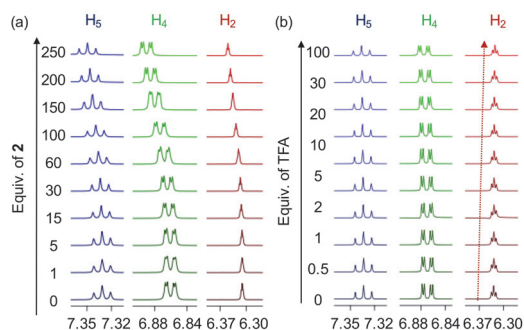


**Figure 5.** Evolution of proton resonances of a 45 mM solution of **1a** in  $\text{CDCl}_3$  at 288 K upon a) addition of up to 250 equivalents of **2** and b) addition of up to 100 equivalents of TFA. The three aromatic proton resonances are shown separately. Upon addition of **2**, all proton resonances shift downfield, whereas upon addition of TFA, an upfield change of chemical shift is observed for  $\text{H}_2$  proton resonance.

changes in the spectra we have observed are not induced by changes in the pH of the solution.<sup>[36]</sup>

Further insight into the possible dominant interactions for complexation was given by DFT calculations. Zuo et al. have calculated the structures and conformational energies for a series of calixarenes<sup>[37]</sup> including oxacalix[4]arene studied in this work. Their choice of the B3LYP functional was in part made because the macrocycle was considered too constrained for the aromatic groups to undergo  $\pi$ - $\pi$  stacking; the main source of deficiency in this functional. Our choice of the functional M06-2X<sup>[38]</sup> was primarily made based on its ability to take into account the dispersion effects of  $\pi$ -electron density around aromatic rings because of their importance in the complex formation<sup>[39]</sup> between **1a** and the guest molecule **2**.

Our conformational analysis of **1a** yielded two low energy conformers (structures shown in Figure S19). The lowest energy structure was similar to the crystal structure. We next investigated the potential interactions between the lowest energy geometry of **1a** and **2**. The choice of initial geometries for complexation between **1a** and **2** was based on a T-shaped  $\pi$ - $\pi$  interaction, an off-center  $\pi$ - $\pi$  interaction and hydrogen-bonding. Three binding geometries gave either one or more of these weak supramolecular interactions (Figure 6). In the lowest energy geometry, benzoic acid made one T-shaped and one off-center  $\pi$ - $\pi$  interaction with phenyl groups in **1a**. Binding geometry II was 0.233 kcal/mol higher in energy and also allowed for the formation of a hydrogen bond between the carboxylic hydrogen and the ether oxygen (2.008 Å), while geometry III relied on one off-center  $\pi$ - $\pi$  interaction and was 2.898 kcal/mol higher in energy than binding geometry I. Even different orientations of the carboxyl group did not allow for hydrogen bonding in this structure (see SI for details). Moreover, we aimed to calculate a fourth binding geometry that forms just one hydrogen bond between **1a** and **2**, however, this structure converted into conformation III in the course of the geometry optimization. It is noted here that these

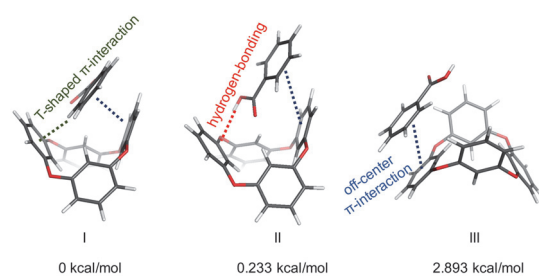


**Figure 6.** The three complexation geometries calculated with DFT calculations in this work. The lowest-energy complexation geometry is without any hydrogen-bonding interactions.

computational results serve as an estimation for interactions for complexation between **1a** and **2** as the binding demonstrated by NMR titration experiments was very weak in methanol- $d_4$ .

Shimizu and coworkers showed ferrocene to complex with nitro-substituted oxacalix[4]arenes,<sup>[40]</sup> which led to our interest whether complexation could be detected with unsubstituted oxacalix[4]arene. The NMR titration results of **1a** and guest **3** showed weak binding (see SI for details). Intriguingly, the peak arising from guest molecule **3** near 4.2 ppm shifted upfield when up to 5 equivalents of the guest was added, followed by downfield shifts thereafter, which could indicate aggregation of the guest species **3** during the titration experiment.

We also observed, albeit weak, complexation of **1a** with 1,5-dimethylnaphthalene (**4**) and neocuproine (**5**) in  $\text{CDCl}_3$  and 3-methylcatechol (**6**) in toluene- $d_6$ . Even though guest species **4**, **5** and **6** showed binding with **1a**, association constant determination was set aside due to the poor solubility of **4**, **5** and **6** in these solvents. The spectra for complexation and the respective changes in chemical shifts for **1a** with **4**, **5**, and **6** are brought in SI. Moreover, calix[*n*]arene derivatives have been shown to complex with fullerene  $\text{C}_{60}$  (**7**) in toluene- $d_6$ ,<sup>[41,42]</sup> however, the oxacalix[*n*]arenes **1a** and **1b** did not show complexation based on the  $^1\text{H}$  or  $^{13}\text{C}$ NMR spectra for a 2:1 molar mixture of the host and the guest species **7**, which could arise from the competitive  $\pi$ - $\pi$  interactions of **1a** with the solvent.

The guest species **2** and **3** were selected to probe complexation with oxacalix[8]arene **1b**. Addition of 100 equivalents of either **2** or **3** showed almost undetectable changes in chemical shifts between the host and the guest molecules (see Table S4). This is likely to arise from a size mismatch between the cavity of the guest molecules or the more flexible nature of the larger host compound.

## Conclusions

In conclusion, the interactions governing the packing of the oxacalix[*n*]arene ( $n=4$  and 8) macrocycles in their unprecedented solid state structures are characterized. Our solution state conformational study coincides with previous reports for

substituted oxacalix[4]arenes and does not allow to differentiate whether the macrocycles are in fast conformational exchange or in a static conformation in solution. NMR titration experiments with benzoic acid and ferrocene show weak complexation at room temperature. The oxacalix[8]arene host does not show detectable complexation in solution with ferrocene and benzoic acid, which is attributed to their size mismatch or the more flexible nature of the host.

### Supporting Information Summary

Detailed experimental section, details of analysis of interaction energies in the crystal structures, variable temperature NMR spectra, NMR spectra for compounds **1a** and **1b** with and without guest species **2-7**, NMR titration experiments results and further DFT calculation details.

### Acknowledgements

This research was supported by the Estonian Ministry of Education and Research through Grants MOBJD39, IUT23-7 and PUT692 and the EU European Regional Development Fund through grant TK134. We would like to acknowledge Kari Rissanen for help with the manuscript.

### Conflict of Interest

The authors declare no conflict of interest.

**Keywords:** conformational study · host-guest complexation · oxacalix[n]arene · NMR titration · nuclear magnetic resonance · single crystal structure

- [1] C. J. Pedersen, *Angew. Chemie Int. Ed. English* **1988**, *27*, 1021–1027.
- [2] M. Hiraoka, *Crown Ethers and Analogous Compounds*, Elsevier, **2016**.
- [3] G. Crini, *Chem. Rev* **2014**, *114*, 10940–10975.
- [4] W. A. Freeman, W. L. Mock, N. Y. Shih, *J. Am. Chem. Soc.* **1981**, *103*, 7367–7368.
- [5] K. I. Assaf, W. M. Nau, *Chem. Soc. Rev.* **2015**, *44*, 394–418.
- [6] M.-Z. Asfari, V. Böhmer, J. Harrowfield, J. Vicens, *Calixarenes 2001*, Springer Science & Business Media, **2007**.
- [7] J. Vicens, V. Böhmer, *Calixarenes: A Versatile Class of Macrocyclic Compounds*, Springer Science & Business Media, **2012**.
- [8] W. Maes, W. Dehaen, *Chem. Soc. Rev.* **2008**, *37*, 2393–2402.
- [9] N. Sommer, H. A. Staab, *Tetrahedron Lett.* **1966**, *7*, 2837–2841.
- [10] J. L. Katz, M. B. Feldman, R. R. Conry, *Org. Lett.* **2005**, *7*, 91–94.
- [11] J. L. Katz, B. J. Geller, P. D. Foster, *Chem. Commun.* **2007**, *10*, 1026–1028.
- [12] W. Van Rossom, J. Caers, K. Robeyns, L. Van Meervelt, W. Maes, W. Dehaen, *J. Org. Chem.* **2012**, *77*, 2791–2797.
- [13] S. Akagi, Y. Yasukawa, K. Kobayashi, H. Konishi, *Tetrahedron* **2009**, *65*, 9983–9988.
- [14] C. Capici, D. Garozzo, G. Gattuso, A. Messina, A. Notti, M. F. Parisi, I. Pisagatti, S. Pappalardo, *Ark. Online J. Org. Chem.* **2009**, *8*, 199–211.
- [15] R. D. Chambers, P. R. Hoskin, A. Khalil, P. Richmond, G. Sandford, D. S. Yufit, J. A. K. Howard, *J. Fluor. Chem.* **2002**, *116*, 19–22.
- [16] W. Van Rossom, K. Robeyns, M. Ovaere, L. Van Meervelt, W. Dehaen, W. Maes, *Org. Lett.* **2010**, *13*, 126–129.
- [17] W. Van Rossom, M. Ovaere, L. Van Meervelt, W. Dehaen, W. Maes, *Org. Lett.* **2009**, *11*, 1681–1684.
- [18] D. Sobransingh, M. B. Dewal, J. Hiller, M. D. Smith, L. S. Shimizu, *New J. Chem.* **2008**, *32*, 24–27.
- [19] N. Manganaro, G. Lando, C. Gargiulli, I. Pisagatti, A. Notti, S. Pappalardo, M. F. Parisi, G. Gattuso, *Chem. Commun.* **2015**, *51*, 12657–12660.
- [20] N. Manganaro, G. Lando, I. Pisagatti, A. Notti, S. Pappalardo, M. F. Parisi, G. Gattuso, *Supramol. Chem.* **2016**, *28*, 493–498.
- [21] J. E. McMurry, J. C. Phelan, *Tetrahedron Lett.* **1991**, *32*, 5655–5658.
- [22] F. Grynszpan, S. E. Biali, *Tetrahedron Lett.* **1991**, *32*, 5155–5158.
- [23] F. Inokuchi, Y. Miyahara, T. Inazu, S. Shinkai, *Angew. Chemie Int. Ed.* **1995**, *34*, 1364–1366.
- [24] Q. Zhou, L. Su, T. Jiang, B. Zhang, R. Chen, H. Jiang, Y. Ye, M. Zhu, D. Han, J. Shen, et al., *Tetrahedron* **2014**, *70*, 1125–1132.
- [25] M. J. Turner, S. Grabowsky, D. Jayatilaka, M. A. Spackman, *J. Phys. Chem. Lett.* **2014**, *5*, 4249–4255.
- [26] C. F. Mackenzie, P. R. Spackman, D. Jayatilaka, M. A. Spackman, *IUCrJ* **2017**, *4*, 575–587.
- [27] J. J. McKinnon, M. J. Turner, D. Jayatilaka, M. A. Spackman, D. J. Grimwood, S. K. Wolff, *Univ. West. Aust.* **2012**.
- [28] C. R. Martinez, B. L. Iverson, *Chem. Sci.* **2012**, *3*, 2191–2201.
- [29] R. D. Chambers, P. R. Hoskin, A. R. Kenwright, A. Khalil, P. Richmond, G. Sandford, D. S. Yufit, J. A. K. Howard, *Org. Biomol. Chem.* **2003**, *1*, 2137–2147.
- [30] M.-X. Wang, H.-B. Yang, *J. Am. Chem. Soc.* **2004**, *126*, 15412–15422.
- [31] C. R. Martinez, B. L. Iverson, *Chem. Sci.* **2012**, *3*, 2191–2201.
- [32] P. Thordarson, *Chem. Soc. Rev.* **2011**, *40*, 1305–1323.
- [33] C. S. Wilcox, *Front. Supramol. Org. Chem. Photochem.* **1991**, 123–143.
- [34] J. B. Milne, T. J. Parker, *J. Solution Chem.* **1981**, *10*, 479–487.
- [35] D. C. Harris, *Quantitative Chemical Analysis*, Macmillan, **2010**.
- [36] Katz et al. reported in their study in Ref. [11] that benzoic acid causes small upfield shifts (<0.05 ppm) in the resonances of oxacalix[4]naphthalene[2]naphthyridine, whereas downfield shifts are observed in this study. The analysis of this discrepancy is beyond the scope of this work, though worth highlighting in itself.
- [37] C. Zuo, O. Wiest, Y. Wu, *J. Phys. Org. Chem.* **2011**, *24*, 1157–1165.
- [38] Y. Zhao, D. G. Truhlar, *Theor. Chem. Acc.* **2008**, *120*, 215–241.
- [39] E. G. Hohenstein, S. T. Chill, C. D. Sherrill, *J. Chem. Theory Comput.* **2008**, *4*, 1996–2000.
- [40] D. Sobransingh, M. B. Dewal, J. Hiller, M. D. Smith, L. S. Shimizu, *New J. Chem.* **2008**, *32*, 24–27.
- [41] J. L. Atwood, G. A. Koutsantonis, C. L. Raston, *Nature* **1994**, *368*, 229–231.
- [42] S. Mized, M. Ashram, D. O. Miller, P. E. Georghiou, *J. Chem. Soc. Perkin Trans. 2* **2001**, 1916–1919.

Submitted: May 25, 2018

Accepted: July 9, 2018



## Appendix 2

### Publication II

Peterson, A.; Ludvig, M-L.; Martõnova, J.; Kaabel, S.; Kerner, P.; Uudsemaa, M.; Trummal, A.; Fomitšenko, M.; Pehk, T.; Aav, R.; Adamson, J. New oxacalix[4]arene carboxylate detects viologen in protic media, *Supramolecular Chemistry* **2020**, 32:5, 313-319.

Authors accepted manuscript reprinted with permission. Copyright © 2019, Informa UK Limited, trading as Taylor & Francis Group.



## New oxalix[4]arene carboxylate detects viologen in protic media

Anna Peterson<sup>a,b</sup>, Mari-Liis Ludvig<sup>a,b</sup>, Jevgenija Martõnova<sup>b</sup>, Sandra Kaabel<sup>b</sup>, Paul Kerner<sup>a</sup>, Merle Uudsemaa<sup>a</sup>, Aleksander Trummal<sup>a</sup>, Maria Fomitšenko<sup>b</sup>, Tõnis Pehk<sup>a</sup>, Riina Aav<sup>b</sup> and Jasper Adamson<sup>a</sup>

<sup>a</sup>Chemical Physics Laboratory, National Institute of Chemical Physics and Biophysics, Tallinn, Estonia; <sup>b</sup>Department of Chemistry and Biotechnology, Tallinn University of Technology, Tallinn, Estonia

### ABSTRACT

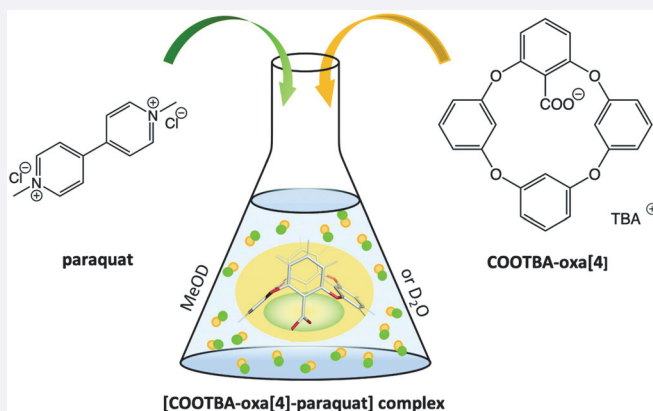
We demonstrate that Ullman fragment-coupling can be used to synthesise an oxalix[4]arene monocarboxylic acid, which provides easy access to its water-soluble carboxylate derivatives. Crystallographic and computational data suggest that the new carboxyl-substituted oxalix[4]arene adopts a 1,3-alternate conformation both in the solid-state and in methanol solution. Its water-soluble tetrabutylammonium derivate can detect the herbicide paraquat at neutral pH in aqueous media ( $K_a = 111 \pm 3 \text{ M}^{-1}$ ) and in methanol ( $K_a = 2020 \pm 70 \text{ M}^{-1}$ ).

### ARTICLE HISTORY

Received 14 July 2019  
Accepted 19 August 2019

### KEYWORDS

Oxalix[4]arene  
carboxylate; herbicide  
sensing; 1,3-alternate  
conformation



## Introduction

Oxalix[*n*]arenes, the oxygen-bridged heterocalixaromatics, are macrocyclic host compounds that provide unique cavity sizes and shapes and capability for hydrogen bonding and  $\pi - \pi$  interactions (1, 2). Nevertheless, this class of aromatic macrocycles has been significantly less explored compared to its carbon-bridged analogues, e.g. calix[*n*]arenes (3, 4), resorcin[*n*]arenes (5–8) and pillar[*n*]arenes (9–12).

Encapsulation of bipyridinium derivatives, including the harmful herbicide molecule paraquat, has seen much interest in supramolecular chemistry with the aim of reducing their toxicity through the development of viologen targeted chemosensors (13). As such, it has been shown that

carboxyl-decorated biphen[4]arene (14) as well as pillar[6]arene (15) can be used in complexation with cationic guest species, including the detection of harmful molecules by encapsulating them through non-covalent interactions (16, 17). This can potentially lead to applications in the treatment of toxicant poisoning by forming stable host-guest complexes with the toxic guest molecule (18). Additional examples of molecular recognition studies of toxicants in water include different-sized  $S_x$ -corona[*n*](het)arenes as host compounds (19, 20). To the best of our knowledge, only one example of an oxalix[*n*]arene, a polycationic tetraammonium macrocycle, that is able to complex with paraquat ( $[(C_6H_7N)_2]Cl_2$ ) in acidic aqueous media (21, 22) has been reported previously.

**CONTACT** Jasper Adamson  jasper.adamson@kbf.ee  Chemical Physics Laboratory, National Institute of Chemical Physics and Biophysics, Akadeemia tee 23, Tallinn 12618, Estonia; Riina Aav  riina.aav@taltech.ee  Department of Chemistry and Biotechnology, Tallinn University of Technology, Akadeemia tee 15, Tallinn 12618, Estonia

 Supplemental data for this article can be accessed here.

© 2019 Informa UK Limited, trading as Taylor & Francis Group

In general, S- and O-bridged [1,*n*]metacyclophanes, as electron-rich heterocalixaromatic macrocycles, have similar affinities towards cations (23–25), while NH-bridged azacalix[*n*]arenes (26) and triazine-containing oxacalix[*n*]arenes (27–29), have been employed mainly in anion recognition studies and complexation studies with neutral aromatic compounds such as C<sub>60</sub> fullerene (25, 30). Studies of oxacalix[4]arene complexation with cations have focused on complexation properties with metal cations by oxacalix[4]crowns (31, 32) and ferrocene and the ferrocenium cation complexes with nitro-substituted oxacalix[4]arenes ( $K_a = 87 \text{ M}^{-1}$  in CH<sub>2</sub>Cl<sub>2</sub>) (33), however, complexation in polar protic solvents remains quite unexplored due to the solubility of the oxacalix[*n*]arene macrocycles. As a scarce example, the aforementioned polycationic oxacalix[4]arene can bind paraquat (21) and neutral aromatic guest molecules (22) in acidic aqueous media with association constant values of  $K_a = 253 \text{ M}^{-1}$  and  $K_a = 44 \text{ M}^{-1}$ , respectively. In comparison, however, Wang and co-workers have shown that S-bridged heterocalixaromatics can bind aromatic dicationic guests (19, 20) with association constants in the range of  $10^3$ – $10^5$ . Therefore, the development of oxacalix[*n*]arene chemosensors that can strongly interact with cationic guest species in polar protic solvents is of great importance for utilising oxacalix[*n*]arenes in paraquat detection. Overcoming the weak complexation and solubility limitations of oxacalix[*n*]arenes by decorating their homooxalix[*n*]arene core could pave the way towards discovering the full potential of using these host molecules as selective chemosensors.

## Results and discussion

Herein, we report the synthesis of an oxacalix[4]arene carboxylic acid **1a**, according to a copper(I) and iron(III)

catalysed Ullman fragment-coupling protocol (34, 35) and convert the macrocycle to its anionic tetrabutylammonium derivative **1b**, shown in Figure 1(a). The **1a** macrocycle adopts a 1,3-alternate conformation in methanol solution, similarly to its solid-state structure, and we further determine that **1b** can bind dicationic paraquat in methanol and at neutral, including physiological, pH conditions in aqueous media.

## Synthesis

The three-step fragment-coupling synthesis procedure that we have explored to prepare unsubstituted oxacalix[*n*]arene (*n* = 4 and 8), previously (34, 35), resulted in **1a** in 14% yield. Details regarding the yield of the macrocycle are brought in ESI p. S3. **1a** could be converted to water-soluble **1b** by treatment with aqueous tetrabutylammonium hydroxide solution. The macrocycles' structures were confirmed by NMR, ESI-HRMS and single-crystal X-ray diffraction.

## Binding studies

In our work, we show that **1b** binds paraquat in protic media. Firstly, we performed <sup>1</sup>H NMR titration experiments in methanol (see ESI Fig. S8), whereby we determined the binding strength to be  $2020 \pm 70 \text{ M}^{-1}$  for this host-guest system [Figure 1(b)]. The fits to the titration data were obtained using a 1:1 binding isotherm in the open-source online fitting tool Bindfit (36). In comparison to previous studies that investigate oxacalix[4]arene macrocycles complexation with organic cations (21), the determined  $K_a$  value for the [**1b**-paraquat] complex in methanol is an order of magnitude larger. Secondly, we tested the ability of **1b** macrocycle to bind paraquat in aqueous solution (see ESI Fig. S10). The observed  $K_a$

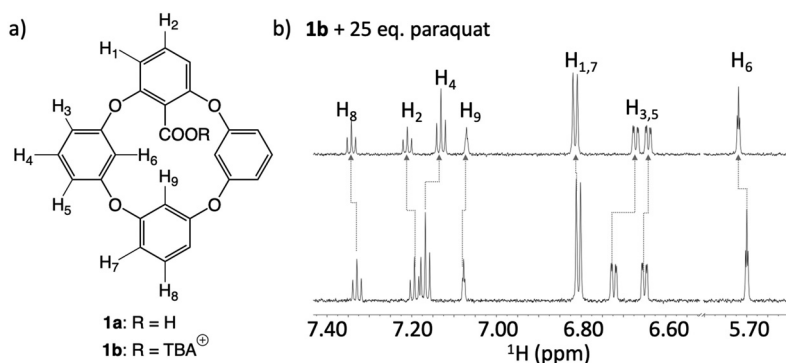


**Figure 1.** (a) Structures and designation of proton positions of the synthesised macrocycles **1a** and **1b** and (b) <sup>1</sup>H NMR spectra of [**1b**-paraquat] complex (top spectrum) and the native **1b** (bottom spectrum) in methanol-d<sub>4</sub> at 298 K.

value was  $111 \pm 3 \text{ M}^{-1}$  for this host-guest complex. The affinity of **1b** for paraquat in aqueous media is comparable to the aforementioned polycationic oxacalix[4]arene (21, 22). It is noteworthy that paraquat detection in aqueous media occurred at neutral pH values, which might be important for detection of paraquat in biological fluids. Moreover, much attention has been attributed to paraquat poisoning by government organisations due to its toxicity, nevertheless, no treatment methodologies with convincing efficiency currently exist (37, 38). This manifests in the need for new paraquat chemosensors that can trap the toxicant in a stable host-guest complex in cases of paraquat poisoning.

Subsequently, we studied the conformation of the **1a** macrocycle in solution and solid-state. The macrocycle **1a** adopts a 1,3-alternate saddle-shape conformation in the solid phase, similarly to the unsubstituted oxacalix[4]arene reported previously (35). However, owing to the strong hydrogen-bonding ability of the carboxylic acid groups, the packing of the **1a** chloroform solvate is directed largely by electrostatic interactions, in contrast to the predominantly dispersion-directed packing of the unsubstituted oxacalixarenes (35). Whole-molecule energy framework analysis (see ESI, pp. S7-S9) using the CrystalExplorer software (39) revealed that the strongest contribution to framework stability comes from the hydrogen bonds between the carboxylic acid groups of two molecules of **1a**,  $d(\text{O}-\text{H}\cdots\text{O}) = 1.76 \pm 0.03 \text{ \AA}$ , which form the dimeric motif (Figure 2). Weak C-H $\cdots$ O hydrogen bonds and aromatic-aromatic interactions, that mainly contribute to the dispersion term, stabilise the side-to-side stacking of the macrocycles into sheets parallel to

the ab-plane of the unit cell (Figure 2). Co-crystallised chloroform molecules are arranged between these sheets, potentially contributing to the observed rapid drying of the crystals when exposed to air.

The NMR spectra of the asymmetric **1a** macrocycle are valuable for providing information regarding its conformation in solution. It was suggested by Lehmann that oxacalix[4]arenes that contain two ortho-connected monomers adopt a saddle (now known as the 1,3-alternate) conformation in solution (40). Lehmann rationalised this based on the very upfield shifts of the inner aromatic protons (5.67 ppm) that relates to their relative position with respect to the anisotropic shielding cones of the adjacent aromatic monomers. In 2005, Katz et al. proposed nitro-substituted oxacalix[4]arenes to adopt the 1,3-saddle conformation, partly to maintain conjugation between the aromatic moieties (41). The experimental difference between the chemical shifts of the **1a** H<sub>6</sub> and H<sub>9</sub> protons that point towards the core of the macrocycle is 1.04 ppm (the protons give signals at 5.66 ppm vs 6.70 ppm, respectively) (40). To gain insight into the conformation of **1a** in solution, we carried out quantum-chemical calculations of the respective structural parameters and corresponding <sup>1</sup>H and <sup>13</sup>C NMR chemical shifts in methanol. Firstly, we optimised the solution-state geometry of the structure that showed a noticeable resemblance to the conformation of **1a** in the crystal structure (Figure S13).

Subsequently, the <sup>1</sup>H NMR chemical shifts were calculated at B3LYP GIAO and MN12-SX CSGT level of theory and the <sup>13</sup>C NMR chemical shifts at B3LYP CSGT and ICPSS GIAO level of theory (see ESI pp. S16-S28). The

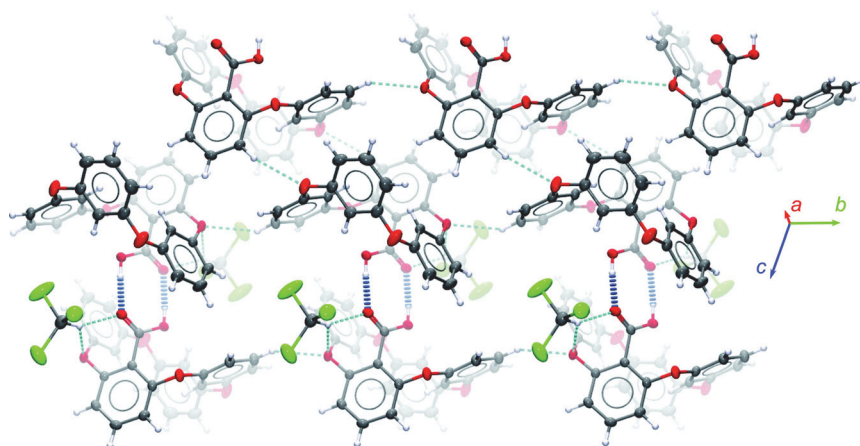


**Figure 2.** (colour online) Single-crystal XRD structure of **1a** showing the hydrogen-bonded dimers (interactions shown with dark blue dotted lines) and the side-to-side stacking of the macrocycles in the ab-plane of the unit cell of **1a** with the co-crystallised chloroform molecules. Crystallographic and computational data.

calculated chemical shifts are in good agreement with the experimental data. In particular, the experimental difference between the chemical shifts of the H<sub>6</sub> and H<sub>9</sub> protons is replicated in the calculations [Figure 3(a, b)]. Analogously to previous studies, this likely arises from the position of these protons with respect to the anisotropic shielding cones of the adjacent aromatic monomers [Figure 3(a)]. It is worth noting that when the adjacent aromatic groups were omitted in calculations, the H<sub>6</sub> proton resonances shifted considerably downfield, which is further discussed in the ESI. This finding and the agreement of experimental and calculated geometries suggest the solution-state conformation of **1a** in methanol to resemble the 1,3-alternate conformation of the solid-state. We hypothesise that the 1,3-alternate conformation is prerequisite for the strong binding in protic solvents discussed above, where two aromatic monomers and the carboxyl group of the third monomer form a defined binding cavity for a cationic guest molecule.

## Conclusion

We have synthesised a new oxacalix[4]arene macrocycle **1a**, which in its anionic form is able to bind with the cationic aromatic guest paraquat in methanol and aqueous media at neutral pH. The high binding affinity in methanol holds potential to contribute to the development of chemosensors that can selectively detect paraquat, *e.g.* in drinking water, and thereby aid to reduce its harmful effects. To the best of our knowledge, the K<sub>a</sub>

value in methanol is the largest reported between an organic cation and oxacalix[4]arene macrocycle to date. The strong binding of an aromatic cationic guest in protic media could arise from the static 1,3-alternate conformation in methanol, which creates a defined binding pocket, surrounded by two aromatic moieties and the carboxylate group.

## <sup>1</sup>H NMR titration

The association constant values for [**1b**-paraquat] complexes were determined from methanol-d<sub>4</sub> and D<sub>2</sub>O. All the solutions were prepared using Hamilton® Gastight syringes and samples were weighed on a Sartorius microbalance with an accuracy of 15 µg. **1b** stock solutions (0.2 mM) were added to a vial containing paraquat to keep the concentration of the macrocycle fixed throughout the titration experiment. Small aliquots from the paraquat stock solution were added increasingly (from 0 to 160–240 µl) to the NMR tube containing 600 µl of the **1b** stock solution. After every addition, the sample was thoroughly shaken using vortex and measured quantitatively, collecting 8 scans with relaxation delay set to 15 s and acquisition time set to 2.4 s. The changes in H<sub>4</sub> and H<sub>6</sub> proton shifts were monitored and after the addition of paraquat the followed protons shifted upfield with an exception of H<sub>6</sub> in methanol. No remarkable changes in chemical shifts of the guest were observed. The K<sub>a</sub> values were determined using non-linear regression analysis. For the fitting of the binding data the 1:1 binding isotherm of BindFit was used (freely

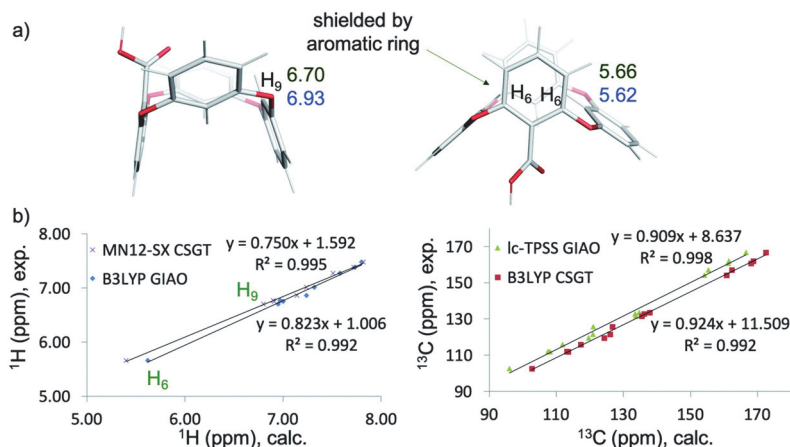


**Figure 3.** (colour online) (a) The positions of H<sub>6</sub> and H<sub>9</sub> protons with respect to the adjacent aromatic rings and their respective calculated and experimental chemical shifts. Numbers in green and blue denote experimental NMR chemical shifts and calculated chemical shifts (B3LYP/GIAO) in ppm, respectively, and (b) correlation between experimental and calculated <sup>1</sup>H and <sup>13</sup>C NMR chemical shifts for **1a** in methanol.

available at <http://supramolecular.org>). Herein, the given standard error depicts error coming from curve fit calculations. In aqueous media, the last titration point, with 23.7 eq of paraquat used as a guest, resulted in 66% of host-guest complex formation. See ESI pp. S10-S14 for further details.

### X-ray crystallography

Single crystals of **1a** were obtained by slow evaporation from chloroform. The small colourless crystals were found to be the chloroform solvate of **1a**, crystallised in the space group *P*-1 (Figure S5). Single crystal X-ray diffraction data was collected on a Rigaku Compact HomeLab diffractometer, equipped with a Saturn 944 HG CCD detector and Oxford Cryostream cooling system, at  $T = 123.0$  (1) K using monochromatic Cu- $K\alpha$  radiation (1.54178 Å) from a MicroMax<sup>TM</sup>.003 sealed tube microfocus X-ray source. The strategy of data collection was calculated using Rigaku *CollectionStrategy* (42), *CrysAlisPro* (43) was used for data reduction and empirical absorption correction using spherical harmonics implemented in *SCALE3 ABSPACK* scaling algorithm (44). The structure was solved using *SHELXT* (45) and refined by full-matrix least-squares method against  $F^2$  with *SHELXL-2016* (46) through *OLEX2* (47) program package. All non-hydrogen atoms were refined with anisotropic atomic displacement parameters. Hydrogen atoms on carbons were treated as riding on their parent atoms, with  $U_{iso}(H) = 1.2U_{iso}(C)$  for CH. The hydrogen atom of the carboxylic acid group was located from the Fourier difference map and refined freely ( $U_{iso}(H) = 0.0531$ ). The figures were drawn using the programs Mercury CSD 3.10 (48) and POV-Ray 3.7 (49).

### Computational data

The crystal structure of **1a** was optimised at B3LYP (50, 51)/6-311 + G(2d,p) (52, 53) level of theory and vibrational normal mode analysis was carried out to confirm the absence of imaginary eigenvalues. The effects of solvation were included in the framework of IEF-PCM (54, 55) dielectric continuum model representing methanol environment for all calculations. Another true minimum confirmation was obtained by 180 degrees rotation of the COOH group while the core of macrocycle remained intact. These two structures, being very close in total energy and resembling the overall appearance of the parent crystal structure, represent the whole conformational space of **1a** in methanol. Nuclear magnetic shielding tensors in gauge-independent atomic orbitals (GIAO) (56–60) and continuous set of gauge transformations (CSGT) (60–62) representations were calculated at B3LYP/6-311 + G(2d,p) level of theory for both hydrogen

and carbon atoms. Additionally, MN12-SX (63)/cc-pVTZ (64) and Ic-TPSSTPSS (65, 66)/cc-pVTZ methods were used for calculations of magnetic shieldings of hydrogens and carbons, respectively. Magnetic shieldings were converted to chemical shifts using TMS at B3LYP/6-311 + G(2d,p) GIAO level as a reference. The calculations were carried out using Gaussian 09 (67) and Gaussian 16 (68) software suites while GaussView package was used for analysing computational NMR data.

### Disclosure statement

No potential conflict of interest was reported by the authors.

### Funding

Our research is sponsored by the Estonian Research Council through grants PRG399, IUT23-7, IUT23-9 and MOBJD39 and the European Regional Development Fund project CoE TK134 and CoE No. 2014-2020.4.01.15-0013 and by ASTRA 'TUT Institutional Development Programme for 2016-2022' Graduate School of Functional materials and technologies (2014-2020.4.01.16-0032).

### References

- (1) Maes, W.; Dehaen, W. Oxacalix [n](het) Arenes. *Chem. Soc. Rev.* **2008**, 37 (11), 2393–2402. DOI: 10.1039/b718356a.
- (2) Wang, M.-X.; Heterocalixaromatics, New Generation Macrocyclic Host Molecules in Supramolecular Chemistry. *Chem. Commun.* **2008**, 38, 4541–4551. doi:10.1039/b809287g
- (3) Ikeda, A.; Shinkai, S. Novel Cavity Design Using Calix[n] Arene Skeletons: toward Molecular Recognition and Metal Binding. *Chem. Rev.* **1997**, 97 (5), 1713–1734. DOI: 10.1021/cr960385x.
- (4) McIldowie, M.J.; Mocerino, M.; Ogden, M.I. A Brief Review of C N-Symmetric Calixarenes and Resorcinarenes. *Supramol. Chem.* **2010**, 22 (1), 13–39. DOI: 10.1080/10610270902980663.
- (5) Tanaka, Y.; Kato, Y.; Aoyama, Y. Two-Point Hydrogen-Bonding Interaction: A Remarkable Chain-Length Selectivity in the Binding of Dicarboxylic Acids with Resorcinol-Aldehyde Cyclotetramer as A Multidentate Host. *J. Am. Chem. Soc.* **1990**, 112 (7), 2807–2808. DOI: 10.1021/ja00163a056.
- (6) Timmerman, P.; Verboom, W.; Reinhoudt, D.N. Resorcinarenes. *Tetrahedron.* **1996**, 52 (8), 2663–2704. DOI: 10.1016/0040-4020(95)00984-1.
- (7) Shivanyuk, A.; Rebek, Jr, J., Jr. Reversible Encapsulation of Multiple, Neutral Guests in Hexameric Resorcinarene Hosts. *Chem. Commun.* **2001**, 23, 2424–2425. doi:10.1039/b109464p
- (8) Evan-Salem, T.; Baruk, I.; Avram, L.; Cohen, Y.; Palmer, L.C.; Rebek, J. Resorcinarenes are Hexameric Capsules in Solution. *Proc. Natl. Acad. Sci.* **2006**, 103 (33), 12296–12300. DOI: 10.1073/pnas.0604757103.

- (9) Xue, M.I.N.; Yang, Y.; Chi, X.; Zhang, Z.; Huang, F. Pillararenes, a New Class of Macrocycles for Supramolecular Chemistry. *Acc. Chem. Res.* **2012**, *45* (8), 1294–1308. DOI: 10.1021/ar2003418.
- (10) Park, C.; Kim, K.T. Pillar [n] Arenes and Other Cavitands: Aspects of Complex Thermodynamics. *Chin. J. Chem.* **2015**, *33* (3), 311–318. DOI: 10.1002/cjoc.201400875.
- (11) Wang, Y.; Ping, G.; Li, C. Efficient Complexation between Pillar [5] Arenes and Neutral Guests: from Host–Guest Chemistry to Functional Materials. *Chem. Commun.* **2016**, *52* (64), 9858–9872. DOI: 10.1039/C6CC03999E.
- (12) Fernando, A.; Mako, T.L.; Levenson, A.M.; Cesana, P.T.; Mendieta, A.M.; Racicot, J.M.; DeBoef, B.; Levine, M. A Polycationic Pillar [5] Arene for the Binding and Removal of Organic Toxicants from Aqueous Media. *Supramol. Chem.* **2019**.
- (13) Sun, Y.; Fu, W.; Chen, C.; Wang, J.; Yao, Y. Water-Soluble Pillar [5] Arene Induced the Morphology Transformation of Self-Assembled Nanostructures and Had Further Application in Paraquat Detection. *Chem. Commun.* **2017**, *53* (26), 3725–3728. DOI: 10.1039/C7CC00291B.
- (14) Ma, J.; Meng, Q.; Hu, X.; Li, B.; Ma, S.; Hu, B.; Li, J.; Xia, X.; Li, C. Synthesis of a Water-Soluble Carboxylatobiphen [4] Arene and Its Selective Complexation toward Acetylcholine. *Org. Lett.* **2016**, *18* (21), 5740–5743. DOI: 10.1021/acs.orglett.6b03005.
- (15) Duan, Q.; Cao, Y.; Li, Y.; Hu, X.; Xiao, T.; Lin, C.; Pan, Y.; Wang, L. PH-Responsive Supramolecular Vesicles Based on Water-Soluble Pillar [6] Arene and Ferrocene Derivative for Drug Delivery. *J. Am. Chem. Soc.* **2013**, *135* (28), 10542–10549. DOI: 10.1021/ja405014r.
- (16) Zhu, K.; Li, S.; Wang, F.; Huang, F. Anion-Controlled Ion-Pair Recognition of Paraquat by a Bis (m-phenylene)-32-crown-10 Derivative Heteroditopic Host. *J. Org. Chem.* **2009**, *74* (3), 1322–1328. DOI: 10.1021/jo802683d.
- (17) Zhou, Y.; Jie, K.; Yao, Y. A Cavity Extended Water-Soluble Resorcin [4] Arene: Synthesis, PH-Controlled Complexation with Paraquat, and Application in Controllable Self-Assembly. *New J. Chem.* **2017**, *41* (3), 916–919. DOI: 10.1039/C6NJ03026B.
- (18) Yu, G.; Zhou, X.; Zhang, Z.; Han, C.; Mao, Z.; Gao, C.; Huang, F. Pillar[6]Arene/Paraquat Molecular Recognition in Water: High Binding Strength, PH-Responsiveness, and Application in Controllable Self-Assembly, Controlled Release, and Treatment of Paraquat Poisoning. *J. Am. Chem. Soc.* **2012**, *134* (47), 19489–19497. DOI: 10.1021/ja3099905.
- (19) Guo, Q.; Zhao, L.; Wang, M. Synthesis and Molecular Recognition of Water-Soluble S6-Corona [3] Arene [3] Pyridazines. *Angew. Chemie Int. Ed.* **2015**, *54* (29), 8386–8389. DOI: 10.1002/anie.201503179.
- (20) Guo, Q.; Zhao, L.; Wang, M. Synthesis, Structure, and Molecular Recognition of S6-And (SO2) 6-corona [6] (het) Arenes: Control of Macrocyclic Conformation and Properties by the Oxidation State of the Bridging Heteroatoms. *Chem. Eur. J.* **2016**, *22* (20), 6947–6955. DOI: 10.1002/chem.201600462.
- (21) Manganaro, N.; Lando, G.; Gargiulli, C.; Pisagatti, I.; Notti, A.; Pappalardo, S.; Parisi, M.F.; Gattuso, G. Unique Binding Behaviour of Water-Soluble Polycationic Oxacalix [4] Arene Tweezers Towards the Paraquat Dication. *Chem. Commun.* **2015**, *51* (63), 12657–12660. DOI: 10.1039/C5CC04079E.
- (22) Manganaro, N.; Lando, G.; Pisagatti, I.; Notti, A.; Pappalardo, S.; Parisi, M.F.; Gattuso, G. Hydrophobic Interactions in the Formation of a Complex between a Polycationic Water-Soluble Oxacalix [4] Arene and a Neutral Aromatic Guest. *Supramol. Chem.* **2016**, *28* (5–6), 493–498. DOI: 10.1080/10610278.2015.1123811.
- (23) Neri, P.; Sessler, J.L.; Wang, M.-X. *Calixarenes and Beyond*; Springer, Switzerland, 2016.
- (24) Lhotak, P.; Chemistry of Thiacalixarenes. *European J. Org. Chem.* **2004**, *2004* (8), 1675–1692. DOI: 10.1002/ejoc.200300492.
- (25) Wang, M.-X.; Nitrogen and Oxygen Bridged Calixaromatics: Synthesis, Structure, Functionalization, and Molecular Recognition. *Acc. Chem. Res.* **2012**, *45* (2), 182–195. DOI: 10.1021/ar200108c.
- (26) Canard, G.; Edzang, J.A.; Chen, Z.; Chessé, M.; Elhabiri, M.; Giorgi, M.; Siri, O. 1, 3-alternate Tetraamido-Azacalix [4] Arenes as Selective Anion Receptors. *Chem. Eur. J.* **2016**, *22* (16), 5756–5766. DOI: 10.1002/chem.201505089.
- (27) Wang, D.-X.; Wang, M.-X. Anion– $\pi$  Interactions: Generality, Binding Strength, and Structure. *J. Am. Chem. Soc.* **2013**, *135* (2), 892–897. DOI: 10.1021/ja310834w.
- (28) Wang, D.-X.; Zheng, Q.-Y.; Wang, -Q.-Q.; Wang, M.-X. Halide Recognition by Tetraoxacalix[2]Arene[2]Triazine Receptors: Concurrent Noncovalent Halide– $\pi$  and Lone-Pair– $\pi$  Interactions in Host–Halide–Water Ternary Complexes. *Angew. Chemie Int. Ed.* **2008**, *47* (39), 7485–7488. DOI: 10.1002/anie.200801705.
- (29) Alberto, M.E.; Mazzone, G.; Russo, N.; Sicilia, E. The Mutual Influence of Non-Covalent Interactions in  $\pi$ -Electron Deficient Cavities: the Case of Anion Recognition by Tetraoxacalix[2]Arene[2]Triazine. *Chem. Commun.* **2010**, *46* (32), 5894–5896. DOI: 10.1039/c0cc01083a.
- (30) Chen, Z.; Canard, G.; Azarias, C.; Jacquemin, D.; Siri, O. Straightforward Metal-Free Synthesis of an Azacalix [6] Arene Forming a Host–Guest Complex with Fullerene C 60. *New J. Chem.* **2017**, *41* (13), 5284–5290. DOI: 10.1039/C7NJ00697G.
- (31) Csokai, V.; Kulik, B.; Bitter, I. The First Synthesis of Functionalized Oxacalix[4]Crown Ethers. *Supramol. Chem.* **2006**, *18* (2), 111–115. DOI: 10.1080/10610270500462296.
- (32) Hou, B.-Y.; Wang, D.-X.; Yang, H.-B.; Zheng, Q.-Y.; Wang, M.-X. Synthesis and Structure of Upper-Rim 1,3-alternate Tetraoxacalix[2]Arene[2]Triazine Azacrowns and Change of Cavity in Response to Fluoride Anion. *J. Org. Chem.* **2007**, *72* (14), 5218–5226. DOI: 10.1021/jo0706168.
- (33) Sobransingh, D.; Dewal, M.B.; Hiller, J.; Smith, M.D.; Shimizu, L.S. Inclusion of Electrochemically Active Guests by Novel Oxacalixarene Hosts. *New J. Chem.* **2008**, *32* (1), 24–27. DOI: 10.1039/B709806E.
- (34) Zhou, Q.; Su, L.; Jiang, T.; Zhang, B.; Chen, R.; Jiang, H.; Ye, Y.; Zhu, M.; Han, D.; Shen, J.; et al., Copper/Iron-Catalyzed Ullmann Coupling of Diiodo- and Dibromoarenes and Diphenols for the Synthesis of Aryl Ether Macrocycles. *Tetrahedron.* **2014**, *70*(6), 1125–1132. doi:10.1016/j.tet.2013.12.089
- (35) Peterson, A.; Kaabel, S.; Kahn, I.; Pehk, T.; Aav, R.; Adamson, J. Unsubstituted Oxacalix [n] Arenes (N= 4

- and 8): A Conformational Study in Solution and Solid State and Interaction Studies with Aromatic Guests. *ChemistrySelect*. **2018**, 3 (31), 9091–9095. DOI: 10.1002/slct.201801590.
- (36) Brynn Hibbert, D.; Thordarson, P. The Death of the Job Plot, Transparency, Open Science and Online Tools, Uncertainty Estimation Methods and Other Developments in Supramolecular Chemistry Data Analysis. *Chem. Commun.* **2016**, 52 (87), 12792–12805. DOI: 10.1039/C6CC03888C.
- (37) Sittipunt, C. Paraquat Poisoning. *Respir. Care*. **2005**, 50 (3), 383–385.
- (38) Goel, A.; Singh, O. *Princ. Pract. Crit. Care Toxicol.* **2019**, 312.
- (39) Wolff, S.K.; Grimwood, D.J.; McKinnon, J.J.; Turner, M.J.; Jayatilaka, D.; Spackman, M.A. *CrystalExplorer (version 3.1)*; The University of Western Australia, 2012.
- (40) Lehmann F, P, A.; Conformations of Highly Hindered Aryl Ethers—XIX: Synthesis and NMR Study of Some Cyclic Aryl Polyethers. *Tetrahedron*. **1974**, 30 (6), 727–733. DOI: 10.1016/S0040-4020(01)97158-3.
- (41) Katz, J.L.; Feldman, M.B.; Conry, R.R. Synthesis of Functionalized Oxacalix[4]Arenes. *Org. Lett.* **2005**, 7 (1), 91–94. DOI: 10.1021/ol047836h.
- (42) CollectionStrategy. *CollectionStrategy*; Rigaku Corp: Tokyo, Japan, 2011
- (43) CrysAlisPro. *Agilent Technologies*; Agilent Technologies UK Ltd, Oxford, UK, 2014. Version 1.171.36.35
- (44) Clark, R.C.; Reid, J.S. The Analytical Calculation of Absorption in Multifaceted Crystals. *Acta Crystallogr. Sect. Found. Crystallogr.* **1995**, 51 (6), 887–897. DOI: 10.1107/S0108767395007367.
- (45) Sheldrick, G.M.; No Title. *Acta Cryst.* **2015**, A71, 3–8.
- (46) Sheldrick, G.M. *Acta Cryst.* **2008**, A64, 112–122. DOI: 10.1107/S0108767307043930.
- (47) Dolomanov, O.V.; Bourhis, L.J.; Gildea, R.J.; Howard, J.A. K.; Puschmann, H. OLEX2: A Complete Structure Solution, Refinement and Analysis Program. *J. Appl. Crystallogr.* **2009**, 42 (2), 339–341. DOI: 10.1107/S0021889808042726.
- (48) Macrae, C.F.; Bruno, I.J.; Chisholm, J.A.; Edgington, P.R.; McCabe, P.; Pidcock, E.; Rodriguez-Monge, L.; Taylor, R.; Streek, J.V.; Wood, P.A. Mercury CSD 2.0—new Features for the Visualization and Investigation of Crystal Structures. *J. Appl. Crystallogr.* **2008**, 41 (2), 466–470. DOI: 10.1107/S0021889808033797.
- ((49)) Persistence of Vision Raytracer. Persistence of Vision Pty. Ltd. Version 3.7 [Computer software], 2004. <http://www.povray.org/download>. No Title (accessed in May, 2019).
- (50) Becke, A.D.; Becke's Three Parameter Hybrid Method Using the LYP Correlation Functional. *J. Chem. Phys.* **1993**, 98, 5648–5652. DOI: 10.1063/1.464913.
- (51) Lee, C.; Yang, W.; Parr, R.G. Development of the Colle-Salvetti Correlation-Energy Formula into a Functional of the Electron Density. *Phys. Rev. B.* **1988**, 37 (2), 785. DOI: 10.1103/PhysRevB.37.785.
- (52) McLean, A.D.; Chandler, G.S. Contracted Gaussian Basis Sets for Molecular Calculations. I. Second Row Atoms, Z= 11–18. *J. Chem. Phys.* **1980**, 72 (10), 5639–5648. DOI: 10.1063/1.438980.
- (53) Frisch, M.J.; Pople, J.A.; Binkley, J.S. Self-consistent Molecular Orbital Methods 25. Supplementary Functions for Gaussian Basis Sets. *J. Chem. Phys.* **1984**, 80 (7), 3265–3269. DOI: 10.1063/1.447079.
- (54) Cancès, E.; Mennucci, B.; Tomasi, J. A New Integral Equation Formalism for the Polarizable Continuum Model: Theoretical Background and Applications to Isotropic and Anisotropic Dielectrics. *J. Chem. Phys.* **1997**, 107 (8), 3032–3041. DOI: 10.1063/1.474659.
- (55) Mennucci, B.; Cancès, E.; Tomasi, J. Evaluation of Solvent Effects in Isotropic and Anisotropic Dielectrics and in Ionic Solutions with a Unified Integral Equation Method: Theoretical Bases, Computational Implementation, and Numerical Applications. *J. Phys. Chem. B.* **1997**, 101 (49), 10506–10517. DOI: 10.1021/jp971959k.
- (56) London, F.; Quantum Theory of Interatomic Currents in Aromatic Compounds. *J. Phys. Radium.* **1937**, 8, 397–409. DOI: 10.1051/jphysrad:01937008010039700.
- (57) McWeeny, R.; Perturbation Theory for the Fock-Dirac Density Matrix. *Phys. Rev.* **1962**, 126 (3), 1028. DOI: 10.1103/PhysRev.126.1028.
- (58) Ditchfield, R.; Self-Consistent Perturbation Theory of Diamagnetism. I. A Gauge-Invariant LCAO Method for NMR Chemical Shifts. *Mol. Phys.* **1974**, 27 (4), 789–807. DOI: 10.1080/00268977400100711.
- (59) Wolinski, K.; Hinton, J.F.; Pulay, P. Efficient Implementation of the Gauge-Independent Atomic Orbital Method for NMR Chemical Shift Calculations. *J. Am. Chem. Soc.* **1990**, 112 (23), 8251–8260. DOI: 10.1021/ja00179a005.
- (60) Cheeseman, J.R.; Trucks, G.W.; Keith, T.A.; Frisch, M.J. A Comparison of Models for Calculating Nuclear Magnetic Resonance Shielding Tensors. *J. Chem. Phys.* **1996**, 104 (14), 5497–5509. DOI: 10.1063/1.471789.
- (61) Keith, T.A.; Bader, R.F.W. Calculation of Magnetic Response Properties Using Atoms in Molecules. *Chem. Phys. Lett.* **1992**, 194 (1–2), 1–8. DOI: 10.1016/0009-2614(92)85733-Q.
- (62) Keith, T.A.; Bader, R.F.W. Calculation of Magnetic Response Properties Using a Continuous Set of Gauge Transformations. *Chem. Phys. Lett.* **1993**, 210 (1–3), 223–231. DOI: 10.1016/0009-2614(93)89127-4.
- (63) Peverati, R.; Truhlar, D.G. Screened-Exchange Density Functionals with Broad Accuracy for Chemistry and Solid-State Physics. *Phys. Chem. Chem. Phys.* **2012**, 14 (47), 16187–16191. DOI: 10.1039/c2cp42576a.
- (64) Kendall, R.A.; Dunning, T.H., Jr; Harrison, R.J. Electron Affinities of the First-row Atoms Revisited. Systematic Basis Sets and Wave Functions. *J. Chem. Phys.* **1992**, 96 (9), 6796–6806. DOI: 10.1063/1.462569.
- (65) Iikura, H.; Tsuneda, T.; Yanai, T.; Hirao, K. A Long-Range Correction Scheme for Generalized-Gradient-Approximation Exchange Functionals. *J. Chem. Phys.* **2001**, 115 (8), 3540–3544. DOI: 10.1063/1.1383587.
- (66) Tao, J.; Perdew, J.P.; Staroverov, V.N.; Scuseria, G.E. Climbing the Density Functional Ladder: Nonempirical Meta-Generalized Gradient Approximation Designed for Molecules and Solids. *Phys. Rev. Lett.* **2003**, 91 (14), 146401. DOI: 10.1103/PhysRevLett.91.146401.
- (67). Gaussian 09. *Gaussian 09, Revision B.01*; Gaussian Inc.: Wallingford, CT, 2009.

(68). Gaussian 16. *Gaussian 16, Revision A.03*; Gaussian, Inc: Wallingford, CT, 2016.

## Appendix 3

### Publication III

Peterson, A.; Kaasik, M.; Metsala, A.; Järving, I.; Adamson, J.; Kanger, T. Tunable chiral triazole-based halogen bond donors: assessment of donor strength in solution with nitrogen-containing acceptors. *RSC Advances*, **2019**, 9, 11718–11721.

Reprinted with permission of The Royal Society of Chemistry.





Cite this: *RSC Adv.*, 2019, 9, 11718

## Tunable chiral triazole-based halogen bond donors: assessment of donor strength in solution with nitrogen-containing acceptors†

Anna Peterson,<sup>‡ab</sup> Mikk Kaasik,<sup>‡</sup> Andrus Metsala,<sup>b</sup> Ivar Järving,<sup>b</sup> Jasper Adamson<sup>\*a</sup> and Tõnis Kanger<sup>‡</sup><sup>id</sup><sup>\*b</sup>

Received 6th March 2019  
Accepted 4th April 2019

DOI: 10.1039/c9ra01692a

rsc.li/rsc-advances

Strong halogen bond (XB) donors are needed for the activation of neutral substrates. We demonstrate that XB donor properties of iodo-triazoles can be significantly enhanced by quaternization in combination with varying the counterion and aromatic substituent, exemplified by association constants with quinuclidine as high as  $1.1 \times 10^4 \text{ M}^{-1}$ .

Halogen bond (XB) based applications utilize the attractive interaction between a Lewis acidic halogen atom and a Lewis base.<sup>1</sup> From the turn of the century numerous publications have focused on the use of XBs in the solid state<sup>2</sup> and more recently, in solution as well.<sup>3</sup> Among these applications the potential of XBs in catalysis<sup>4</sup> and anion recognition should be highlighted.<sup>5</sup> As shown by Huber *et al.* these fields can be closely associated, exemplified by halide abstraction reactions.<sup>6</sup>

Compared to anion recognition, the recognition of neutral species in solution has received less attention. Studies with neutral acceptors have a primary focus on the fundamental nature of halogen bonding, such as the influence of the solvent and the structure of the XB donor/acceptor on the strength of XBs.<sup>7</sup> Amines have usually been used as neutral acceptors in these studies for their high affinity towards XB donors. This property can potentially be utilized in the detection of biologically relevant amines by XBs.<sup>8</sup> From the synthetic point of view, the activation of neutral species through XBs is also a topic of high interest.<sup>9</sup> In general, compared to anions, neutral acceptors form weaker complexes with organic XB donors.<sup>1d,3c</sup> Therefore, XB donors with stronger halogen bonding ability should be used for the activation of neutral compounds. From a catalyst design perspective, information on the extent different structural fragments affect XB donor ability is of great value.

Recently, we became interested in applying XBs in asymmetric catalysis. Chiral 5-halo-1,2,3-triazoles are among the best

candidates of catalysts to achieve this goal.<sup>6b,9b,d</sup> The triazoles are readily available through a Cu-catalysed click reaction<sup>10</sup> and access to a broad range of alkynes with the possibility to quaternize the triazole core makes it feasible to enhance the donor ability of the triazole. In addition, the availability of many chiral azides offers wide opportunities for the design of new chiral XB donor systems.<sup>11</sup> We have shown the potential of these compounds to interact with various possible substrates and in enantiodiscrimination.<sup>12</sup> Due to relatively low affinity constants with thiourea acceptors, it was difficult to fully assess how structural modifications affect XB donors' binding ability. Therefore, a stronger XB acceptor has to be selected for this kind of analysis. Anionic species are known to give large affinity constants with halo-triazolium salts,<sup>13</sup> however, in these complexes charge attraction plays a key role in XB formation. We therefore chose quinuclidine,<sup>7d,h-k</sup> a neutral monodentate XB acceptor with a readily accessible lone pair, for screening of the effect of XB donor analogues (Fig. 1) on XB strength. Herein we describe the formation of complexes between triazole-based XB donors and quinuclidine in solution with emphasis on the influence of aromatic substituents and counterions on XB donor strength and investigate the XB donors' ability to discriminate between enantiomers of chiral imines and amines.

A collection of monodentate XB donors shown in Fig. 1 were synthesized (see ESI† for details). To determine the effect of structural changes, the triazolium salts were modified by introducing a perfluorophenyl or a *p*-nitrophenyl substituent instead of a phenyl substituent, changing the counterions and varying the halogen atoms. The XB donor ability of the synthesized compounds was determined through their respective association constants with quinuclidine in CDCl<sub>3</sub> based on <sup>1</sup>H NMR titration experiments. To evaluate the XB strength more accurately, the titration experiments were carried out in duplicate. The results are summarized in Table 1.

<sup>a</sup>Chemical Physics Laboratory, National Institute of Chemical Physics and Biophysics, Akadeemia tee 23, 12618, Tallinn, Estonia. E-mail: jasper.adamson@kbfi.ee

<sup>b</sup>Department of Chemistry and Biotechnology, School of Science, Tallinn University of Technology, Akadeemia tee 15, 12618 Tallinn, Estonia. E-mail: tonis.kanger@taltech.ee

† Electronic supplementary information (ESI) available: Experimental procedures, titration experiments, computational information and copies of <sup>1</sup>H and <sup>13</sup>C NMR spectra. See DOI: 10.1039/c9ra01692a

‡ These authors contribute equally to this work.



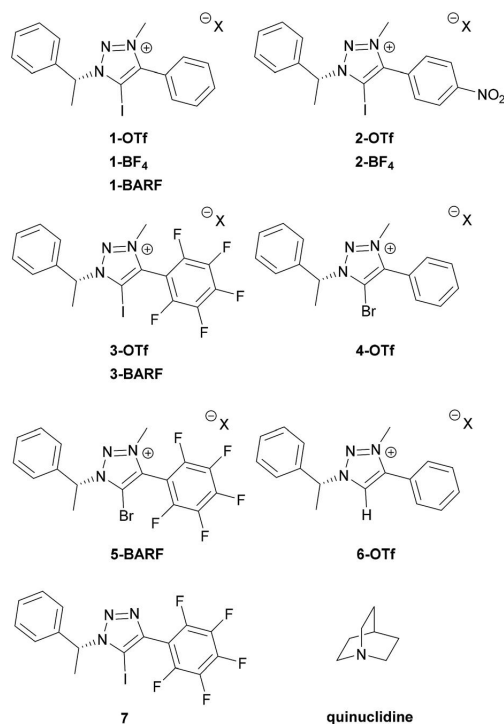


Fig. 1 XB donors and reference compound under study.

Table 1 Association constant  $K_a$  values<sup>a</sup> of the XB donor–quinuclidine pairs

Entry	XB donor	$K_a$ , M <sup>-1</sup>
1	1-OTf	57 ± 5
2	1-BARF	(1.23 ± 0.01) × 10 <sup>3</sup>
3	2-OTf	257 ± 12
4	2-BF <sub>4</sub>	284 ± 12
5	3-OTf	703 ± 6
6	3-BARF	(1.1 ± 0.3) × 10 <sup>4</sup>
7	4-OTf	<1
8	5-BARF	n.d. <sup>b</sup>
9	6-OTf	<1
10	7	2.0 ± 0.3

<sup>a</sup> Association constant  $K_a$  measured in CDCl<sub>3</sub> at 298 K and determined by fitting the <sup>1</sup>H NMR titration data to 1 : 1 binding isotherm of BindFit.<sup>15</sup> The given  $K_a$  and standard error are the calculated mean values of two parallel experiments. Full details given in the ESI. <sup>b</sup>  $K_a$  could not be determined due to the instability of XB donor during the experiment.

To evaluate the influence of substituents of the aromatic ring that connects directly to the triazolium core on XB formation ability of the triazolium salts, a perfluorinated and a nitro-substituted derivative (3-OTf and 2-OTf, respectively) were compared with the unsubstituted phenyl derivative 1-OTf (Table 1, entries 1, 3 and 5). The affinity towards quinuclidine

decreases in the order of 3-OTf > 2-OTf > 1-OTf which corresponds to the decrease of the size of the  $\sigma$ -hole on the iodine atom.<sup>14</sup> The perfluorinated XB donor had more than twice as high affinity towards quinuclidine as the NO<sub>2</sub>-containing XB donor and over an order of magnitude higher affinity when compared to 1-OTf. The strong XB donating ability of perfluorinated XB donors is explained by its highly electronegative fluorine substituents that significantly increase the polarization of the C–X bond, therefore increasing the  $\sigma$ -hole.<sup>7d,7i</sup> The electron-withdrawing nitro group in compound 2-OTf is similarly essential to enhance its XB donor ability, albeit less strongly compared to the more electron deficient perfluorophenyl group in 3-OTf. To determine that the changes in chemical shifts were indeed induced by halogen bonding, the nonhalogenated analogue 6-OTf was synthesized which expectedly did not interact favourably with quinuclidine (Table 1, entry 9).

The effects of anionic counterions were characterised based on triflate (1-OTf, 2-OTf, 3-OTf), tetrafluoroborate (2-BF<sub>4</sub>) and tetrakis[3,5-bis(trifluoromethyl)phenyl]borate (1-BARF, 3-BARF) containing triazolium salts. Due to poor solubility, the comparison to 1-BF<sub>4</sub> could not be made. In general, the change of the counterion affected XB strength substantially in accordance with their coordination ability.<sup>16</sup> The less coordinating tetrafluoroborate containing triazolium salt 2-BF<sub>4</sub> showed higher affinity towards quinuclidine compared to the triflate containing salt 2-OTf (Table 1, entries 3 and 4). The introduction of the BARF counterion increased XB strength by more than one order of magnitude (Table 1, comparing entries 1 and 5 to entries 2 and 6). To the best of our knowledge, the obtained affinity constant between quinuclidine and 3-BARF is among the highest affinities reported so far for a neutral acceptor.<sup>3e,7</sup> Usually XBs are stronger in apolar solvents than in more polar solvents<sup>7e,f,i</sup> and as a comparison, the association constant is only a magnitude smaller than that for the complex between quinuclidine and I<sub>2</sub> measured in heptane.<sup>7h</sup>

The strength of the XB is known to decrease based on the polarization of the halogen atom and the increase of electronegativity in the order of I > Br > Cl > F.<sup>1</sup> In our <sup>1</sup>H NMR titration study, the iodo-triazolium analogue (1-OTf) displayed moderate affinity towards quinuclidine whereas the corresponding bromine analogue (4-OTf) did not show any affinity towards quinuclidine altogether (Table 1, entry 7, also see ESI† for details). The absence of complex formation with the bromine derivative agrees with a similar outcome in our previous investigation.<sup>12</sup> In an attempt to obtain a complex containing a bromine atom as the donor, a bromo-triazolium salt 5-BARF with the strongly electronegative pentafluorophenyl substituent was synthesized. Nevertheless, the changes undertaken made the donor too labile and upon the titration experiment dehalogenation prevented the determination of the affinity constant (Table 1, entry 8, also see ESI† for details).

Quaternization of the triazole core has been critical to obtain compounds with sufficient XB donor ability.<sup>13b,17</sup> To ascertain the impact of charge in the triazole core, neutral perfluorinated triazole 7 was also titrated with quinuclidine. The obtained affinity constant is indeed very low. However, this result is of importance in its own right as there are only a few examples



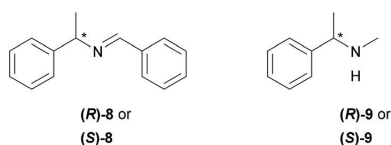


Fig. 2 Chiral XB acceptors under study.

describing complex formation in solution between a neutral halo-triazole and a neutral acceptor.<sup>18</sup> The difference between the neutral XB donor (7) and its charged derivative (3-OTf) is more than two orders of magnitude (Table 1, entries 5 and 10). However, if the counterion acts as an acceptor and competes with quinuclidine for XB formation, triazole 7 should be compared to 3-BARF, which has the less coordinating BARF counterion and therefore provides a better representation for a “naked” cationic backbone. In this case, the difference in binding ability of four orders of magnitude was observed (Table 1, entries 6 and 10).

Furthermore, <sup>1</sup>H NMR titrations measurements were performed using both enantiomers of chiral imine 8 and amine 9 (Fig. 2) to determine whether the XB donors are able to selectively interact with chiral substances. For these experiments, 3-BARF was chosen as the donor due to the highest binding affinity towards quinuclidine. The XB donor showed no preference towards either enantiomer of the selected acceptors since no differences between the two enantiomers  $K_a$  values were observed in either case (Table 2, entries 1 and 2; entries 3 and 4). Nevertheless, the affinity constant between amine 9 and 3-BARF is considerably higher compared to the only reported example, where the XB strength between an organic XB donor and secondary amine was measured.<sup>7</sup> The affinity constant between perfluorohexyl iodide and piperidine was <1 in all three solvents used in that study. The difference compared to the binding strength of quinuclidine can partly be explained by the fact that cyclic amines are better acceptors than acyclic amines.<sup>7</sup>

Calculations were performed on the CAM/B3LYP<sup>19</sup> level of theory using DEF2TZVP basis set<sup>20</sup> to model the interaction between both enantiomers of amine 9 and 3-OTf. The calculated complexes in the vacuum and in CHCl<sub>3</sub> had similar energy values (see ESI† for details). The substituents on the triazole core are most likely not sufficiently bulky to differentiate between the two enantiomers through steric repulsion or by

Table 2 Association constant  $K_a$  values<sup>a</sup> of the chiral acceptor and 3-BARF pairs

Entry	XB acceptor	$K_a$ , M <sup>-1</sup>
1	(R)-8	6.1 ± 0.7
2	(S)-8	6.0 ± 0.8
3	(R)-9	94 ± 7
4	(S)-9	91 ± 5

<sup>a</sup> Association constant  $K_a$  measured in CDCl<sub>3</sub> at 298 K and determined by fitting the <sup>1</sup>H NMR titration data to 1 : 1 binding isotherm of BindFit.<sup>15</sup> The given  $K_a$  and standard error are the calculated mean values of two parallel experiments. Full details given in the ESI.

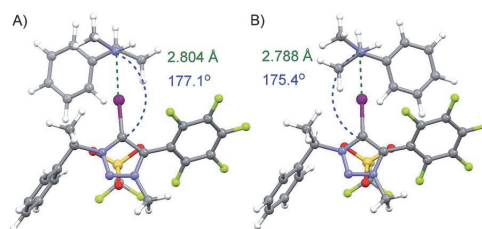


Fig. 3 Calculated minimum energy complexes formed through a XB between donor 3-OTf and (S)- or (R)-enantiomer of amine 9 (A and B respectively).

other noncovalent interactions (Fig. 3). This could also explain our previously obtained results of enantiodiscrimination experiments, where Takemoto's catalyst<sup>21</sup> was used as an acceptor and that suggest that both hydrogen and halogen bonding interactions influenced the binding of enantiomers.<sup>12</sup> Therefore, a more beneficial approach would be to use multi-dentate or bifunctional XB donors that form more rigid complexes. For example, Beer *et al.* has shown that chiral bidentate XB donors that contain at least two halo-triazole cores are suitable for differentiating between enantiomers.<sup>13a,22</sup>

In conclusion, we have once again shown the pivotal role of charge on XB donor strength. In addition, by changing the aromatic substituent and the counterion, the XB donor properties of triazole-based donors can be enhanced even further. This is exemplified by the fact that the donors form complexes with quinuclidine with association constants covering almost four orders of magnitude. To the best of our knowledge, the reported association constants are comparable to the largest described between an amine and an organic XB donor in solution. Enantiodiscrimination of acceptors 8 and 9 by the most powerful donor 3-BARF was not observed. However, information obtained during this study can aid to move towards more selective donors.

## Conflicts of interest

There are no conflicts to declare.

## Acknowledgements

The present study was supported by Estonian Ministry of Education and Research (Grant No. IUT 19-32, IUT 19-9, IUT 23-7, PUT1468 and PRG399) and the Centre of Excellence in Molecular Cell Engineering 2014-2020.4.01.15-0013 as well as the Centre of Excellence TK134. We thank Dr Aleksander-Mati Müürisepp for the IR spectra, Dr Kadri Kriis and Mrs Egle Rinaldo for their help on the synthesis.

## Notes and references

- (a) Á. M. Montaña, *ChemistrySelect*, 2017, 2, 9094; (b) G. Cavallo, P. Metrangolo, R. Milani, T. Pilati, A. Priimagi, G. Resnati and G. Terraneo, *Chem. Rev.*, 2016, 116, 2478; (c) H. Wang, W. Wang and W. J. Jin, *Chem. Rev.*, 2016, 116,



- 5072; (d) L. C. Gilday, S. W. Robinson, T. A. Barendt, M. J. Langton, B. R. Mullaney and P. D. Beer, *Chem. Rev.*, 2015, **115**, 7118.
- 2 (a) J.-C. Christopherson, F. Topić, C. J. Barrett and T. Friščić, *Cryst. Growth Des.*, 2018, **18**, 1245; (b) B. Li, S.-Q. Zang, L.-Y. Wang and T. C. W. Mak, *Coord. Chem. Rev.*, 2016, **308**, 1; (c) G. Berger, J. Soubhy and F. Meyer, *Polym. Chem.*, 2015, **6**, 3559; (d) A. Mukherjee, S. Tothadi and G. R. Desiraju, *Acc. Chem. Res.*, 2014, **47**, 2514; (e) R. W. Troff, T. Mäkelä, F. Topić, A. Valkonen, K. Raatikainen and K. Rissanen, *Eur. J. Org. Chem.*, 2013, **2013**, 1617; (f) K. Rissanen, *CrystEngComm*, 2008, **10**, 1107.
- 3 (a) A. V. Jentzsch, *Pure Appl. Chem.*, 2015, **87**, 15; (b) A.-C. C. Carlsson, A. X. Veiga and M. Erdélyi, *Top. Curr. Chem.*, 2014, **359**, 49; (c) T. M. Beale, M. G. Chudzinski, M. G. Sarwar and M. S. Taylor, *Chem. Soc. Rev.*, 2013, **42**, 1667.
- 4 (a) M. Breugst and D. von der Heiden, *Chem.–Eur. J.*, 2018, **24**, 9187; (b) D. Bulfield and S. M. Huber, *Chem.–Eur. J.*, 2016, **22**, 14434; (c) S. Schindler and S. M. Huber, *Top. Curr. Chem.*, 2014, **359**, 167.
- 5 (a) R. Tepper and U. S. Schubert, *Angew. Chem., Int. Ed.*, 2018, **57**, 6004; (b) A. Brown and P. D. Beer, *Chem. Commun.*, 2016, **52**, 8645.
- 6 (a) F. Heinen, E. Engelage, A. Dreger, R. Weiss and S. M. Huber, *Angew. Chem., Int. Ed.*, 2018, **57**, 3830; (b) A. Dreger, E. Engelage, B. Mallick, P. D. Beer and S. M. Huber, *Chem. Commun.*, 2018, **54**, 4013; (c) S. H. Jungbauer and S. M. Huber, *J. Am. Chem. Soc.*, 2015, **137**, 12110; (d) F. Kniep, S. H. Jungbauer, Q. Zhang, S. M. Walter, S. Schindler, I. Schnapperelle, E. Herdtweck and S. M. Huber, *Angew. Chem., Int. Ed.*, 2013, **52**, 7028; (e) F. Kniep, L. Rout, S. M. Walter, H. K. V. Bensch, S. H. Jungbauer, E. Herdtweck and S. M. Huber, *Chem. Commun.*, 2012, **48**, 9299.
- 7 (a) A. M. S. Riel, M. J. Jessop, D. A. Decato, C. J. Massena, V. R. Nascimento and O. B. Berryman, *Acta Crystallogr., Sect. B: Struct. Sci., Cryst. Eng. Mater.*, 2017, **73**, 203; (b) G. Ciancaleoni, A. Macchioni, L. Rocchigiani and C. Zuccaccia, *RSC Adv.*, 2016, **6**, 80604; (c) R. Puttreddy, O. Jurčák, S. Bhowmik, T. Mäkelä and K. Rissanen, *Chem. Commun.*, 2016, **52**, 2338; (d) O. Dumele, D. Wu, N. Trapp, N. Goroff and F. Diederich, *Org. Lett.*, 2014, **16**, 4722; (e) S. H. Jungbauer, D. Bulfield, F. Kniep, C. W. Lehmann, E. Herdtweck and S. M. Huber, *J. Am. Chem. Soc.*, 2014, **136**, 16740; (f) C. C. Robertson, R. N. Perutz, L. Brammer and C. A. Hunter, *Chem. Sci.*, 2014, **5**, 4179; (g) B. Hawthorne, H. Fan-Hagenstein, E. Wood, J. Smith and T. Hanks, *Int. J. Spectrosc.*, 2013, **2013**, 1; (h) C. Laurence, J. Graton, M. Berthelot and M. J. El Ghomari, *Chem.–Eur. J.*, 2011, **17**, 10431; (i) M. G. Sarwar, B. Dragisic, L. J. Salsberg, C. Gouliaras and M. S. Taylor, *J. Am. Chem. Soc.*, 2010, **132**, 1646; (j) R. Cabot and C. A. Hunter, *Chem. Commun.*, 2009, 2005; (k) P. Metrangolo, W. Panzeri, F. Recupero and G. Resnati, *J. Fluorine Chem.*, 2002, **114**, 27.
- 8 X. X. Zhang, J. S. Bradshaw and R. M. Izatt, *Chem. Rev.*, 1997, **97**, 3313.
- 9 (a) G. Bergamaschi, L. Lascialfari, A. Pizzi, M. I. M. Espinoza, N. Demitri, A. Milani, A. Gori and P. Metrangolo, *Chem. Commun.*, 2018, **54**, 10718; (b) R. Haraguchi, S. Hoshino, M. Sakai, S. Tanazawa, Y. Morita, T. Komatsu and S. Fukuzawa, *Chem. Commun.*, 2018, **54**, 10320; (c) J.-P. Gliese, S. H. Jungbauer and S. M. Huber, *Chem. Commun.*, 2017, **53**, 12052; (d) D. von der Heiden, E. Detmar, R. Kuchta and M. Breugst, *Synlett*, 2017, **28**, 1307.
- 10 (a) J. M. Pérez, P. Crosbie, S. Lal and S. Díez-González, *ChemCatChem*, 2016, **8**, 2222; (b) J. García-Álvarez, J. Díez and J. Gimeno, *Green Chem.*, 2010, **12**, 2127; (c) J. E. Hein, J. C. Tripp, L. B. Krasnova, K. B. Sharpless and V. V. Fokin, *Angew. Chem., Int. Ed.*, 2009, **48**, 8018; (d) B. H. M. Kuipers, G. C. T. Dijkmans, S. Groothuys, P. J. L. M. Quaedflieg, R. H. Blaauw, F. L. van Delft and F. P. J. T. Rutjes, *Synlett*, 2005, 3059.
- 11 M. Kaasik, S. Kaabel, K. Kriis, I. Järving and T. Kanger, *Synthesis*, 2019, DOI: 10.1055/s-0037-1610864.
- 12 M. Kaasik, S. Kaabel, K. Kriis, I. Järving, R. Aav, K. Rissanen and T. Kanger, *Chem.–Eur. J.*, 2017, **23**, 7337.
- 13 (a) J. Y. C. Lim, I. Marques, V. Félix and P. D. Beer, *Chem. Commun.*, 2018, **54**, 10851; (b) R. Tepper, B. Schulze, M. Jäger, C. Friebe, D. H. Scharf, H. Görls and U. S. Schubert, *J. Org. Chem.*, 2015, **80**, 3139.
- 14 M. Kaasik, A. Metsala, S. Kaabel, K. Kriis, I. Järving and T. Kanger, *J. Org. Chem.*, 2019, **84**, 4294–4303.
- 15 Freely available at <http://www.supramolecular.org> (accessed February 22, 2019).
- 16 (a) I. Krossing and I. Raabe, *Angew. Chem., Int. Ed.*, 2004, **43**, 2066; (b) S. H. Strauss, *Chem. Rev.*, 1993, **93**, 927.
- 17 (a) B. Nepal and S. Scheiner, *Chem.–Eur. J.*, 2015, **21**, 13330; (b) B. Nepal and S. Scheiner, *J. Phys. Chem. A*, 2015, **119**, 13064.
- 18 L. Maugeri, J. Asencio-Hernández, T. Lébl, D. B. Cordes, A. M. Z. Slawin, M. Delsuc and D. Philp, *Chem. Sci.*, 2016, **7**, 6422.
- 19 T. Yanai, D. Tew and N. Handy, *Chem. Phys. Lett.*, 2004, **393**, 51.
- 20 F. Weigend and R. Ahlrichs, *Phys. Chem. Chem. Phys.*, 2005, **7**, 3297.
- 21 T. Okino, Y. Hoashi and Y. Takemoto, *J. Am. Chem. Soc.*, 2003, **125**, 12672.
- 22 (a) A. Borisso, J. Y. C. Lim, A. Brown, K. E. Christensen, A. L. Thompson, M. D. Smith and P. D. Beer, *Chem. Commun.*, 2017, **53**, 2483; (b) J. Y. C. Lim, I. Marques, L. Ferreira, V. Félix and P. D. Beer, *Chem. Commun.*, 2016, **52**, 5527.



## Author's other publications and conference presentations

### Other publications

1. Balčiūnas, S.; **Peterson, A.**; Ivanov, M.; Adamson, J.; Banys, J. Dielectric properties of one dimensional ice in HHTP-4H<sub>2</sub>O crystallites. *Ferroelectrics*, **2018**, 533, 192–197.
2. Fomitšenko, M.; **Peterson, A.**; Reile, I.; Cong, H.; Kaabel, K.; Prigorchenko, E.; Järving I.; Aav R. A quantitative method for analysis of mixtures of homologues and stereoisomers of hemicucurbiturils that allows us to follow their formation and stability. *New Journal of Chemistry*, **2015**, 41, 2490–2497.

### Conference publications

1. **Peterson, A.**; Ludvig, M-L.; Martõnova, J.; Kaabel, S.; Uudsemaa, M.; Trummal, A.; Pehk, T.; Aav, R.; Adamson, J. New oxacalix[4]arene macrocycles: a conformational and interaction study. 15th International Conference on Calixarenes (Calix-2019), **2019**, Cassis, France. (oral presentation and poster)
2. **Peterson, A.**; Kaabel, S.; Kahn, I.; Pehk, T.; Aav, R.; Adamson, J. Synthesis and Properties of Oxacalix[n]arenes. 13th International Symposium on Macrocyclic and Supramolecular Chemistry (ISMSC 2018), **2018**, Quebec City, Canada. (poster)
3. **Peterson, A.**; Kaabel, S.; Kahn, I.; Pehk, T.; Aav, R.; Adamson, J. Synthesis and Properties of Oxacalix[n]arenes. International Conference on Organic Synthesis (BOS 2018), **2018**, Tallinn, Estonia. (poster)
4. **Peterson, A.**; Kaabel, S.; Aav, R.; Pehk, T.; Adamson, J. Synthesis and properties of oxacalix[n]arenes. AMPERE NMR School, **2017**, Zakopane, Poland. (poster)

# Curriculum vitae

## Personal data

Name: Anna Cowart (Peterson)  
Date of birth: 06.07.1992  
Citizenship: Estonian

## Contact data

E-mail: anna.cowart@kbfi.ee

## Education

2016 – ... Tallinn University of Technology, Chemistry and Biotechnology, Ph.D.  
2014 – 2016 Tallinn University of Technology, Applied Chemistry and Biotechnology, M.Sc.  
2011 – 2014 Tallinn University of Technology, Applied Chemistry and Biotechnology, B.Sc.  
1999 – 2011 Jakob Westholm Secondary School

## International research experience

Sept 2019 – Jan 2020 Visiting PhD student, Department of Chemistry, University of Jyväskylä, Finland. Research supervisor Dr. Elina Kalenius.

## International studies

Aug 2015 – Jan 2016 Student exchange, Linköping University, Sweden.

## Language competence

Estonian native  
English fluent  
Russian beginner  
Swedish beginner

## Professional employment

2016 – ... National Institute of Chemical Physics and Biophysics, Department of Chemical Physics; junior researcher.

## Honors and awards

2019, Anna Peterson, Dora Pluss T1.1 short-term mobility grant (The Archimedes Foundation, Estonia)  
2019, Anna Peterson, Dora Pluss T1.2 student mobility grant (The Archimedes Foundation, Estonia)  
2019, Scholarship for Full time Students (Estonian Students Fond in USA)  
2018, Scholarship for Full time Students (Estonian Students Fond in USA)  
2017, Scholarship for Full time Students (Estonian Students Fond in USA)

## Supervised theses

Mari-Liis Ludvig, M.Sc., 2019

*Synthesis of unsubstituted and substituted oxalix[n]arenes* Tallinn University of Technology, Department of Chemistry; National Institute of Chemical Physics and Biophysics (co-supervisors: Dr. Jasper Adamson, Prof. Riina Aav)

## Teaching experience

Spring 2020 Analytical chemistry, practice (undergraduate course)  
Spring 2018 Nuclear Magnetic Resonance, exercises (graduate course)

## Elulookirjeldus

### Isikuandmed

Nimi: Anna Cowart (Peterson)  
Sünniaeg: 06.07.1992  
Kodakondsus: eesti

### Kontaktandmed

E-post: anna.cowart@kbfi.ee

### Hariduskäik

2016 – ... Tallinna Tehnikaülikool, keemia ja biotehnoloogia, Ph.D.  
2014 – 2016 Tallinna Tehnikaülikool, rakenduskeemia ja biotehnoloogia, M.Sc.  
2011 – 2014 Tallinna Tehnikaülikool, rakenduskeemia ja biotehnoloogia, B.Sc.  
1999 – 2011 Jakob Westholmi Gümnaasium

### Rahvusvaheline teadustöö

Sept 2019 – Jan 2020 külalisdoktorant, Keemia osakond, Jyväskylä Ülikool, Soome.  
Teadustöö juhendaja Dr. Elina Kalenius.

### Rahvusvaheline õppetöö

Aug 2015 – Jan 2016 vahetusüliõpilane, Linköpingi Ülikool, Rootsi.

### Keelteoskus

eesti emakeel  
inglise kõrgtase  
vene algtase  
rootsi algtase

### Teenistuskäik

2016 – ... Keemilise ja Bioloogilise Füüsika Instituut, nooremteadur

### Teaduspreemiad ja tunnustused

2019, Anna Peterson, Dora Pluss T1.1 lühiajalise õpirände stipendium (SA Archimedes, Eesti)  
2019, Anna Peterson, Dora Pluss T1.2 doktorantide õpirände stipendium (SA Archimedes, Eesti)  
2019, Täisajalise Üliõpilase stipendium (Eesti Üliõpilaste Toetusfond USAs)  
2018, Täisajalise Üliõpilase stipendium (Eesti Üliõpilaste Toetusfond USAs)  
2017, Täisajalise Üliõpilase stipendium (Eesti Üliõpilaste Toetusfond USAs)

### Juhendatud väitekirjad

Mari-Liis Ludvig, M.Sc., 2019  
*Asendamata ja asendatud oksakaliiks[n]areenide süntees* Tallinna Tehnikaülikool, Keemia ja biotehnoloogia instituut; Keemilise ja Bioloogilise Füüsika Instituut (kaasjuhendajad: Dr. Jasper Adamson, Prof. Riina Aav)

### Õpetamiskogemus

Kevad 2020 Analüütiline keemia, praktikumid (bakalaureuseõpe)  
Kevad 2018 Tuumamagnetresonants spektroskoopia, harjutustunnid (magistriõpe)

ISSN 2585-6901 (PDF)  
ISBN 978-9949-83-680-2 (PDF)